Investigation into the Mechanisms of UV Transmission to Follicular Stem Cells and Implications for Melanoma Development

A thesis submitted to Auckland University of Technology in fulfilment of the requirements for the degree of

Doctor of Philosophy (PhD)

Author: **Xiyong Huang**

Supervisors: Michael Protheroe, Ahmed Al-Jumaily

July 2019

Institute of Biomedical Technologies
School of Engineering
Faculty of Design & Creative Technology
Auckland University of Technology
Auckland, New Zealand

AUT INSTITUTE OF BIOMEDICAL TECHNOLOGIES

AUT
TE WĀNANGA ARONUI O TĀMAKI MAKAU RAU

Abstract

Children are particularly vulnerable to sun exposure; excessive sun exposure during their childhood can result in increased melanoma incidence in later life. It is hypothesized that the reasons for the vulnerability of children to sun exposure is related to their hair follicles.

The melanocyte stem cells (McSCs) in hair follicles have been identified as a possible origin of melanoma upon exposure to ultraviolet radiation (UVR). Those cells in the vellus hairs (predominant type of hair before puberty) are much shallower than in the terminal hairs (predominant type of hair after puberty). Using the Monte Carlo (MC) method for photon transport in skin alone, we have shown that the McSCs in vellus hair follicles (VHF) would receive and absorb significantly higher UV than those in the terminal hair follicles (THF). Furthermore, as a consequence of the thinner epidermis in children, the cells would absorb about 1.9- and 3.2-times greater UVA and UVB respectively compared to adult skin.

Due to the unique morphologies of vellus hairs, it is also hypothesized that they contribute to the solar UV transmission in the skin to the McSCs. To validate this, Caucasian scalp and body hairs have been used to measure their transmission properties in the UV wavelength range, using a CRAIC^{TM} microspectrophotometer. The measured properties are then implemented into realistic skin-hair models. The simulated results show that a higher level of UV is delivered to the McSCs in the skin model with vellus hairs, as compared to hairless skin. The relative increase in energy absorbed in the stem cells when vellus hair is present to hairless skin varies from 4.6% to 52.0% over the UVA – UVB wavelength ranges. For skin with terminal hair, this relative increase in energy absorbed varies from 16.7% to 55.6% over the same wavelength range. Skin with shaved vellus hair will further enhance the UV transmission into the skin.

In conclusion, this research provides possible explanations as to why children are particularly vulnerable to sun exposure: 1) the shallower depth of McSCs in the VHF than in the THF result in significantly higher UV absorption; 2) relatively thinner epidermis of child's skin increases the UV absorption even more; 3) the presence of vellus hair provides an additional optical pathway, contributing to the overall solar UV transmission into the skin. These findings also explain the positive correlation between the incidence of melanoma in adults' bodies and the number of vellus hair in these areas. This research may lead to the improvement of melanoma prevention, e.g. improvement of the efficacy of sunscreens.

Acknowledgements

First and foremost, I would like to thank my supervisors Dr. Mike Protheroe and Prof. Ahmed Al-Jumaily from Auckland University of Technology (AUT) for their support and encouragement throughout the years of this research. They have been working closely with me to ensure the success of the research.

I would like to express my gratitude to my advisors Dr. Sharad Paul and Dr. Andrew Chalmers for providing expertise in the skin cancer and optics fields respectively.

I would like to acknowledge Prof. Shuao Wang, Prof. Juan Diwu and Dr. Wei Liu in Soochow University's Centre of Nuclear Environmental Chemistry in People's Republic of China for providing the access and supervision in the use of the CRAIC^{TM} microspectrophotometer. Thanks to Prof. Yuan Feng from Shanghai Jiao Tong University for organizing the measurements in Soochow University.

In addition, the author would like to express thank to Robin Hankin and Sharita Meharry of AUT for providing expert advice on statistical analysis and hair sample preparation respectively.

I would like to thank both the moral and financial supports from my family and AUT (Vice Chancellor's Doctoral Scholarship). Working in AUT's Institute of Biomedical Technologies (IBTec) has been a pleasure. I also want to take this opportunity to appreciate the help and kindness I received from my colleagues at IBTec.

Last but not the least, the research would not be carried out without the time and effort the Auckland University of Technology Ethics Committee (AUTEC) put in approving the ethics application (No. 18/11) in March 2018.

Attestation of Authorship

I hereby declare that this submission is my own work and that, to the best of my knowledge and belief, it contains no material previously published or written by another person, nor material which to substantial extent has been accepted for the award of any other degree or diploma of a university or other institution of higher learning, except where due acknowledgement within this document.

Xiyong Huang

Signature

Date 29/07/2019

Table of Contents

List of Figures

List of Tables

Abbreviations

Abbreviation	Description
ANOVA	Analysis of Variance
CCD	Charge-coupled device
CPU	Central processing unit
GPU	Graphic processing unit
MC	Monte Carlo
MCX	Monte Carlo eXtreme
McSCs	Melanocyte stem cells
OLCR	Optical low-coherence reflectometry
RTE	Radiative transfer equation
UV	Ultraviolet
UVA	Ultraviolet A (λ: 315 ~ 400 nm)
UVB	Ultraviolet B (λ: 290 ~ 315 nm)
UVR	Ultraviolet Radiation
UV-VIS-NIR	Ultraviolet-Visible-Near Infrared wavelength
THF	Terminal hair follicle
VHF	Vellus hair follicle

Nomenclature

Symbol	Definition
c	Speed of light in vacuum (m/s)
d_C	Effective diameter of cortex (μm)
d_H	Diameter of hair shaft (μm)
d_M	Diameter of medulla (μm)
E	Solar irradiance ($\mu W/cm^2.nm$)
E_P	Photon energy (J)
g	Anisotropy factor
g_{dermis}	Anisotropy factor of dermis
$g_{epidermis}$	Anisotropy factor of epidermis
$g_{stratum}$	Anisotropy factor of stratum corneum
h	Plank constant (J.s)
I_b	Light intensity of background (W)
I_D	Light intensity of dark scan (W)
I_{hair}	Light intensity through hair (W)
I_R	Light intensity of reference scan (W)
I_S	Light intensity through hair sample (W)
K	Ratio of absorption to attenuation coefficient
n	Refractive index

Symbol	Definition
n_{dermis}	Refractive index of dermis
$n_{epidermis}$	Refractive index of epidermis
$n_{stratum}$	Refractive index of stratum corneum
p	Probability distribution function
T	Transmittance
μ_t	Attenuation coefficient (mm^{-1})
μ_a	Absorption coefficient (mm^{-1})
μ_s	Scattering coefficient (mm^{-1})
μ_s'	Reduced scattering coefficient (mm^{-1})
$\mu_{a,stratum}$	Absorption coefficient of stratum corneum (mm^{-1})
$\mu_{a,epidermis}$	Absorption coefficient of epidermis (mm^{-1})
$\mu_{a,dermis}$	Absorption coefficient of dermis (mm^{-1})
$\mu_{s,stratum}$	Scattering coefficient of stratum corneum (mm^{-1})
$\mu_{s,epidermis}$	Scattering coefficient of epidermis (mm^{-1})
$\mu_{s,dermis}$	Scattering coefficient of dermis (mm^{-1})
$\mu_{t,cortex}$	Attenuation coefficient of cortex (mm^{-1})
$\mu_{t,medulla}$	Attenuation coefficient of medulla (mm^{-1})
λ	Wavelength （nm）

Chapter 1 Introduction

1.1 Background

Melanoma, also known as malignant melanoma, is one of the deadliest skin cancers in humans. Over the last half century, the incidence of melanoma, different to many other cancer types, has been increasing steadily [1]. Although melanoma makes up less than 10% of all skin cancers, it is responsible for the majority of skin cancer-related deaths because of its high metastatic potential and resistance to therapy [2]. Once melanoma grows to a critical thickness of about 4 mm and indicates a high risk of metastasis, then the cure and survival rate drop significantly: 10-year survival of patients with metastases is less than 10% [3].

The melanoma incidence in children younger than 18 is extremely rare (2.5 per million children) as presented in a 35-year population-based review (1979 to 2014) in British Columbia [4]. However, immigrant and epidemiological studies provide convincing evidence showing that children are more vulnerable to sun exposure; sunburn or excessive sun exposure during childhood can lead to increased risk of melanoma in later life [5-10]. The explanation for the correlation of high sun exposure in childhood and increased risks of melanoma in later life is not yet known.

The top layers of human skin are made up of the epidermis and dermis. Figure 1-1 illustrates a schematic diagram of human skin containing vellus hair follicle (VHF) and terminal hair follicle (THF), which are the predominant type of body hair in children and adult respectively. More explanation of the diagram will be introduced in Section 2.3. The cells of origin and mechanisms of melanoma initiation remain unclear. However, it is generally agreed that ultraviolet radiation (UVR) is the main extrinsic causative factor in the induction of melanoma, which arises from the mature melanocytes in the basal layer of the epidermis (see Fig. 1-1) [11]. Due to their high levels of UVR, New Zealand and Australia are reported to have the highest melanoma rates in the world [12]. Other risk factors for melanoma include inherited traits like fair skin, red hair or family history [13, 14].

Ultraviolet radiation of sunlight can be classified into three groups based on the wavelength: UVA ($\lambda = 315 - 400$ nm), UVB ($\lambda = 280 - 315$ nm) and UVC ($\lambda = 100 - 280$ nm). The stratospheric ozone layer completely blocks UVC radiation and

UVB wavelengths below 290 nm [15]. The solar UVR reaching the earth's surface is comprised of 90-95% of UVA radiation, with UVB accounting for the remainder.

Whether the UVB or UVA plays a more important role in melanoma development is still controversial [16]. Although UVB makes up only a very small portion of the total UV radiation that reaches the surface of earth, it is the major contributor to sunburn. UVB can be substantially absorbed by DNA, causing direct DNA damage; and its effective role in melanomagenesis has been demonstrated in mice [17, 18]. Although in these studies, UVB has been shown to be more effective than UVA in initiating melanoma, the role of UVA in melanoma development remains significant. UVA can penetrate deeper in the skin than UVB [19], and it is capable of causing oxidative damages to the DNA in an indirect manner [20]. In addition, recently it has been shown that human melanocytes have low repair capacity to oxidative DNA damage [21], indicating melanoma formation is mainly due to DNA breakdown induced by UVA.

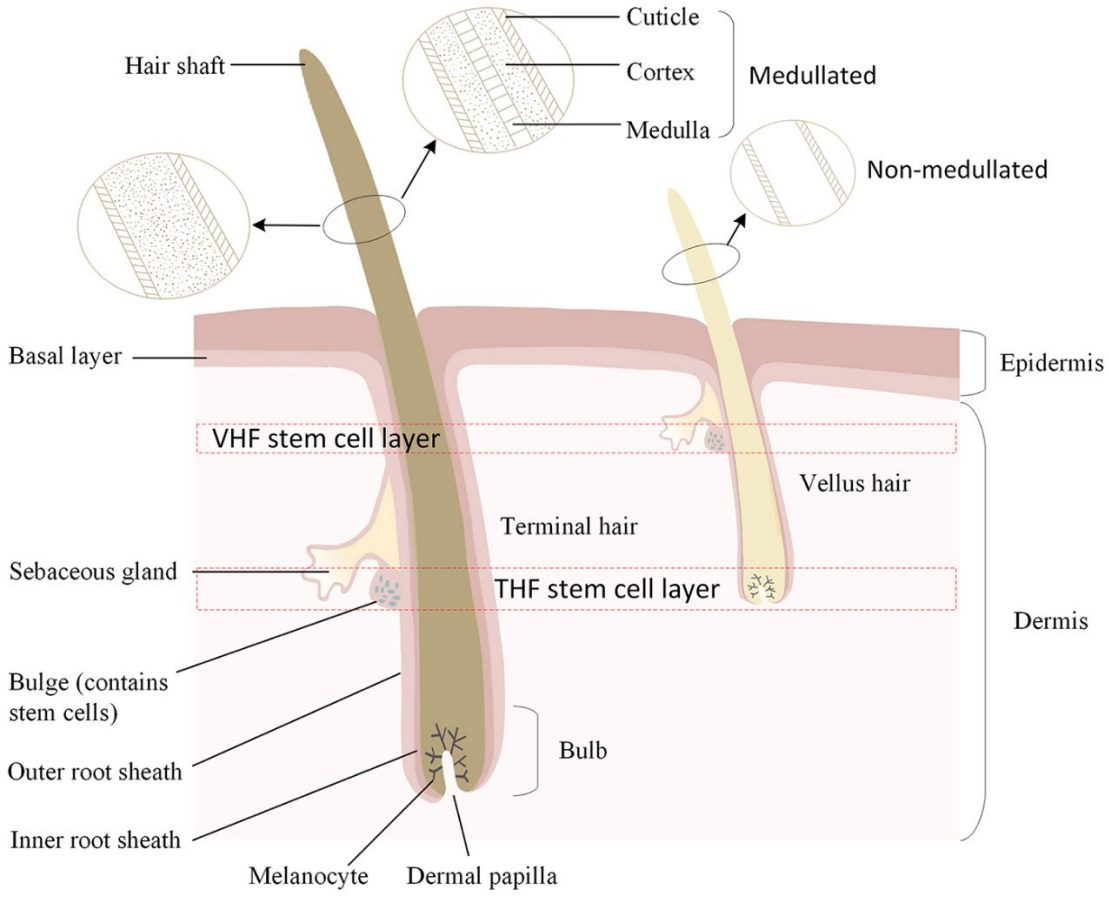

Figure 1-1: Schematic diagram of skin layers containing terminal and vellus hair follicles. The outer most skin layer is the epidermis. It is made up of the stratum corneum and cellular epidermis. The dermis is the next inner skin layer. The bulge regions of hair follicles are positioned in the dermis layer. They house melanocyte stem cells. The bulge region of vellus hair is about three times shallower than that of terminal hair.

1.2 Hypothesis

No significant difference was found in the UV sensitivity of children and adults' skins, with respect to UV induced skin reactions and anatomic structures [22-24], which led to further research into current knowledge of melanoma development. Recent studies have shown that the melanocyte stem cells (McSCs) in the bulge of the hair follicle (see Fig. 1-1) could also be the origin of melanoma upon exposure to UVR [25, 26].

In addition, Fig. 1-2 shows that positive correlation exists between the incidence of melanoma in adults' bodies and the number of vellus hair in these areas [27], which again implies the possible involvement of the follicular stem cells in melanoma development.

A study has shown that in response to wounding or UV irradiation, the McSCs can exit the bulge of the hair follicle and migrate toward the basal layer of the epidermis and differentiate into functional epidermal melanocytes [28, 29]. We hypothesize that the McSCs in VHF receive relatively more UVR prior to puberty, as compared to those in terminal hair (predominant type of hair in adulthood), resulting in a higher risk of initiating melanoma due to DNA damage or stem-cells' activation and translocation in later life [25]. More specifically, the mutations could occur in quiescent stem cells upon UVR exposure in childhood without the presence of preceding tumors; but the cumulatively mutated stem cells have the potential to materialize into melanoma in later life. This hypothesis is further supported by Fang et.al who found that melanomas contain a stem cell population [30].

We speculate that the relatively higher dose of UV received by the McSCs in the VHF could come from the photon transmission in both the skin and the hair shafts. In other words, the differences in child and adult skin and hair, could be the reasons for the vulnerability of children to sun exposure.

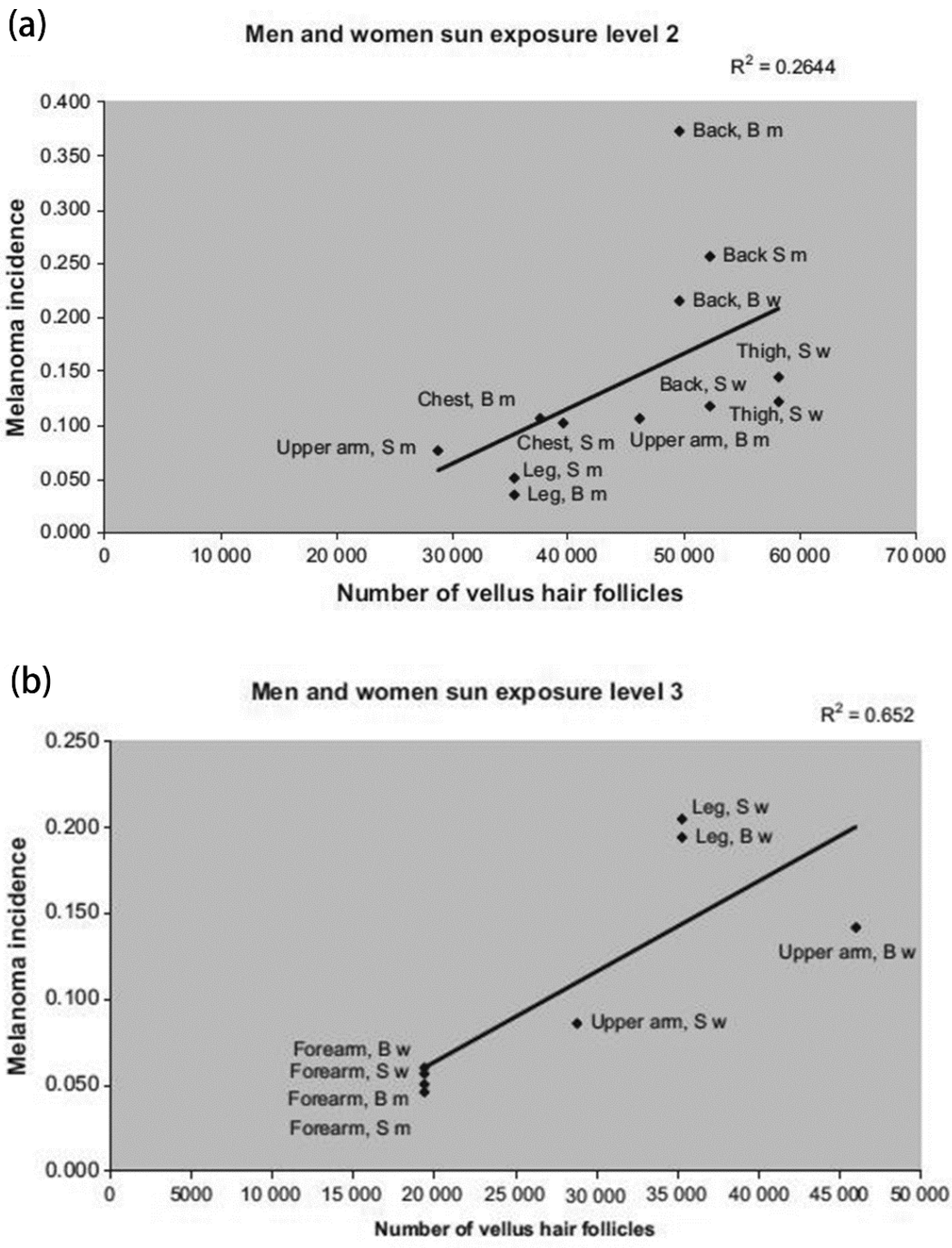

Figure 1-2: Positive correlation between the incidence of melanoma in adults' bodies and the number of vellus hair follicles in these areas. Level 2 and 3 are the scales used to describe low lifetime and high lifetime mainly intermittent sun exposure. The number of the vellus hair follicles varies with body site. S m, S w, B m, B w represent Swiss men, Swiss women, British Columbian men, and British Columbian women, respectively. Reproduced figures [27].

1.3 Thesis structure

The main body of the thesis is composed of several journal and conference articles (See Appendix A for more detail). They have been organized in an order designed to give readers the best flow of the thesis.

Chapter 2 delivers a review of the background knowledge of the link between melanoma development and hair follicles, and studies on the optical properties of human hair. Specific research objectives will be introduced at the end of the chapter.

Children typically have thinner skin layers [31, 32], which will allow more UV photons to transmit deeper into the skin. In addition, the McSCs in the VHF are much shallower in the dermis than those in the terminal hair [33]. How these factors affect the UV dose received by the McSCs will be investigated in **Chapter 3** using a Monte Carlo (MC) simulation of photon propagation.

As early as about three decades ago, it was observed that lightly pigmented human hairs may transmit visible light along their shafts to the follicular epithelium and dermis [34]. Human hair shafts were shown to possibly transmit ultraviolet light down to the bulb region a decade later [35]. We hypothesize that vellus hair, due to its unique morphologies, may contribute to the transmission of harmful UV energy to McSCs. The first step in testing this hypothesis is to determine the optical properties of human hair. Caucasians are the most vulnerable group of humans to sun exposure [36]. **In Chapter 4**, the transmission property of the hair samples collected from Caucasian children and adults, in the UV wavelength range, is investigated using a CRAIC^{TM} micro-spectrophotometer.

To reveal the roles vellus and terminal hair play on the solar UV transmission in the skin to McSCs, the measured optical properties of human hairs in the UV wavelength range are applied to the MC simulations (**Chapter 5**).

As the primary reason for skin cancer-relevant death, melanoma is notoriously famed for its metastatic ability [37]. The propensity of melanoma cells for distance metastasis closely resembles the migratory feature of McSCs [29]. If the hypothesis holds true, it may not only rationalize the phenomenon seen in the immigrant and epidemiological studies and build up the current knowledge of melanomagenesis, but also explain the reasons for recurrence of melanoma years or decades later after treatment. The success of this research may have significant implications for primary prevention through, for example, public awareness and improvement of sunscreen, e.g. for coating hair as well as skin.

Chapter 2 Literature Review

2.1 Introduction

Chapter 2 firstly reviews the evidence suggesting the vulnerability of children to sun exposure (Section 2.2). Section 2.3 introduces the anatomy of human hair to provide necessary background for understanding its possible connection to melanoma development. This is followed by a brief introduction to the optical properties and experimental measurement techniques used in biological tissues (Section 2.4). Sections 2.3 and 2.4 offer biological and optical knowledge for the later sections. Section 2.5 is the focus of this chapter. It delivers a review of the optical studies of human hair up to date, which include the details of sample preparation, experimental methods, results and statistical analysis. Knowing the UV optical properties of hair enables the radiant energy/power in the stem cell region from sun exposure to be determined and this is critical to test the hypothesis. Therefore, Section 2.6 reviews the Monte Carlo method of photon transport simulation used in human hair studies. Section 2.7 outlines the possible application of this research. Finally, in Section 2.8, current knowledge of the optical properties of human hair in the literature are discussed, together with their possible contribution to melanoma development; and the necessary work needed to test the hypothesis is suggested. The goals of this review chapter are 1) to review the studies of the optical properties of human hair in the literature and discuss whether current knowledge is able to support the hypothesis; 2) provide detailed experimental measurement methods and analysis to guide researchers in future investigations. The research gaps will be narrowed down in Section 2.9, which are considered to be feasible in the time frame of a PhD.

2.2 Vulnerability of children to sun exposure

A study of immigrants to Australia (511 cases and 511 controls) indicated that immigrants arriving before the age of 10 suffer similar incidence of melanoma to native born Australians, whereas immigrants arriving after age 15 account for only about a quarter of this [5]. An epidemiological study (412 cases and 445 controls) in Europe involving patients from Germany, Belgium and France also confirmed this finding: individuals arriving in a sunny location before age 10 exhibited a four times higher risk of developing melanoma in later life [6]. Similarly, individuals who spent more than one year in sunny

geographies (either the Mediterranean, subtropics or tropics) prior to the age of 10 presented a four-fold higher risk of melanoma, while people who only resided in those areas in their adulthood did not show major increased risk of melanoma [6]. Studies in the United States and New Zealand also show similar trends [7-9]. These immigrant and epidemiological studies suggest that children are more vulnerable to sun exposure, and that sunburn or excessive sun exposure at an early age could lead to increased risk of melanoma in later life [10].

This critical period of sun exposure seems to coincide with the ages before puberty (approximately 11 – 14 years in girls and 13 – 16 years in boys [38]). However, the explanation for the correlation of high ultraviolet exposure in childhood and increased risks of melanoma in later life is not yet known, although the differences of skin and hair in childhood and adulthood have been hypothesized to be the causes [27, 39].

2.3 Hair anatomy and melanoma

This section describes the anatomy of human hair, to provide an understanding of the possible involvement of hair in melanoma development and provide biological background for the optical studies to be presented and discussed in Sections 2.4 – 2.6.

The hair shaft is mainly composed of keratin (a type of protein). It is generated by the living portion of hair called the hair follicle, a complex mini-organ of the skin [40]. Fig. 1-1 illustrates a schematic diagram of hair follicles. The cuticle is the outermost layer of the hair shaft, which is composed of multiple thin overlapping layers (total thickness < 5 μm). It is translucent so allows light to penetrate into the inner cortex layer. The cortex is the bulk of the hair shaft, which contains longitudinally oriented cells [41]. The medulla is a vertical column of horizontal cells and large air spaces, located at the centre of the cortex (Fig. 2-1) [41]. The medulla cells have distinct keratins compared to any other cells of the hair follicle and epithelium [41]. Melanin is a skin pigment [42] and there are two types of melanin found in the cortex of hair: eumelanin and pheomelanin. It is known that light coloured hair (e.g. red and blond) has predominantly pheomelanin whereas eumelanin is responsible for dark coloured hair (e.g. black and brown) [43]. Melanin has a significant effect on light absorption, especially at shorter wavelengths (e.g. the UV region) [44].

Vellus and terminal hairs have distinct morphologies. Vellus hair is short (< 2 mm), fine (< 30 μm in diameter) and unpigmented or lightly pigmented [45, 46]. Vellus hairs are

present extensively in children before puberty, although they are barely noticeable [47]. Due to hormonal changes that occur during puberty, a large proportion of vellus hair will develop into terminal hair. In contrast to vellus hair, terminal hair is coarse and pigmented, with length and diameter longer than 2 mm and thicker than 60 μm [45, 46]. Unlike vellus hair consisting of only the cuticle and cortex, terminal hair also contains the medulla, which has high light scattering characteristics [48]. In studies on morphology of scalp hairs and the presence of medullas, Wynkoop noted that only a minority (40%) of hair in people aged 0-9 had medullas, whereas at ages 10-19, a significant majority (82%) had medullas [49].

Overall, the anatomy of hair suggests that UV radiation might transmit along vellus hair more easily than terminal hair. Furthermore, the bulge in the outer root sheath of the hair follicle, that houses the stem cells, is located approximately 1200 μm from the exposed skin surface in the terminal hair, which is more than 3 times deeper than the location of the bulge in the vellus hair, at about 360 μm [33], implying that the stem cells in the vellus hair follicles are less protected from sun exposure than THF.

It is hypothesized that the unique morphologies of vellus hair may provide an additional optical path, contributing to the overall UV transmission received by McSCs. The cumulatively damaged McSCs then have the potential to become melanoma.

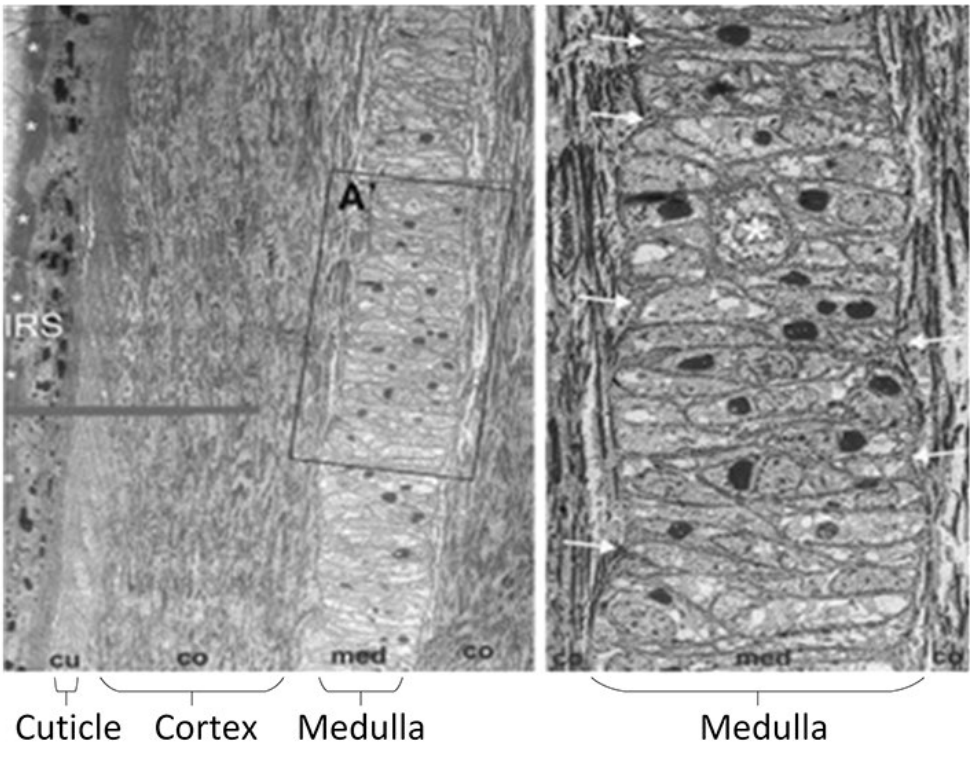

Figure 2-1: Images of the longitudinal section of human hair taken by electron microscope [41]

As the first step to proving the hypothesis, the optical properties of human hair (vellus and terminal hair) need to be well understood. More specifically, the overall optical properties of vellus hair are thought to be responsible for deeper penetration depth of UV radiation than in terminal hair.

Vellus hairs grow in the areas of the body that appear hairless. Even on the scalp, which is usually considered to have only terminal hair, vellus hair may still account for 7% - 25% of the total hair population. Furthermore, there are 'miniaturized' terminal hairs in the scalp with hair shaft diameter $\leq$ 30 μm, which can be classified as 'vellus-like' hair [50]. 'Hair loss' is the result of transition of terminal hairs to vellus hair [51].

Human skins are classified into six groups based on the reactiveness to sun exposure, according to the 'Fitzpatrick skin typing system' [52]. From skin type I to VI, the sensitivity to sun exposure decreases. For example, people with the skin type I and II have sunburn easily without tan or minimal tan. They are fair-skinned individuals with blue, hazel or green eyes, blond, red or brown hair. Whereas highly pigmented skin type VI is insensitive to the sun exposure and never burns.

2.4 Introduction to the optical properties of tissue

Section 2.4 briefly introduces the properties used to describe the optical characteristics of biological tissues and the different measurement techniques for determining these properties.

2.4.1 Optical properties of biological tissues and measurement methods

Absorption and scattering are the two phenomena that occur when light interacts with biological tissue. The optical properties that are commonly used to describe the light propagation in tissue, are the scattering coefficient μ_s, absorption coefficient μ_a, scattering phase function p, and refractive index n [53]. The absorption and scattering coefficients are commonly measured in inverse millimeters and their reciprocal are the average distance that photons will travel before being absorbed or scattered in tissues, respectively. The scattering phase function is used to describe the angular distribution of photons after a single scattering. When multiple scattering occurs in thick tissues, the scattering profile is conveniently described by a dimensionless parameter, the anisotropy factor g (mean cosine of the scattering angle), which characterizes the tissue scattering pattern by its asymmetry [53, 54]. As g approaches 1, 0 and -1, the scattering even tends

to be dominantly forward, isotropic and extremely backward, respectively [54]. The reduced scattering coefficient μ_s', combines the scattering coefficient and the anisotropy factor as $\mu_s' = \mu_s(1-g)$. The sum of the absorption and scattering coefficients is called the attenuation coefficient μ_t, which determines how far light can propagate in tissues before being scattered or absorbed. The refractive index describes how light refracts/bends when it encounters an interface between different media.

Optical properties of biological tissues can be calculated by converting measurements of observable quantities into standard parameters [54]. Measurement techniques are classified into two categories: direct and indirect methods. Direct methods use basic principles of light to calculate the optical properties of optically thin tissue sections (single scattering) from measured quantities, which do not involve the use of a model of light transport in tissue. For instance, the attenuation coefficient of a sample can be calculated from the collimated transmittance measurement using Beer's law [55]. By contrast, indirect methods involve measuring quantities such as diffuse reflection and transmission, from which the optical properties of optically thick tissue sections (multiple scattering) can be determined by solving an 'inverse problem' based on a model of light transport in tissue [54, 56-58]. A common indirect technique involves measurements using integrating spheres (Fig. 2-2). The inverse Monte Carlo method is then used to estimate the optical properties of the tissues by fitting the simulated results to the experimentally measured quantities [59-61].

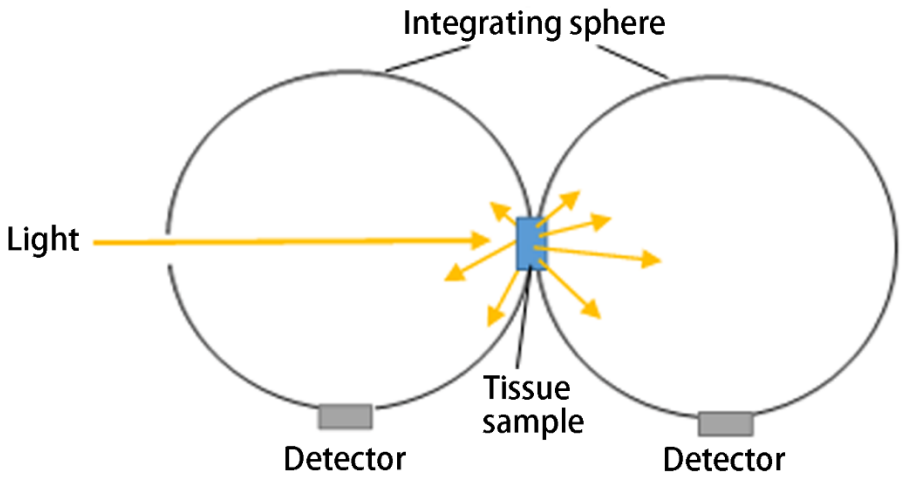

Figure 2-2: Double integrating sphere for measuring the diffuse reflectance and transmittance from an optically thick section

2.4.2 Light Propagation model – Monte Carlo method

Light transport in biological tissues can be modeled analytically by the radiative transfer equation (RTE) as well as numerically by the Monte Carlo (MC) method. Radiative transport theory describes the energy transfer through a turbid medium [57]. As radiative transport theory states, the radiance $L(r,s)$(W.m^{-2}sr^{-1}) of light at position r and moving in the unit direction vector s is attenuated by absorption and scattering but its energy is gained from the light that is scattered from s' direction [54]. Radiative transport in tissue is governed by Eq. (2-1)

$$s \cdot \nabla L(r,s) = -\mu_t L(r,s) + \mu_s \int_{4\pi} p(s,s') L(r,s') d\omega' \qquad 2\text{-}1$$

Finding closed-form solutions to the RTE is often not possible. Therefore, Diffusion Approximation Theory is often used for simplification. However, assumption of isotropic scattering and matched boundary conditions in turn bring inaccuracies, especially in the region close to the light source and boundaries [62].

The MC method, as a statistical approach to light transport in tissues, requires calculating the propagation of considerable number of photons, thus significant computation time, to establish an accurate simulation to reality. The MC modelling of photon transport in multi-layered tissues was developed and coded in Standard C language by Wang et al. in the 1990s [63], and modified by many other researchers for different applications [64-67]. It is based on the fact that photons exhibit 'random walk' as they propagate in a medium which involves scattering and absorption. The MC technique has been used to solve both forward [68] and inverse problems [59-61]. The experimentally determined optical properties (μ_a, μ_s, g, n) of tissues are required as input parameters to simulate light distribution; whereas in the inverse application, the optical properties are estimated by fitting the simulated results to the experimental measured quantities.

The algorithm of a Monte Carlo simulation is briefly explained as follows. Figure 2-3 shows a flow diagram of the MC method applied to photon transport in tissues. Each photon pack is assigned an initial weight. Once the photon pack is launched, a step size s, is calculated based on the probability distribution of the photon free path length and the attenuation coefficient of the tissue [63]. After the photon pack has entered the tissue and moved by distance s, an absorption event occurs: a fraction weight of the photon pack is absorbed according to the absorption probability and scored in the Absorbance Array.

The remaining weight is then scattered by a new step. The scattering angle is randomly sampled base on its probability distribution [63]. If the photon pack is about to hit the boundary, it will either transmit through or be reflected from the boundary; this probability is governed by Snell's law and Fresnel's equation [68]. The photon pack will travel in the tissue model step by step until it escapes from the model or is terminated by the program.

The MC method is considered to be more suitable for this investigation because more realistic skin-hair 3D models can be built for accurate simulations.

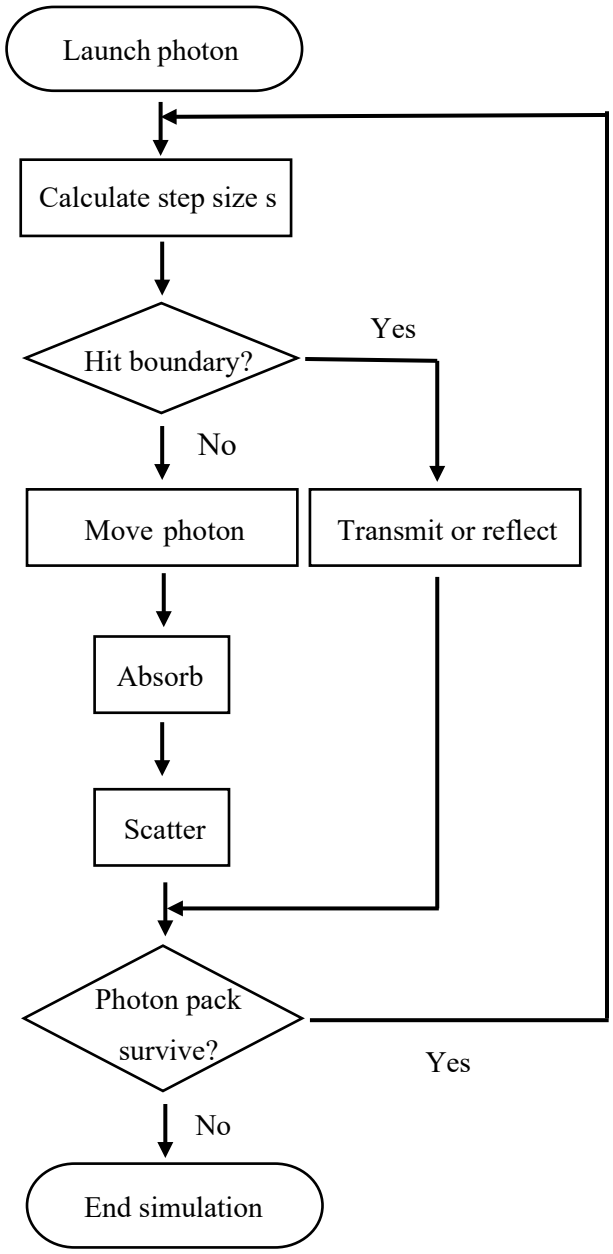

Figure 2-3: Flow diagram for the principle of the Monte Carlo method for photon transport in tissues

2.5 Experimental measurement of optical properties of hair

Human hair is delicate, and its average diameter is smaller than that of some common optical fibers. Therefore, holding the hair sample in place for precise optical measurement is challenging. The optical properties of human hair have been investigated by a number of groups. Among them, some works were mainly devoted to the optical properties of the hair surface [48, 69-73], while others contributed to the knowledge of light propagation through hair [74-79]. This section describes in detail the experimental investigations of light propagation properties of hair.

2.5.1 Sample preparation

The hair samples should be free of contaminants (e.g. dirt and oil), which could influence the measured results. This can be achieved by cleaning the samples with ethanol or shampoo before any measurements [74, 75]. For the micro-spectrophotometry of hair, the samples can be placed between a microscope slide and a cover slip [77, 78] or mounted on a tri-holed metal slide [74]. Some sample holders can also be used to mount the hair and adjust its position and orientation [75, 79]. The refractive index of human hair is about 1.54, which is higher than that of air [80]. So some researchers used a refractive-index-matching liquid to minimize the light loss from the surface scattering in measurement [77-79], whereas others included the mismatch of refractive index on the measurement results [74-76]. It is noted that the refractive index matching liquid (mounting media) should not degrade the hair sample nor absorb UV [74]. When UV light is involved in the measurement, a quartz microscope slide needs to be used instead of a glass one as glass absorbs UV and could mask the spectral result.

The optical properties in the transversal (cross-sectional) direction of hair were studied by most of the groups because of the relatively simple sample preparation procedures [74-79]. In contrast, the properties in the longitudinal direction of hair were rarely examined due to the difficulties of achieving a flat cross section of hair and positioning it accurately for illumination. However, one group achieved this by mounting the properly cleaved hair to a thin metal wire, wrapped with double-sided tape [75]. Although there are several techniques for preparing the hair samples with neat cross sections through several steps, involving the use of mounting media (e.g. paraffin and resin) and microtome sectioning, they are technically more difficult and time-consuming to implement [81-86]. In one case, it was found that hairs with different colours sectioned from a microtome were too short to give discrimination in the spectrophotometry readings [78]. Also, when paraffin is used

as a mounting medium, since the keratin of hair is harder than paraffin, the hair could split, break or move within the block [82].

2.5.2 Measurement techniques

The optical properties of biological tissues are commonly measured using an integrating sphere (Fig. 2-2) [58, 87]. However, human hair has never been studied using this method due to the difficulty of accurately focusing light onto a hair shaft inside an integrating sphere. Nevertheless, the optical characteristics of some relatively larger mammals' hair have been investigated using this techniques [88, 89]. Instead, human hair was primarily studied using a common confocal setup [48, 69-79].

A confocal setup of collimated transmittance measurement, as shown in Fig. 2-4, was constructed by Kharin et al. to examine the attenuation coefficient of human scalp hair [79]. Five laser sources with different wavelengths ranging from 409 to 1064 nm were used to examine the wavelength dependence of the optical properties of different hairs. In addition, for the first time in the literature, a multi-order wave plate was used in this study to rotate the light polarization for studying the sensitivity of the optical properties to polarization of light.

Constructing a confocal setup for optical measurements of such a small object could be costly and time consuming, if starting from scratch. Alternatively, given the advantages of accurately focusing light onto hair using an optical microscope, a video camera and a light source that are attached to an optical microscope has been commonly used in the past to study the optical properties of human hair [74, 76-78]. The CRAIC^{TM} Micro-spectrophotometer and Jasco Spectrophotometer are two modern instruments in the market that can be used to study the optical properties of microscale materials [90, 91].

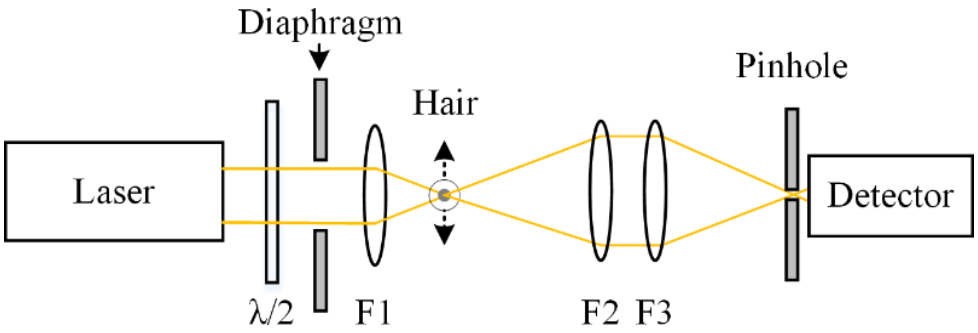

Figure 2-4: Schematic diagram of the confocal setup used for the measurement of collimated transmittance through a hair: λ/2, a multi-order half-lambda waveplate; F1, a 20 x 0.4 NA microscope objective; F2, a 40-mm-focal-distance lens; F3, a 100-mm-focal-distance lens. Reproduced figure with permission [79].

They are powerful but expensive devices that combine the techniques of microscopy and spectrophotometry, providing measurement of the UV-VIS-NIR range of transmission, absorbance and reflectance for sampling areas as small as 6 μm × 6 μm [91]. In the micro-spectrophotometry studies of hair, the incident light is focused down to a size smaller than the diameter of human hair to obtain the absorbance or transmission spectra of hair samples [74, 77, 78]. A dark scan and a reference scan are required during measurement to obtain accurate spectra graphs. At a given wavelength, transmittance, T for example, is calculated using Eq. (2-2), where I_D is the dark reading measured by a detector when the light source is turned off while I_R is the reference reading when the hair sample is absent in the light path; and I_{hair} is the reading when the hair sample is in place. To reduce the uncertainties of the result on each hair, I_{hair} is determined by averaging multiple measurements along the length of the hair shaft [74, 77, 79].

$$T = \frac{I_{hair} - I_D}{I_R - I_D} \qquad 2\text{-}2$$

From the transmittance measurement, the attenuation coefficients of hairs were estimated using Beer's law, as shown in Eq. (2-3), where L is the thickness of the material [77, 79]. The diameters of the hair samples have been measured conveniently using a video camera that is fitted to the microscope [76, 77, 79].

$$\mu_t = -\frac{Ln(T)}{L} \qquad 2\text{-}3$$

However, by assuming the measured transmitted light is collimated, the attenuation coefficients are underestimated. Another limitation of only conducting the transmittance measurement is the difficulty of distinguishing the absorption and scattering coefficient from the attenuation coefficient on its own. Rather than calculating the attenuation coefficient from Beer's law, Bashkatov et al. took a similar approach using a digital video microscopic system [76]. The images of hairs in the reflectance and transmittance modes of a microscope are acquired and analysed. From the colour images of hair shafts, their absorption and reduced scattering coefficient are estimated using the inverse Monte Carlo method. Readings from white and black papers are used as a reference and a background signal in the reflectance measurement, while the readings from a transparent glass are used as a reference in the transmittance measurement.

The refractive index of scalp hair can be determined by increasing the refractive index of the hairs' mounting media in small intervals until they match, in which case the hair became invisible under a transmittance microscope [80, 92]. Wang et al. used the optical low-coherence reflectometry (OLCR) technique to investigate the refractive index of human scalp hair at a wavelength of 850 nm [75]. Different single hair shafts are scanned both longitudinally and transversely. The refractive index of hair is calculated as a ratio of the scan length of the reference mirror in the OLCR result and the physical length of the hair shaft. Although the attenuation coefficients were not reported in Wang et al.'s study, they were estimated by Kharin et al. using Beer's law based on the magnitude of the interference signals in the OCLR graph [79].

2.5.3 Hair optical properties

Wells observed that grey hair acts as a natural optical fiber, transmitting light along the hair shaft [34]. The transmittance microscope image of hair in his work illustrated that the cortex of the hair behaved like the core of an optical fiber, allowing the passage of light. In contrast to the cortex, the air-filled medulla at the centre of the shaft appeared dark, implying no light transmitted through this region. Wells also pointed out that the colour of hair is the most important factor affecting the light transmission along the shaft: darkly pigmented brown hair transmitted little or no light. Although no corresponding optical properties of hair were reported, these findings were confirmed by other later studies that presented numerical values [75-77, 79].

The attenuation coefficient is the most commonly reported property of human hair in the literature because it can be estimated conveniently by applying Beer's law. Figure 2-5 illustrates a summary of the attenuation coefficient of different coloured hairs at different wavelengths, obtained from three research groups [75, 77, 79]. These studies show that highly pigmented brown and black hairs have, as expected the highest absorption and attenuation coefficients, while little- or un-pigmented blond and grey hairs have the least values. Among these studies, Kharin et al. demonstrated that the attenuation coefficient of the medulla was dramatically higher than that of the cortex, especially in blond and grey hairs [79]. This explains why the cortex of the grey hair appeared extremely bright while the medulla appeared completely dark in Wells' study. In contrast with other measurement and analysis methods, Bashkatov et al. discriminated between the absorption and reduced scattering coefficient [76]. However, lightly pigmented blond and grey hairs showed significantly higher reduced scattering coefficient, which is

inconsistent with Wang's results [75]. This great inconsistency of results may be due to the fact that hair samples with and without medulla were studied by the two research groups, respectively.

Apart from the dependence of the optical properties of hair on its colour and the presence of a medulla, the attenuation, absorption and reduced scattering coefficients all increase with a decrease in the wavelength [76, 79]. In addition, the difference between the optical properties in highly and lightly pigmented hair increases with a decrease in wavelength [76, 79]. These relations can be seen from Kharin et al.'s results in Fig. 2-5 [79]. This observed result is primarily due to the fact that the absorption and scattering coefficients of melanin become progressively more significant as the wavelength decreases [93, 94]. Therefore, it is inferred that the difference between the optical properties (absorption and scattering coefficients) of highly- and un-pigmented hairs (e.g. terminal and vellus hair) will peak in the UV wavelength region. This means that UV rays are expected to penetrate more deeply in vellus hair than in terminal hair.

Table 2-1 summarizes the varied experimental factors (different hair samples, experimental methods, directions of measurement and refractive-index-matching conditions) in these studies, which may result in the difference seen in their results.

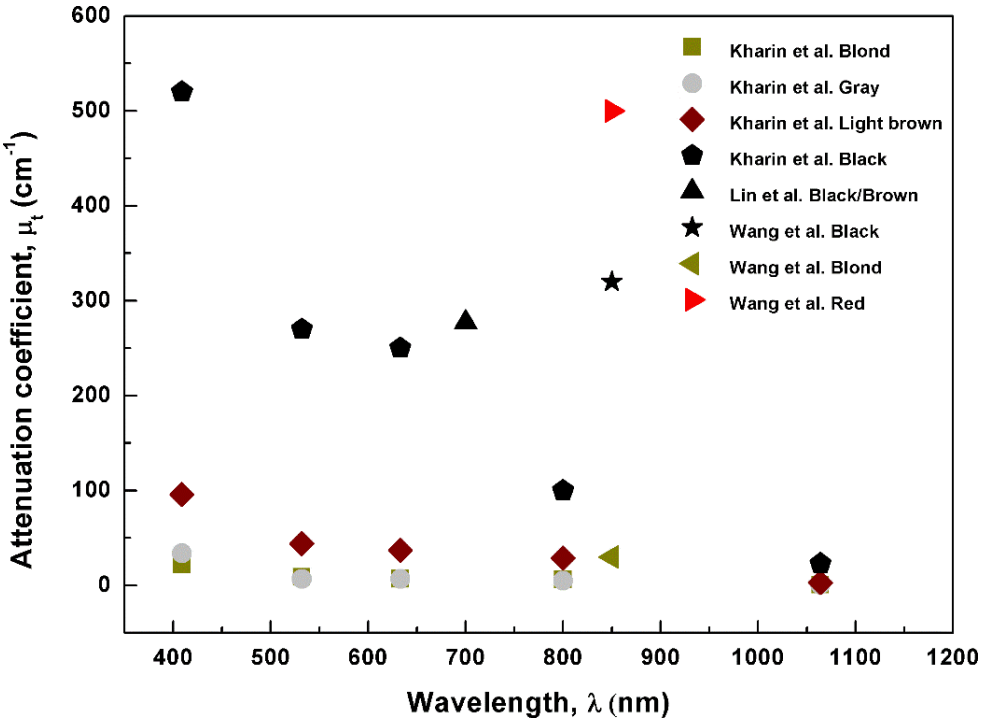

Figure 2-5: Attenuation coefficient of human hair with different colours. Data is obtained from Kharin et al. [79], Lin et al. [77] and Wang et al. [75]. The properties of the black and blond hair samples in Wang et al.'s study are measured in the longitudinal direction while the rest data are all measured in the transverse direction.

Table 2-1: Summary of the experimental factors in the studies of the attenuation coefficient of human hair [75, 77, 79]. The details of the hair samples used by Wang et al. are not reported.

	Hair sample	Experimental Method	Direction of measurement	Refractive index matching
Kharin et al. [79]	Non-medullated scalp hair	Collimated transmittance measurement	Transverse	Yes
Lin et al. [77]	Medullated body hair	Micro-spectrophotometry	Transverse	Yes
Wang et al. [75]	-	Optical low-coherence reflectometry	Transverse & longitudinal	No

The attenuation coefficient of black hair at the wavelength of 700 nm determined by Lin et al. [77] is inconsistent with the wavelength-dependency of the black hair observed in Kharin et al.'s work [79]. This inconsistency is probably attributed to the presence of medulla since the high scattering effect of medulla can contribute to overall attenuation coefficient of hair. In contrast, the attenuation coefficient of black hair reported by Wang et al. [75] again differs to the other two studies. One fact is that, Wang et al. [75] performed the measurement in air, in which the surface scattering effect is taken into the total attenuation coefficient. Furthermore, the black and blond hair were measured in the longitudinal direction by Wang et al. [75], whereas the rest were measured in the transverse direction. The attenuation coefficient of red hair measured in the transverse direction is surprisingly much higher than that of black hair at the same wavelength, both determined by Wang et al. [75]. It is too early to draw a solid conclusion that the optical properties are different in the transverse and longitudinal directions since other variables such as measurement techniques and hair samples, which are different in the different studies, may all affect the published results.

The lowest attenuation coefficient is expected to be observed in the cortex of the blond hair because it mainly contains pheomelanin. The attenuation coefficient of the cortex of hair in Kharin et al.'s study shows an exponential relation with the wavelength. Based on the current knowledge, the cortex of the blond scalp hair is considered to be mostly close to that of vellus hair. Therefore, we extrapolate the attenuation coefficient of the cortex of blond hair at a wavelength of 350 nm to be 26 cm^{-1}. By assuming the absorption to be dominant to the scattering in the cortex of blond hair, we estimated its penetration depth (at 350 nm wavelength) to be 376 μm, which is about six times deeper than that of fair

Caucasian skin [95], implying that UV may penetrate much deeper in vellus hair than skin. The contribution of vellus hair in the UV energy delivery is to be verified by determining the UV optical properties of vellus hair.

As presented by Barrett et al, the absorbance spectra (200 – 700 nm) of scalp hairs with different colours peaked in a wavelength range of 300 – 400 nm [74]. However, no numerical values of the optical properties of hairs were reported and the absorbance spectra graphs have no scale for comparison. In another spectrophotometry study of red and brown hair, the absorbance spectra (400 – 800 nm) of hairs from red-haired people differed noticeably to those from brown-haired people, but both peaked at a wavelength of about 440 nm [78]. In contrast, the absorbance spectra of melanin isolated from red and black hairs continuously decreased in the wavelength range of 270 – 700 nm; while a more marked decrease was observed in red hair [96]. Greenwell et al. found that regardless of age, gender and race, the refractive index of the cuticles of hairs varied slightly from 1.543 to 1.554. As noted in this study, females and children have similar values of the refractive index, which tend to be higher than that of males [80]. In contrast, Wang et al. showed that the refractive indices of the hair cortical regions were in a range of 1.56 – 1.59 [75].

Studies in the literature so far have mainly looked at the influence of colour on the optical properties of scalp hair in the visible and infrared range of wavelength. In addition, the hair examined was primarily adult terminal hair, and very little investigation was done on children's hair and none on vellus hair. All in all, current knowledge of the optical properties of hair cannot provide enough evidence to support our hypothesis.

2.5.4 Statistical analysis

The anatomy of human hair varies with colour, age, gender, race and body site. Achieving statistically significant optical properties requires a substantial number of samples.

Statistically significant results of the refractive index of human scalp hairs (2529 hairs from 97 individuals) were obtained by Grenwell et al., taking into consideration different races, sexes and ages [78]. The dispersion of the result was about 1%. Similarly, a large number of samples (1080 hairs from 54 brown haired individuals, 420 hairs from 21 red haired individuals) were used in Nicholls' study to determine their absorbance spectra.

Wang et al. also investigated the refractive index of the cortical region (cortex and medulla) in the longitudinal direction of scalp hairs [75]. However, the identities of the

hairs and the number of samples were not reported. Kharin et al. used five hair samples from single individuals with different hair colour (Black, light brown, grey and blond) [79]. Again, the age and gender of the individuals were not specified.

Over 30 hair samples each from 10 individuals were used in Bashkatov et al.'s study [76]. The age, gender and hair colour were specified in the paper. Barrett et al. also used five natural scalp hair samples each from seven groups of colour (each group consisting of 1-5 individuals) to study the variation in their absorbance spectra due to the different levels of brown and blond colours [74]. However, no other information about the characteristics of the hair samples was given.

In Lin et al.'s study, about five body hair samples each from about 45 individuals were used to determine the attenuation coefficient of human body hair [77]. This study calculated the mean attenuation coefficient of the hairs with different colours (auburn, brown and black), from different gender, body sites (back, forearm, thigh, lower leg, shoulder etc), and ages (21-61). However, due to the randomness of the samples measured and multiple colours of hair samples involved, the statistical dispersion is more significant than scalp hair, as it can be seen from Table 2-2. Table 2-2 presents a summary of the optical properties of black hair and their standard deviation (SD), for wavelengths from 600 to 700 nm.

In the literature, the influences of gender, age, race and, more importantly, hair type, on the optical properties of hair have not been investigated deeply. Since there are vellus and terminal hairs existing at different sections of human bodies and their morphologies vary greatly, if human body hairs are to be examined, the colour, type and site of hair are the main categories to be considered in any future statistical analysis.

Table 2-2: summary of the optical properties of black hair in the transverse direction and their standard devivation [76, 77, 79]

	Wavelength (nm)	Optical property (cm^{-1})	SD (±)
Bashkatov et al. [76]	600	28.5[a]	6.3
		37.5[b]	18.8
Kharin et al. [79]	633	250[c]	20
Lin et al. [77]	700	277[d]	111

[a] Absorption coefficient of scalp hair
[b] Reduced scattering coefficient of scalp hair
[c] Attenuation coefficient of the cortex of scalp hair
[d] Attenuation coefficient of body hair

2.6 Monte Carlo method for photon transport in skin and hair

Stem cells can be found approximately 360 and 1200 μm from the exposed skin surface in vellus and terminal hair follicles, respectively. Examination of the significances in magnitude of the radiant energy density in these locations due to sun exposure may provide more information and evidence to support the hypothesis.

Radiant energy transfer to the hair follicle through the skin due to light exposure has been simulated using the MC method for the application of epilation (hair removal) [97-100]. Figure 2-6 shows a diagram of the principle of using a MC simulation to determine the energy exposure of the hair follicle from a Ruby laser beam [97].

Broadband light sources that deliver polychromatic light with various intensities at different wavelengths have also been commonly used for epilation. The principle of this method is to select the appropriate wavelength, pulse duration and fluence (radiant exposure) from a broadband light source to damage the stem cells of hair follicles (for permanent hair removal) with the least interference to the surrounding tissues (selective photothermolysis). The MC method requires the input of the optical properties of the tissues (epidermis, dermis and hair), which are strongly wavelength dependent. Averaged values over the range of the light source spectrum cannot be used. For this reason, implementing the MC photon simulation to tissues subjected to light with varied wavelengths is challenging [98, 99]. To overcome this challenge, Ash et al. ran the MC photon simulation simultaneously for each wavelength comprising the spectrum of the broadband light source [99]. In contrast, Sun et al. applied a spectrum-intensity-weighted method to estimate the effective absorption and scattering coefficients of the tissues [98].

Table 2-3 summarizes the optical properties of hair reported in Sun et al. and Ash et al.'s publications. However, the optical properties of the hair, epidermis and dermis in their numerical model were only estimations. The absorption and scattering coefficients of hair were estimated by assuming the melanin and water contents to be 0.3 and 0.25 respectively [98]. The temperature of the hair follicle in the simulation was validated by measuring the temperature values in a two-layered, agar gel skin phantom using a thermocouple [98]. The agar gel skin model, having the same optical properties as skin was made by dissolving the granulated agar, dyes and milk into boiling distilled water. The refractive-index-mismatch of hair and skin was taken into consideration in Ash et al.'s simulation [99, 100].

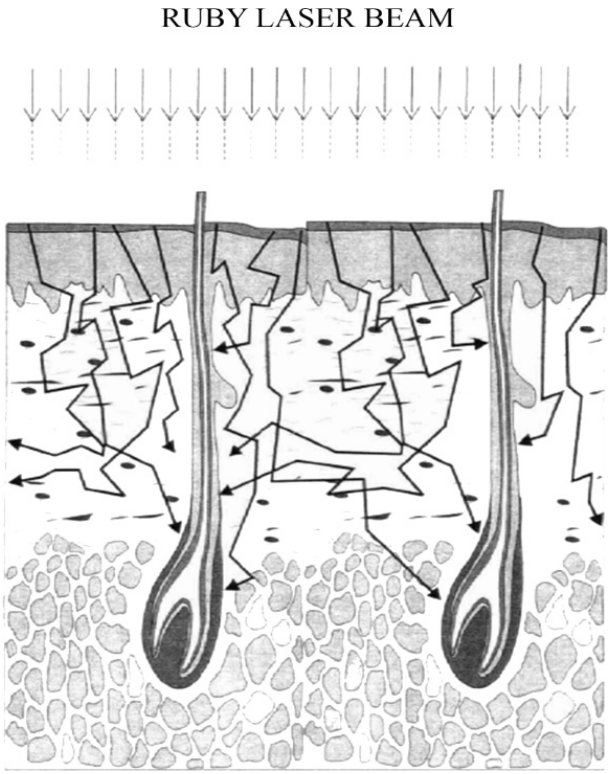

Figure 2-6: Diagram of the principle of the Monte Carlo photon simulation in the skin and hair follicle. Reproduced figure with permission [97].

Theoretically, the Monte Carlo photon simulation in hair requires the knowledge of its absorption coefficient, scattering coefficient, refractive index and anisotropy factor. However, it is difficult to experimentally determine all the properties, due to the small size of hair. In addition, the inhomogeneous structures of hair make realistic photon simulation more challenging. Therefore, the refractive index and anisotropy factor of hair are usually assumed, and the hair is often simply modeled as a cylinder in the MC simulation [97-100].

Table 2-3: Summary of the optical properties of hair (estimated) used in MC simulation [98-100]. The absorption and scattering coefficients of hair are not reported in Ash et al.'s publication.

	Absorption coefficient (cm^{-1})	Scattering coefficient (cm^{-1})	Refractive index	Anisotropy factor
Sun et al. [98]	36.61	13.45	1.37	0.79
Ash et al. [99, 100]	-	-	1.7	0.789

2.7 Protection from sun damage

Hair, like skin, can also be damaged by the UV rays. For example, prolonged sun exposure can cause hair to develop split ends, brittleness, dryness and colour fading through photoaging and photodegradation processes [101-103]. The influence of sun exposure on the appearance of scalp hair has drawn more attention recently. Several sunscreens that can be used for hair (both body and scalp hair) are available in the market [103-107]. Unlike skin, the human hair shaft is nonliving and carcinogenesis within the hair is not possible. If human hair is damaged by sun exposure, it will be replaced by new grown hair in the next hair cycle. Therefore, lack of UV protection for hair does not seem life-threatening. However, if hair shafts act like UV transmitting media and have the potential to cause damage to the hair follicle and skin, resulting in skin cancers, developing sunscreens that provide effective photo-protection for the skin and the hair becomes essential; and the effectiveness of current sunscreens on hair becomes worth investigating.

2.8 Chapter summary

The optical properties of human hair have most commonly been studied using the optical spectral measurements based on an optical microscope. Those studies have shown that the optical properties of human hair depend strongly on the type and concentration of melanin contained in the hair shafts, the site of the hair, the presence of the medulla and the wavelength being measured. It is well accepted that eumelanin-dominated dark hair has higher absorption and scattering coefficients than pheomelanin-dominated light hair. The optical properties (absorption coefficient, reduced scattering coefficient, and attenuation coefficient) of hair increase with a decrease in wavelength, meaning fewer photons at shorter wavelengths are transmitted through hair. This phenomenon is much more pronounced for dark hair. Therefore, based on the unique morphologies of vellus hair (absence of medulla and little or no melanin present), it is inferred that UV radiation would penetrate deeper in lightly or non-pigmented vellus hair than highly pigmented terminal hair. However, the studies in the literature have focused only on examining the optical properties of human scalp hair (terminal hair) in the visible and infrared range of wavelength; so current knowledge of the optical properties of hair cannot provide enough evidence to support our hypothesis. Therefore, the UV optical properties of vellus hair

need to be explored; whether vellus hair transmits more UV light than terminal hair is yet to be answered.

Since preparing hair samples for the measurement in their transverse direction is relatively easy, the knowledge of the optical properties of hair from the literature are primarily limited to its transverse direction. The properties in the longitudinal direction of hair shafts need to be investigated further, which will require proper hair sample preparation, precise instrumentation and statistical analysis of the results. In addition, the cortex of hair has been found to have a much lower attenuation coefficient than the medulla, which is a strongly scattering structure in the centre of the hair shaft, implying that the light is primarily propagated in the cortex. It is possible that UV penetrates through the cuticle of vellus hair from all directions and travels in the cortex of the hair shafts deeper into the follicle region. Some of the transmitted light is then scattered to the stem cells, possibly causing damage to these cells. The cumulatively damaged stem cells have the potential to become melanocytes and melanomas in later life. If this hypothesis is proved to be true, it may reveal why children are more vulnerable to sun exposure, and the consequent increased melanoma incidence seen in adults who have experienced excessive sun exposure or sunburn in their childhood. It would also explain the positive correlation between the incidence of melanoma in the areas of adults' bodies and the number of vellus hair follicles in these areas.

Children younger than 10 have a noticeable proportion of 'vellus-like' scalp hair and their terminal hairs on the scalp are generally finer than those of adults [49, 50]. Therefore, children's scalp hair could be studied more conveniently by researchers than fine and short bodily vellus hair. The wide variations of the optical properties of hair indicate that statistically significant measurements of hair properties need to be achieved for reliable comparisons.

As human skin is exposed to the sunlight, the energy may not only penetrate through the skin but also hair. Examining and comparing the radiant energy in the bulge regions of hair follicles using the Monte Carlo photon simulation could provide evidence to support the hypothesis. It will also allow us to visualize the contribution of hair, as an energy conduit, in the energy transfer process. The outcome of this research may contribute to the prevention of melanoma.

2.9 Research objectives and methodology

It is hypothesized that the McSCs in vellus hair follicles can receive relatively higher dose of UV than those in the terminal hair follicles. This may be the result of the differences between child and adult skin, and vellus and terminal hairs. To validate the hypothesis, the objectives and methodology are described as follows:

1) To determine the influence of the differences between the child and adult skin on the UV dose absorbed by McSCs (Ignoring the influence of hair)

The vulnerability of children to sun exposure could be due to the differences in child and adult skin alone. Therefore, in Chapter 3, MC simulations will be used to investigate the differences in the UV absorption in the stem cells in child and adult skin, based on the current knowledge of the optical properties of human skin. Two main differences between child and adult skin will be considered: the skin layer thicknesses and the depth of the McSCs.

2) To determine the difference in the UV absorbed by McSCs in the bulge region between vellus and terminal hair follicles, considering the differences between hairs

To achieve that, the MC simulations will be carried out in skin models with vellus and terminal hairs. This will require the optical properties of vellus and terminal hairs. The optical properties of human hair in the UV wavelength range are essential in validating the hypothesis, and these are missing in the literature. Therefore, the first step to achieve this objective is to measure the transmittance spectra of hairs in the UV wavelength range (Chapter 4). The hair samples used in this research will mainly comprise of scalp hair because it is easier to acquire than fine body hair. A CRAIC^{TM} Microspectrophotometer will be used to investigate the optical properties of hair in the UV wavelength range. Although the optical properties of hair in the longitudinal direction could be different to that in the transverse direction, this research will focus on the measurement in the transverse direction of hair due to the difficulties and disadvantages encountered when preparing samples (as discussed in Section 2.5.1).

The transmittance spectra of hairs will further be converted into the attenuation coefficients, which will be implemented in the simulations. Finally, in Chapter 5, two realistic skin models, one having vellus hairs and the other one having terminal hairs, will be used to determine the difference in the UV dose received by McSCs using the MC simulation.

Chapter 3 Solar UV transmission in child and adult skin

3.1 Introduction

Although different morphologies of vellus and terminal hairs could result in their different UV transmission properties, skin still remains as a major pathway for UV transmission. This chapter considers the influences of the differences between child and adult skin in the transmission of UVR.

Children typically have thinner skin layers than adults [31, 32], which will allow more UV photons to transmit into the deeper skin layers. In addition, the McSCs in VHF are much shallower in the dermis than those in the THF [33]. Therefore, the McSCs in children's skin could be subjected to higher doses of UVR from transmission through the skin alone. To quantify the solar UV dose absorbed by the follicular stem cells (which could be an indication of their relative risks of developing melanoma), we used the MC method for photon transport. The MC method of modelling light transport in skin layers has been implemented in several investigations [108-110]. However, it is noticed that in these studies, the thickness of the skin layers and some of their optical properties are often assumed. In addition, the solar UV transport in the human skin is rarely studied. In this part of the research, we have applied the UV optical properties and typical thicknesses of skin layers for Caucasian children and adults in a MC model [31, 32, 111]. The objective of this part of the research is to quantify the radiant power absorbed by the entire horizontal skin layer where the stem cells reside in child and adult skin from the solar UVR. A series of simulations were conducted to obtain the results over the effective UV wavelength range (290 – 400 nm). Since the focus of this chapter is to investigate the differences of child and adult skin on its own with respect to UV absorption in the stem cells, the hair shafts were excluded in the MC model. A more realistic skin model with hair shafts, will be set up for simulation in Chapter 5, after the optical properties of hair are determined in Chapter 4.

3.2 Materials and methods

3.2.1 Monte Carlo method for light transport in skin

When UV rays reach the skin, a small fraction of the incident radiation is reflected from the surface of the skin to the air [44]. The rest of the light is refracted beneath the skin

surface. As the photons propagate in the skin, they will be either absorbed by tissue cells or scattered to the surrounding skin cells. These two processes together determine the energy distribution within the tissue. Due to the nature of the MC method, intense computation of photon transport is required to accurately simulate reality, which made it time-consuming initially. This drawback has been improved significantly in the past decades using a variety of techniques [68].

In this work, we employ the GPU-based Monte Carlo eXtreme (MCX) to achieve a much faster acceleration in the computation time than conventional CPU based Monte Carlo algorithms [112]. The tissue is considered to be made of voxels with assigned optical properties. Statistically significant numbers of photons are launched into the tissue in a sequential order. Each photon with an initial pack weight of 1 repeatedly experiences scattering and absorption until it exits the domain or its remaining weight is insignificant [112]. The scattering length x, is calculated based on the probability distribution of the photon free path length and the scattering coefficient of the tissue [63, 113]. The probability distribution for the cosine of the deflection angle, $P(cos\theta)$ is expressed by the Henyey-Greenstein phase function [63], as shown in Eq. (3-1), where g is the anisotropy factor.

$$P(cos\theta) = \frac{1 - g^2}{4\pi(1 + g^2 - 2gcos\theta)^{\frac{3}{2}}} \qquad 3\text{-}1$$

A proportion of the photon's weighting is subtracted from it and added to the voxel according to the absorption probability at the end of each scattering event. When the photon pack hits a boundary layer, it will either transmit through or be reflected from the boundary according to Snell's law and Fresnel's equation. The accuracy of MCX has been validated with the analytical method from the diffusion theory [112].

3.2.2 Physical model of skin in MC simulation

Human skin is a complex heterogeneous medium. The first two upper layers of skin are the epidermis and dermis. The epidermis consists of the stratum corneum and the cellular epidermis. Since the stem cells are housed in the bulge region of the hair follicle in the dermis, we model the skin as a three-layer tissue, which includes the stratum corneum, epidermis and dermis, as shown in Fig. 3-1.

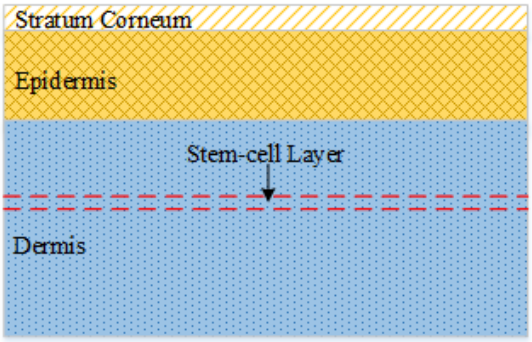

Figure 3-1: Schematic diagram of a three-layered skin model built in MCX. The stem cell layer refers to the layer of skin at the depth of follicular stem cells.

Although the epidermis can be further stratified, current knowledge of the optical properties is limited to stratum corneum and epidermis (bulk quantity). The stratum corneum is treated separately from the rest of the epidermis because its optical properties have been reported to differ considerably to the overall epidermis [44, 111, 114]. Each tissue layer is modelled to be flat with uniform optical properties.

The thickness of skin increases gradually from birth to adulthood [115] and noticeable differences between the thickness of skin before and after puberty has been observed [116]. In terms of UV protection, the thicknesses of the stratum corneum and epidermis are considered important in reducing the amount of UV reaching deeper into the skin [117]. In Caucasians, the thickness of both the stratum corneum and cellular epidermis have been found to be greater in young adults (after puberty) than children [31, 32].

The thickness of the bulge region in the vellus and terminal hair are approximately 90 and 240 μm, respectively [33]. We define the skin layer that houses the McSCs as the stem cell layer (Fig. 3-1). This layer has depths of 360 and 1200 μm (measured from the center of the layer to the skin surface). Table 3-1 presents typical thicknesses of the stratum corneum, cellular epidermis, bulge region and the depth of the bulge region in the child and adult skin.

Table 3-1: Summary of typical thicknesses of the stratum corneum [31], epidermis [31, 32] and dermis in child and adult skin, and the thicknesses and the depths of the bulge regions in vellus and terminal hair follicles [33].

Skin layer	Stratum corneum		Cellular epidermis		Bulge region		Bulge depth	
Classification	Child	Adult	Child	Adult	Vellus	Terminal	Vellus	Terminal
Thickness (**μm**)	28.8	35.4	62.0	77.0	90	240	360	1200

3.2.3 UV optical properties of human skin

In contrast to the differences reported in the anatomy of child and adult skin, there is very little knowledge about the optical properties of child skin. The primary skin types found in Caucasians' skin are skin type I and II [52]. According to the Fitzpatrick scale, skin type I and II always burn easily and never (or only minimally) tan. In addition, the increase in melanin content in Caucasians' skin after days of UV irradiation is negligible [118]. Therefore, the melanin fraction (the primary UV filter in the epidermis) is considered to be the same in Caucasian child and adult skin. Furthermore, the difference in the UV sensitivity of child and adult's skin from the aspects of UV induced skin reactions and anatomic structures has not been identified as significant [22, 23]. In this study, the optical properties of Caucasian child and adult skin are assumed to be the same.

The UV properties of the stratum corneum, epidermis and dermis are reviewed in the following paragraphs prior to the simulation of UV transport in the skin. For the optical properties represented graphically in the literature, a series of data points was determined by using graphic scaling tools. The least-squares technique was then applied to find a set of equations that best describe the optical properties relative to wavelength. These equations were then coded in Matlab for the MC simulation.

The stratum corneum has an approximate anisotropy factor value of 0.9 in the UV region, indicating its highly forward scattering characteristics [114]. Due to the lack of the knowledge of refractive index of human stratum corneum in the UV range, it is assumed to be constant at 1.55 [44]. The absorption coefficient of the stratum corneum increases relatively rapidly with a decrease in the wavelength [111]. There is a gradual increase in its scattering coefficient as the wavelength decreases [111]. The absorption and scattering coefficients are estimated by Eqs. (3-2) and (3-3). The units of μ_a and μ_s are mm^{-1} and wavelength λ has a unit of nm.

$$\mu_{a,stratum} = 16 + \frac{1063}{\lambda - 269.8} \qquad 3\text{-}2$$

$$\mu_{s,stratum} = 186.8 + \frac{5.679 \times 10^6}{\lambda^2} \qquad 3\text{-}3$$

The scattering coefficients of the human epidermis and dermis are similar in value and both increase with a decrease in wavelength at a similar rate in the UV-visible spectral

range [61, 111]. Using the data from Van Gemert et al. [111], the absorption and scattering coefficients of epidermis and dermis are expressed in Eqs. (3-4) – (3-6).

$$\mu_{a,epidermis} = -1.125 + \frac{1011}{\lambda - 265.8} \quad \textit{3-4}$$

$$\mu_{a,dermis} = 10.94 - \frac{8201}{\lambda} + \frac{1.673 \times 10^6}{\lambda^2} \quad \textit{3-5}$$

$$\mu_{s,epidermis} = \mu_{s,dermis} = 600.26\, exp(-0.005\lambda) \quad \textit{3-6}$$

Bruls and van der Leun found that the anisotropy factor of the epidermis varies linearly with wavelength in the range of 302 – 546 nm [114]. The value of this factor for the dermis at 633 nm from Jacques et al. [119] fits well to the extrapolated epidermal g factor from Bruls and van der Leun. As a result, the anisotropy factor of the epidermis and dermis are considered to be close and follow the same wavelength dependency as expressed in Eq. (3-7) [111]. In the UV wavelength range, the anisotropy factors of the epidermis and dermis vary from about 0.7 to 0.74, indicating their strongly forward scattering characteristics.

$$g_{epidermis} \approx g_{dermis} = 0.62 + 2.9 \times 10^{-4}\lambda \quad \textit{3-7}$$

According to a study of the refractive index of human skin in the wavelength range between 300 – 1600 nm [120], the values of the epidermis and dermis are steady in longer wavelength ($\lambda > 400\ nm$) but rise gradually in the UV region. These relations can be described in Eqs. (3-8) and (3-9) [120]. The coefficients of the equation for the epidermis are not presented in the publication, so they were estimated using the curve fitting technique to the published graph. Figure 3-2 is plotted using Eqs. (3-2) – (3-9). It illustrates the relationship between the optical properties of Caucasian's skin layers and wavelength in the UV range of 280 – 400 nm.

$$n_{epidermis} = 1.395 + \frac{26.57}{\lambda} + \frac{0.2203}{\lambda^{3.5}} \quad \textit{3-8}$$

$$n_{dermis} = 1.3696 + \frac{3916.8}{\lambda^2} + \frac{2558.8}{\lambda^4} \quad \textit{3-9}$$

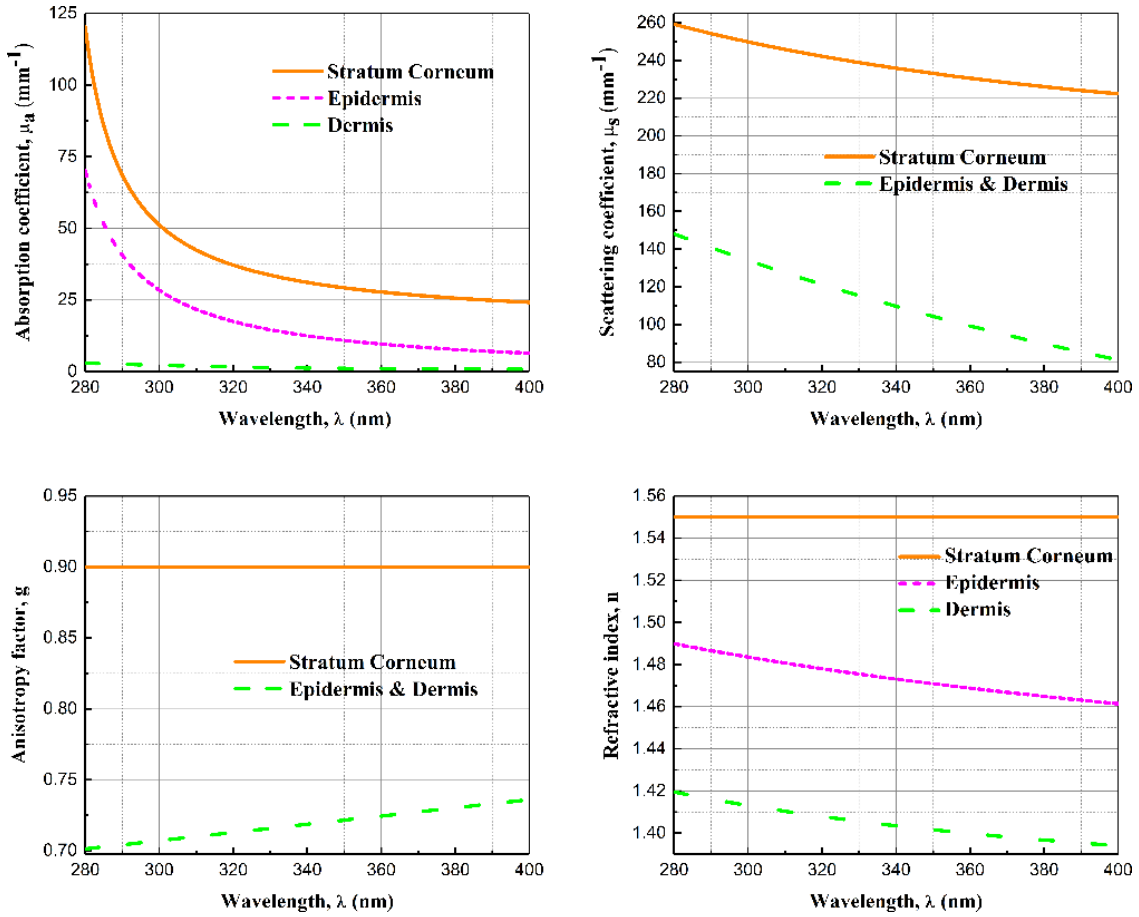

Figure 3-2: Optical properties of Caucasians' skin layers for the ultraviolet wavelength range of 280 – 400 nm. Graphs are generated using Eqs. (3-2) – (3-9), where the data is obtained from various published experimental results. (a) and (b) The absorption and scattering coefficients of stratum corneum, epidermis and dermis are derived from the data reported graphically by Van Gemert et al. [111]. (c) The anisotropy factor of stratum corneum, epidermis and dermis are obtained from the data and equation reported by Bruls et al. [114]. (d) The refractive index of stratum corneum is acquired from Anderson's publication [44]; the refractive indices of epidermis and dermis are obtained from the data and equation in Ding's publication [120].

3.2.4 Simulation and data processing techniques

The skin model is constructed as a three-dimensional block in Matlab, which consists of 400 x 400 x 750 cubical voxels in the x-y-z directions respectively. Each voxel has a size dimension of 2 μm. A uniform beam with a diameter of 800 μm illuminates the top surface of the skin model with a direction normal to the surface. The thickness of each skin layer is constructed according to Table 3-1.

In our simulation, we employ the solar spectrum measured in a clear day in January at noon in Melbourne, Australia [15], as shown in Fig. 3-3. This would provide as the worst case scenario. For better visualization in terms of the units, we convert the solar irradiance, *E* into the number of photons by applying Planck's equation, as expressed in Eq. (3-10),

where E_p is the energy of a photon at a wavelength λ , h is the Planck constant, and c is the speed of light in vacuum. The number of photons, N_P launched from the sun per second reaching Melbourne at any wavelength is then equal to E/E_P. The number of photons absorbed in the stem-cell layer from the sun is then the product of N_P and the absorption in that layer. The UV solar spectrum reaching the earth's surface is comprised of UVB ($\lambda = 290 - 315$ nm) and UVA ($\lambda = 315 - 400$ nm). Both UVB and UVA can initiate melanoma [16], therefore the multiple MC simulations are run in the skin model comprising the entire solar UV spectrum ($\lambda = 290 - 400$ nm) in 1 nm steps. Each run corresponds to the optical properties of skin layers given at each wavelength (Fig. 3-2). Each simulation is executed with 10^8 photon packs for calculating the absorption fraction in each voxel.

$$E_p(\lambda) = \frac{hc}{\lambda} \qquad 3\text{-}10$$

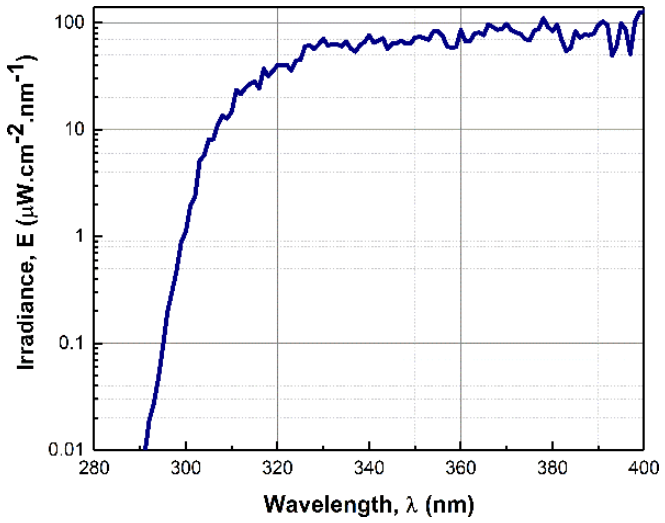

Figure 3-3: Solar spectrum measured in a clear day in January at noon in Melbourne, Australia. The graph is generated using the tabulated data reported by Diffey [15]. The irradiance of the UV below 290 nm was effectively zero. The solar spectrum has an irradiance of 211.6 $\mu W \cdot cm^{-2}$ in UVB and 6026.6 $\mu W \cdot cm^{-2}$ in UVA.

3.3 Results and discussion

The simulated results were obtained using the solar irradiance ($\mu W/cm^2$) for an uniform beam with a diameter of 800 µm. When larger skin areas are exposed to the sun (higher solar UV power), the power absorbed in the stem-cell layer will simply be the product of the absorption fraction, solar irradiance and exposure area. The results can be converted into energy by multiplying by the exposure duration. 10^8 of photons have been used in each MC simulation to obtain the results. During simulations, it has been noticed that this quantity of photons is sufficient to achieve the desired accuracy.

Figure 3-4 illustrates the absorbed power map of the central slice in the child and adult skin models. A wavelength of 350 nm is selected for demonstration. Since the same optical properties of human skin layers have been assumed in both models, the maps show similar patterns. In Caucasian skin, the stratum corneum is identified to be the main site of UV filtration [121]. This can be observed from the high-power absorption in the stratum corneum layer in Fig. 3-4. In addition, the cellular epidermis, which contains melanins, provides another shielding layer from UVR reaching deeper cells. These results demonstrate that the epidermis is responsible for the majority of UV absorption. To be more specific, 96% and 97% of photons at 350 nm are absorbed by the epidermis in the child and adult skin respectively. These percentages vary from approximately 93% to 99% from 400 nm to 290 nm for both child and adult skin.

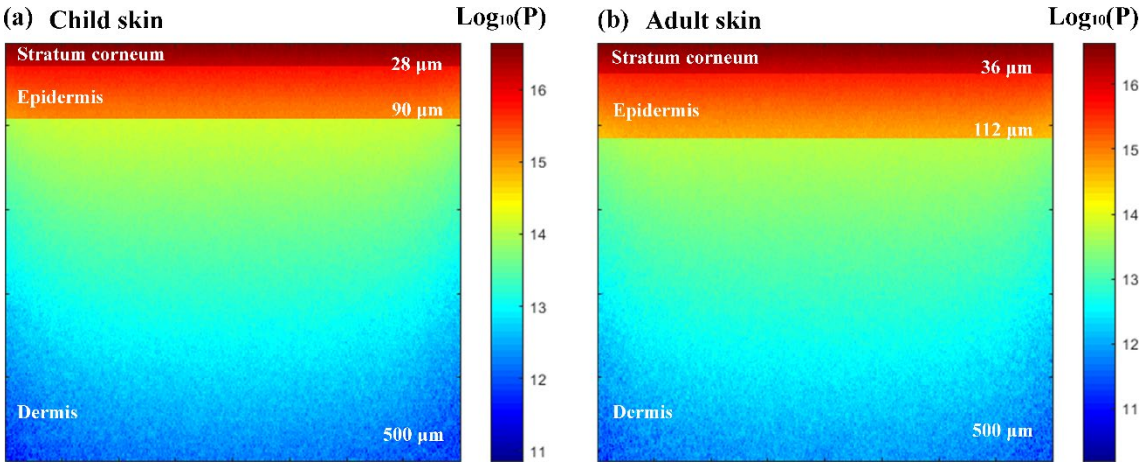

Figure 3-4: Power absorption graphs at 350 nm. (a) and (b) represent the power (P) maps of the central slice (x:1~400, y=200, z:1~250 voxels) of the child and adult skin models respectively, in terms of the number of absorbed photons per cm^3 per second. The depths of the boundaries for each layer are included in the figure.

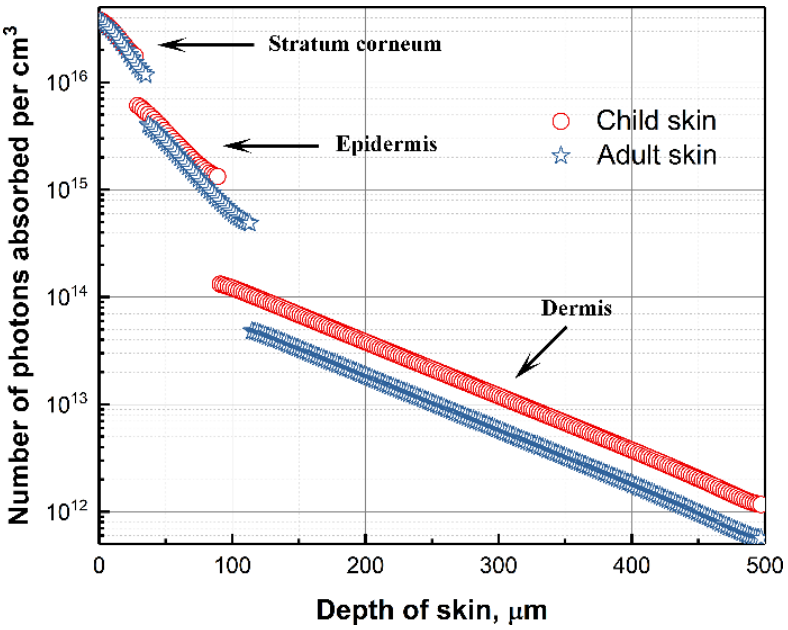

Figure 3-5: Power attenuation along the depth of the child and adult and skin models at 350 nm, in terms of the number of photons absorbed in each voxel layer per second. Each voxel layer has a thickness of 2 μm. The power absorbed by the voxel layer declines almost linearly along the depth of the skin in a logarithmic scale. Due to different optical properties of each skin layer, the absorbed power shows discontinuities at the boundary layers. The result is shown for a skin thickness of 500 μm, corresponding to Fig. 3-4.

The adult epidermis absorbs slightly more UV power due to its greater thickness. For the same reason, approximately double the UV photons at 350 nm is transmitted through the dermis in child skin relative to adult skin, as shown in Fig. 3-5. Figure 3-5 presents an indication of the number of photons absorbed along the depth of the skin. The absorption attenuation trend is observed as discontinuous at the boundary layers because of the distinct optical properties of the stratum corneum, epidermis and dermis.

Next, we look at the UV power (in terms of the number of photons per second) absorbed in VHF and THF stem cell layer in child and adult skin. Figure 3-6 shows these results for the UV wavelength range. The radiant power absorbed by the stem cell layer from the solar UVR is the product of the absorption fraction in that layer and the solar spectral irradiance, where the absorption fraction is determined by the optical properties of the skin. The absorption and scattering coefficients of the skin layers all increase as the wavelength decreases. This increase is more dramatic in the UVB range (Fig. 3-2). On the other hand, the solar irradiance in the UVA band is about 28 times greater than that of UVB band (Fig. 3-3). These two contributing factors lead to the computed power-wavelength profile in the stem-cell layer (Fig. 3-6).

It is important to note that not all the photons absorbed in the stem cell layers have effects on the stem cells in the bulge regions. Some of the photons are likely to be absorbed by the dermis without any influence on the stem cells. Nevertheless, the results indicate the relative dose of UVR absorbed in the follicular stem cells from sun exposure and their relative risks of developing into melanoma.

In both child and adult skin, the power absorbed by the VHF stem cell layer (Fig. 3-6 (a)) is greater than that of THF stem cell layer (Fig. 3-6 (b)). This is attributed to the fact that the stem cells are situated at about 3 times shallower in the VHF than the THF. Although, it is noticed that the power from the UVB band absorbed in the stem-cell layer has a relatively insignificant magnitude as compared to UVA, the effect of UVB on the stem cells cannot be simply neglected. This is because the higher energy of the UVB photons is more effective than UVA in initiating melanoma by causing direct DNA damage [18]. On the other hand, the relatively more penetrative UVA is also considered important since it is associated with melanoma in an indirect manner, as discussed in Chapter 1 [21].

While the role of UVA and UVB and their significances in melanoma development are still debatable [16], we present the ratio of the UV absorption in the stem-cell layers in these categories as a reference for future research (Table. 3-2 & 3-3).

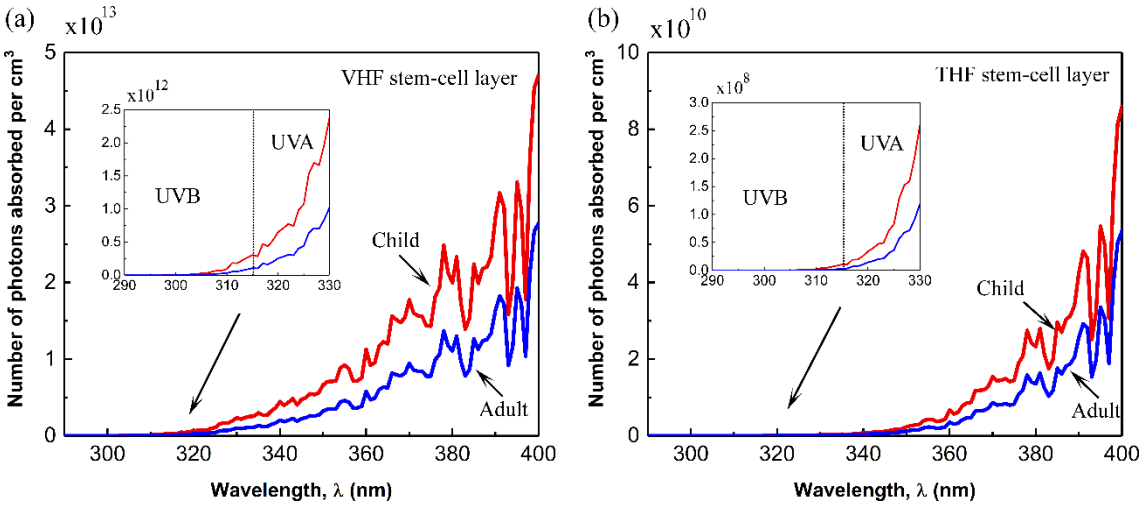

Figure 3-6: The number of photons absorbed per second from the sun in the stem-cell layers as a function of wavelength in the child and adult skin models. Power absorbed in the (a) VHF stem-cell layer and (b) THF stem-cell layer in both child and adult skin models. UVA ranges from 315 to 400 nm. UVB ranges from 290 to 315 nm.

Table 3-2: Ratio of the UV absorption in the skin at the depths of the VHF and THF stem-cell layer

	Child skin (VHF/THF)	Adult skin (VHF/THF)
UVA	255	252
UVB	11000	14000

Table 3-3: Ratio of the UV absorption in the skin at the stem-cell layer between child and adult skin

	VHF (child/adult)	THF (child/adult)
UVA	1.9	1.8
UVB	3.2	4.1

Table 3-2 shows the ratio of the UV power absorbed by the skin at the depth of the VHF and THF stem-cell layers from solar UVR in both child and adult skin. The power absorbed in the VHF stem-cell layer is dramatically greater than that in the THF stem-cell layer in both types of skin in the entire UV wavelength range. This suggests that the shallower stem cells in the bulge of the VHF are much more likely to be involved in melanomagenesis from the UV exposure. Since the most common type of body hair in children before puberty is vellus hair, our simulated results may help to explain why there is an increased risk of melanoma in individuals who have experienced excessive sun exposure during their childhood [10].

Considering the typical thicknesses of child and adult skin, the UVA and UVB power absorbed in the VHF stem-cell layer of child skin are found to be respectively about 1.9 and 3.2 times larger than in adult skin (Table 3-3). While a proportion of vellus hair still remains in adulthood, we extrapolate that their stem cells continuously receive sufficient solar UV photons for melanoma activation, although the amount has reduced due to the thickened epidermis. This may explain the positive correlation between the incidence of melanoma in adults' bodies and the number of vellus hair follicles in these areas [27].

The optical properties of child and adult skin are treated the same in the simulation due to the lack of knowledge of child skin. As more knowledge about the blood volume fraction, the arterio-venous oxygen saturation of hemaglobin in the blood, the average water content and pigment content for child and adult skin become available in the literature, the difference in the optical properties of skin can be integrated in the simulation for more accurate comparison [53].

The solar UV power absorbed in the stem-cell layers may appear insignificant (with a reference to Fig. 3-6), especially when compared to the radiant power absorbed in the

epidermis's basal layer, which is commonly believed to be the original site of melanoma initiation [11]. Nevertheless, this does not affect our hypothesis due to the two proven findings in the literature: 1) the stem cells in the bulge region of hair follicles can develop into melanoma via melanocyte-stem-cell activation and translocation after exposure to UVR [25]; 2) skin regions with higher numbers of vellus hair follicles are associated with higher melanoma incidences [27]. Furthermore, melanocyte stem cells could be more sensitive to UV exposure than the mature melanocytes in the epidermis's basal layer.

3.4 Chapter summary

In this chapter, we have applied the Monte Carlo photon simulation to quantify the dose of solar UV power absorbed in the stem cell layer of Caucasian child and adult skin, when exposed to the sun in a clear summer day at noon in Melbourne. The stem cells in the VHF have been found to absorb significantly more UVR than those in the THF due to their shallower residences. As a consequence of the thinner epidermis, the VHF stem cell layer in child skin absorbs about 1.9 and 3.2 times greater UVA and UVB respectively, than that in adult skin.

Our simulated results suggest that children having a much higher proportion of vellus hair as compared to adults, are at significantly higher risk in later life of developing melanoma by exposing their shallower follicular stem cells to solar radiation. Their relatively thinner epidermis further increases this risk.

Furthermore, the distinct morphologies of vellus hair and terminal hair have also directed us to consider whether vellus hairs contribute to transmitting additional UVR to the stem cells in their bulge regions. The significance of vellus hair in transmitting UV photons will be introduced in the following chapters, as we seek the reasons for the extreme vulnerability of children to sun exposure and the increased risk of melanoma seen in the adults who experienced excessive sun exposure in their childhood.

Chapter 4 Measurement of UV transmission property of human hair

4.1 Introduction

As discussed previously, recent studies have shown that the melanocyte stem cells in the bulge region of hair follicles could also be the origin of melanoma upon exposure to UV [25, 26, 122]. As shown in the previous chapter, the shallower location of the melanocyte stem cells in vellus hair has been considered as one of the reasons for the vulnerability of children to sun exposure, regarding melanoma [123]. Furthermore vellus hairs, with their unique morphology, are thought to contribute to the passage of harmful UV photons to the McSCs, which can experience the activation and translocation processes [25], ultimately resulting in melanoma. To determine whether the vellus hair shaft exhibits greater UV transmission characteristics when compared to the terminal hair and skin is a major purpose of this chapter [124].

The optical properties of human hair have been investigated by several groups [74-79, 125], as discussed previously. However, the hair examined was primarily adult terminal hair, and children's hair or vellus hair were not included. Among these studies, the attenuation coefficient of hair is the most commonly reported optical property because it can be estimated conveniently from the collimated transmission measurement [75, 77, 79]. Given the ability to focus incident light precisely onto hair using an optical microscope, the absorbance spectra or transmission properties of hair samples at single wavelengths or a band of wavelengths have been studied [74, 76-78]. However, the optical properties of human hair in the UV wavelength range have not been reported in the literature.

Therefore, to study the optical properties of human hairs in the UV wavelength range, a CRAIC 20/30 PV^{TM} Microspectrophotometer in Soochow University (Fig. 4-1) was used to measure their transmittance spectra. The CRAIC Microspectrophotometer is a powerful device that combines the advantages of a microscope and a spectrometer, providing measurement of the UV-visible-NIR range of transmission for sampling areas as small as 6 μm x 6 μm. The transmittance spectra of hair samples were then used to estimate their attenuation coefficients using Beer's law.

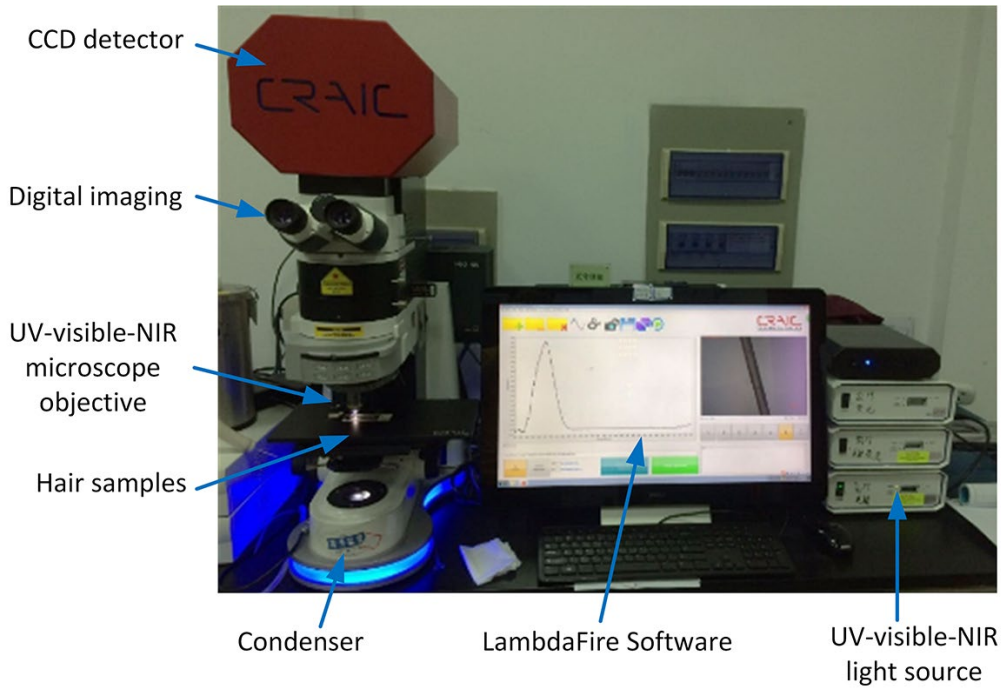

Figure 4-1: Physical photo of CRAIC Microspectrophotometer

A positive correlation exists between the incidence of melanoma in adults' bodies and the number of vellus hairs in these areas [27]. However, this trend was not observed for terminal hair. Therefore, one of the focuses of this study is to compare the attenuation coefficient of the cortex of vellus and terminal hair in the UVA and UVB wavelength ranges. Moreover, the attenuation coefficients of the medulla in terminal hair in the UV wavelength range are also of interest in revealing the overall optical properties of terminal hair.

Measuring the optical properties of short and fine body hair is, however, technically difficult. Most of the scalp hair is terminal hair. Fine vellus hair can be found in bald scalps. Nevertheless, it is found that children younger than age of 10 have a noticeable proportion of "vellus-like" scalp hair, which is non-medullated and finer than that of adults [49, 50, 126]. Therefore, it is considered reasonable to use light blond scalp hair harvested mainly from children to represent vellus hair, from the perspective of hair morphology and optical properties (Figs. 4-6 and 4-9). In this research, we have collected blond and brown scalp hair samples from fair-skinned Caucasian children and adult participants (skin type I and II) [52], who are the most vulnerable group of humans to sun exposure.

4.2 Materials and methods

4.2.1 Hair samples

The hair samples were harvested from the scalps of 16 fair-skinned Caucasian participants from three different families, whose skins are identified as skin types I and II. They are made up of 10 adults (5 males and 5 females with an age range from 22 to 45) and 6 children (3 boys and 3 girls with an age range from 1 to 7). Five to ten samples from each participant were collected for the statistical analysis. The hair samples used in this study are of natural colours and with no history of chemical treatment. For easier implementation, the majority of hair samples are collected from the scalp. The arm hair samples were also collected from one female blond-haired adult for comparing their optical properties with scalp hair. After taking the measurements (photomicrographs and transmittance spectra), the samples are classified into four categories based on their colours. Table 4-1 presents the statistics for the hair samples used in this study. The group of medullated hair includes the hair samples with the presence of medulla, regardless of their colours. The reason will be explained in Section 4.3.2.

Table 4-1: Statistical information of the hair samples.

	Light blond	Dark blond	Light brown	Dark brown	Medullated hair
Number of samples (adult/children)	Total 18 5/13	Total 31 23/8	Total 20 16/4	Total 17 16/1	Total 20 11/9
Number of individuals	8	11	9	6	9
Number of males/females	3/5	5/6	5/4	4/2	6/3

4.2.2 Instrument and methodology

A CRAIC 20/30 PV^{TM} Microscpectrophotometer was used to measure the transmittance spectra of hair samples with UV-VIS-NIR light with wavelength in the range of 200 to 900 nm. Fig. 4-2 (a) illustrates the schematic diagram of the instrument, comprising the essential components. The CRAIC Microspectrophotometer is provided with the CRAIC LambdaFire^{TM} Software, which is used to control the measurement and process the data. In the software, the number of scans to be averaged and the resolution factor were set to 40 and 5 nm respectively to reduce the noise on the transmittance spectra. The transmittance spectra measured in the CRAIC Microspectrophotometer were used as the

collimated transmittance spectra for estimating the attenuation coefficients of the hairs, as shown in Fig. 4-2 (b).

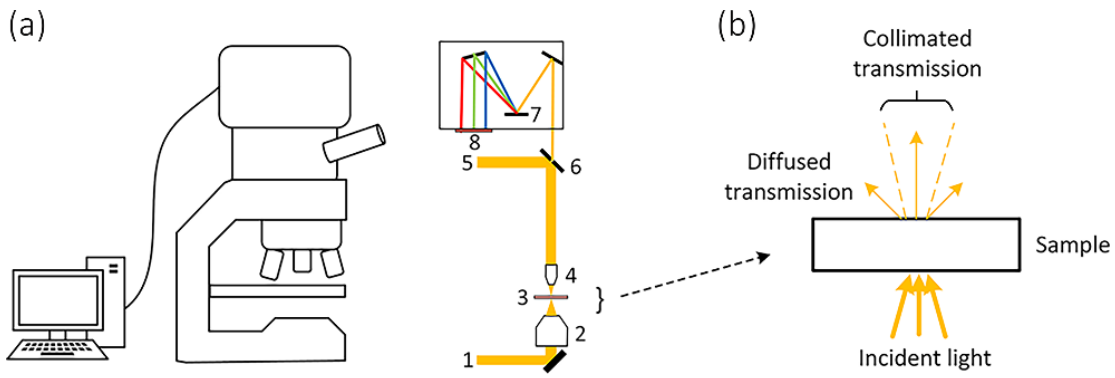

Figure 4-2: (a) Schematic diagram of a CRAIC micro-spectrophotometer. A CRAIC micro-spectrophotometer combines an optical microscope and a highly sensitive spectrophotometer. It includes eight major components: (1) UV-visible-NIR light source, (2) condenser, (3) sample, (4) UV-visible-NIR microscope objective, (5) high resolution digital imaging, (6) mirrored aperture, (7) holographic grating, (8) CCD detector. The overall magnification used in this measurement is 100X. (b) Schematic diagram of the optical principle applied in this study for estimating the attenuation coefficient of samples from the transmittance spectra.

Collimated transmission refers to the portion of transmitted photons which have not experienced scattering. This unscattered light is attenuated exponentially following Beer's law. Since human hair is sufficiently thin, there is minimal chance of multiple scattering. Therefore, the transmittance spectra of the hair samples measured in the microspectrophotometer are regarded as the result of collimated transmission for the purpose of estimating their attenuation coefficients.

4.2.3 Sample preparation and measurement procedures

To minimize the influence of contaminants (e.g. dirt and oil) on the results, all samples were washed with ethanol prior to the measurement. Glass is known to absorb a significant amount of UV, whereas quartz does not (see Fig. 4-3). Therefore, quartz slides and coverslips have been used to hold the hair samples in place. The quartz slides used in the measurement gave excellent UV transmission (about 90%) under the micro-spectrophotometer, which has delivered sufficient intensity of UV for accurate measurement of our samples.

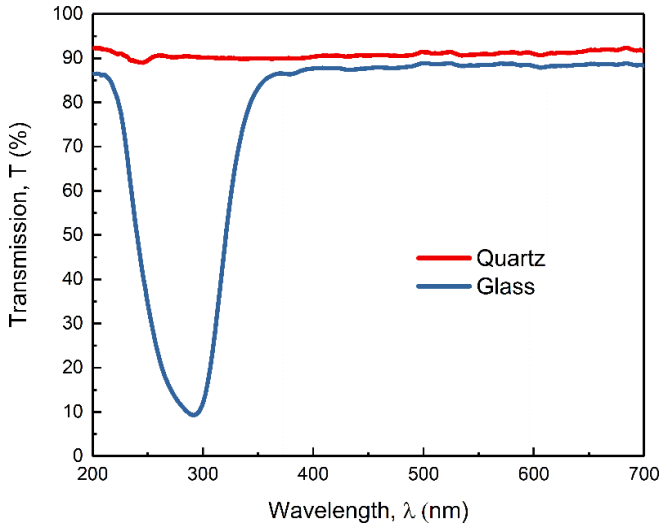

Figure 4-3:Transmission spectra of a quartz and glass slide in the wavelength range of 200 and 700 nm. Glass is shown to absorb significant amount of UV.

Several hair samples with suitable lengths from the same individual were first placed on a quartz microscope slide. This was followed by mounting the samples with glycerin and a quartz coverslip. After the samples have stabilized, the incident light was focused using the smallest aperture (about 6 µm x 6 µm) onto the centre of the width of the hair sample. Next, the aperture was moved off the sample before optimizing the sampling time. The sampling time was optimized to approximately 30 to 40 ms for each hair sample for the wavelength range of 200 to 900 nm. After that, a background and a reference scan were taken for subtraction in later measurements. Next, the aperture was moved to the centre of the width of the hair sample to take the measurement of the transmittance spectra. The formula used for calculating the transmittance spectra of a sample, *T*, is shown as Eq. (4-1), where I_s is the light intensity scan through the sample, I_b is the light intensity from the background when the light source is turned off and I_r is the light intensity scan of the reference when the sample is absent.

$$T(\lambda) = \frac{I_s - I_b}{I_r - I_b} \qquad 4\text{-}1$$

A preliminary analysis was carried out to select the most suitable mounting media. Figure 4-4 (e) shows the transmission spectra for a single light brown hair, using different mounting media. The red line is the result for the sample sandwiched between a quartz slide and coverslip without any mounting media. This method would show the attenuation effect of the hair, which includes the scattering on the surface. However, the drawback is that with the strong scattering from the surface of the hair sample; the internal structure

of hair becomes invisible under the micro-spectrophotometer, as shown in Fig. 4-4 (a). It is known that the medulla, if it exists in the hair shaft, exhibits dramatically different optical properties than the cortex [126]. Therefore, it is essential to know which internal structure the light spot is focused onto. To improve the visibility, we tested three different mounting media, Glycerin, Paratone and Ethyl cinnamate, with refractive indices of 1.47, 1.48 and 1.56 respectively, which are close to that of human hair (n=1.54) [80]. Using these three mounting media, the internal structures of the hair are clearly revealed under the micro-spectrophotometer, as shown in Fig. 4-4 (b-d). However, it has been observed that the transmission spectra of the hair sample mounted in Paratone and Ethyl cinnamate show a trough shift in the UV range. It is attributed to the fact that these two media absorb considerable amounts of UV, thus masking the hair transmission spectrum. In contrast, Glycerin did not show such a noticeable shift in the transmission spectrum. Its higher transmission spectrum (than the one without mounting media) is mainly due to the minimization of surface scattering. Therefore, glycerin was chosen as the most suitable mounting medium for the measurements, which agrees with other studies in the literature [74, 127].

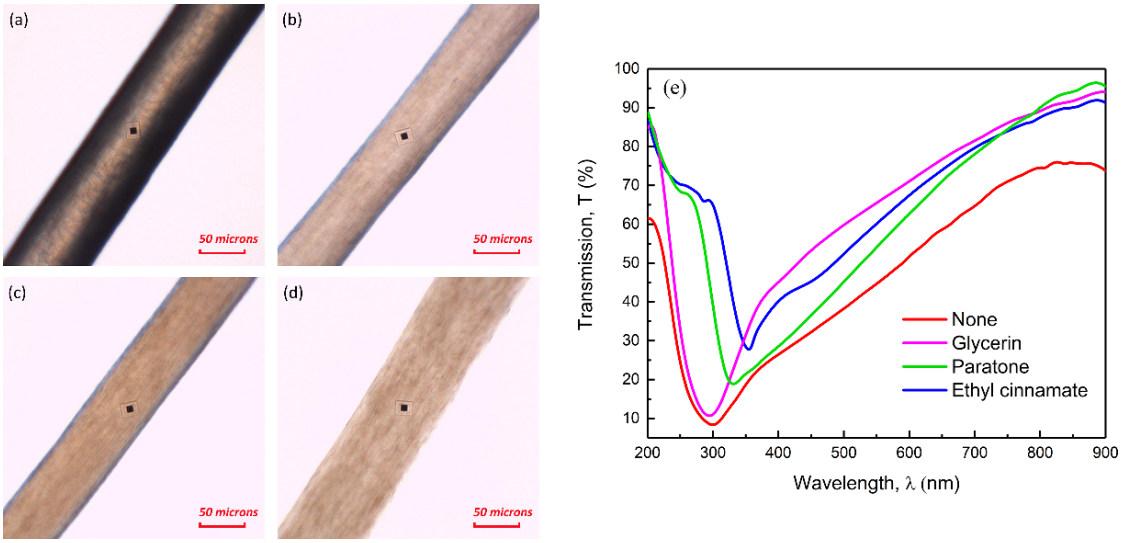

Figure 4-4: (a) – (d) Photomicrographs of a single light brown scalp hair mounted in different media and (e) their corresponding transmission spectra in the wavelength range of 200 to 900 nm. (a) No mounting medium is used. Strong scattering occurs on the surface of the hair, which results in invisibility of the internal structure. (b) Glycerin, (c) Paratone and (d) Ethyl cinnamate have refractive indices close to that of hair, which minimizes the light loss on the surface of hair. Thus, clear internal structures of hair are revealed. As can be seen from (e) paratone and ethyl cinnamate absorb significant amounts of UV. The transmission spectra of hair mounted in these two media have shown shifts in the UV wavelength range. No spectrum shift is observed in the hair sample with Glycerin.

When measuring the transmittance spectra of the medulla, the aperture was moved to the centre of the medulla. To account for any variance along a single hair shaft, five scans were randomly taken along the hair shaft for each sample, which were then averaged using the CRAIC LambdaFire^{TM} Software. The spectral data were transferred to an Excel spreadsheet for further processing. The diameters of the cortex and medulla were measured from the captured images by assuming that they are circular in cross-section.

4.2.4 Data processing

The refractive index of the cortical region of hair (cortex and medulla) is reported to be 1.56 [75], which is very close to that of the cuticle, which has a value of 1.54 [80], and the selected mounting medium. Therefore, the light attenuation is dominated by hair cells' absorption and scattering. The collimated or unscattered photons are attenuated exponentially in the medium following Beer's law, $T = e^{-\mu_t d}$, where μ_t, the attenuation coefficient is the sum of absorption μ_a and scattering coefficient μ_s and d is the diameter of the medium. Rearranging the equation, the attenuation coefficient of the sample can be calculated using Eq. (4-2).

$$\mu_t(\lambda) = -\frac{1}{d} ln\, T(\lambda)\, [mm^{-1}] \qquad 4\text{-}2$$

The diameters of human hairs are comparable with a mean free path of a photon in the media, which is $1/\mu_t$, which makes Beer's law a good estimation, as studied by several groups [75, 77, 79]. In the case that the objective lens collects scattered photons, contributing to the transmission spectra, the attenuation coefficients of samples would be slightly underestimated.

The non-medullated hair samples are used to determine the attenuation coefficient of the cortex and cuticle (Fig. 4-5, light path 1). The thin translucent cuticle appears invisible within the mounting medium (yielding minimal scattering), as shown in Fig. 4-6 and 4-7. Therefore, the attenuation effect of a non-medullated hair in this measurement can be attributed predominantly by the cortex because the absorption by the thin cuticle is considered to be significantly less than that of the cortex. As a result, the sum of the attenuation coefficient of the cuticle and cortex will be treated as the cortex only, for the purpose of simplicity.

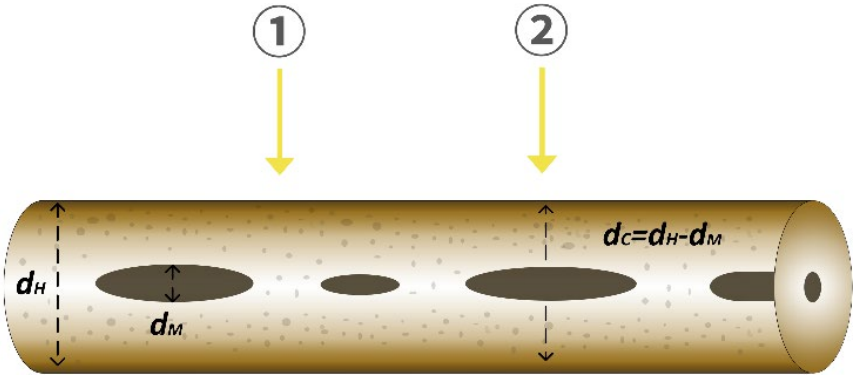

Figure 4-5: Schematic diagram of light illumination on a hair shaft at (1) non-medullated portion and (2) medullated portion. By measuring the transmittance spectra of non-medullated and medullated parts of a single hair, and the diameter of the cortex and medulla, the attenuation coefficient of medulla can be determined.

To quantify the attenuation coefficient of the medulla, the collimated transmission measurement has to be performed on the medullated hair through both the non-medullated and medullated portions, as illustrated in the Fig. 4-5 (light path 1 & 2). After obtaining the attenuation coefficient of the cortex, $\mu_{t,C}$ and the medullated part of hair, $\mu_{t,H}$, the attenuation coefficient of the medulla, $\mu_{t,M}$ can be estimated using Eq. (4-3), where d_H, d_C and d_M are the diameters of the hair, cortex and medulla respectively.

$$-\ln T(\lambda) = \mu_{t,H} d_H = \mu_{t,C} d_C + \mu_{t,M} d_M \qquad 4\text{-}3$$

4.2.5 Statistical analysis

The IBM SPSS Statistics Software is used to perform the statistical analysis. The Shapiro-Wilk test is used to identify the normality of the data [128]. One-way analysis of variance (ANOVA) is used to evaluate the statistical differences between the mean attenuation coefficient of the cortex of the light blond hair and the other three colours of hair. The Levene's test is used to examine the homogeneity of variances among the four categories of hairs [128]. If the assumption of the homogeneity of variances is tenable, the ANOVA and Tukey's test is performed to calculate the significance p-value between the categories. Otherwise, the Welch's test and Games-Howell's test are used for the case of violation of homogeneity of variances [129].

4.3 Results and discussion

4.3.1 Photomicrographs of the cortex and medulla

The type and quantity of melanin in the hair shaft are considered to be the most important factors in influencing its optical properties [126]. And since hair colour is predominantly determined by melanin content, the hair samples are classified into four categories based on the colour: light blond, dark blond, light brown and dark brown. Fig. 4-6 illustrates the typical microscopic images of these four types of non-medullated scalp terminal hair taken using the CRAIC Microspectrophotometer. The light blond hairs were mainly collected from child participants. It is known that blond and brown hairs have predominant proportions of pheomelanin (yellow-reddish colour) and eumelanin (black-brown colour) [43]. It is the ratio of pheomelanin and eumelanin that gives the hair its final colour. The following results were analysed in these four categories. It is noticed that the light blond scalp hairs have little pheomelanin and almost no eumelanin, and it is the closest group to vellus hair in terms of hair morphology.

The medulla, which is only present in terminal hair, exhibits strong light scattering characteristics [126]. As a result, it appears black in the photomicrographs shown in Fig. 4-7. It is speculated that the scattering effect of medulla remains high in the UV wavelength range.

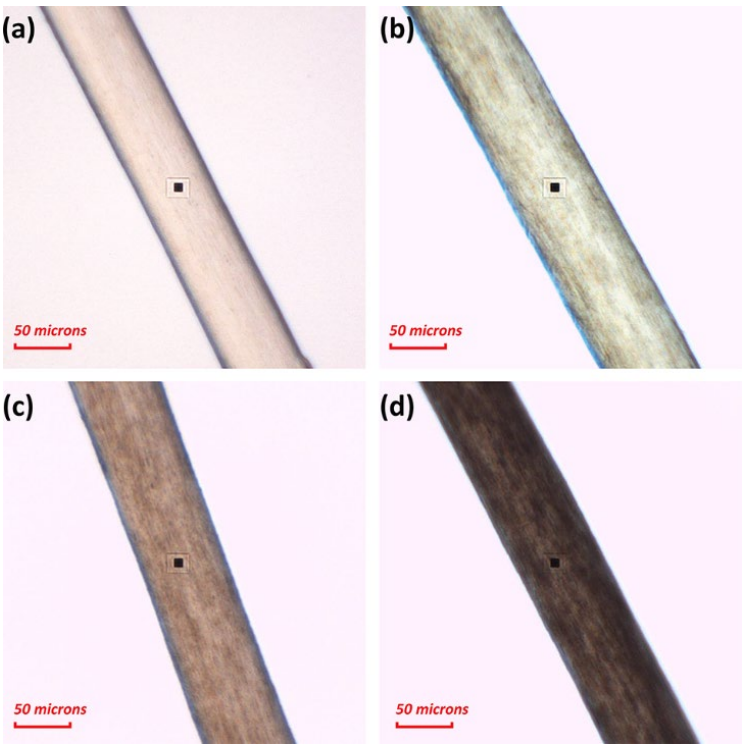

Figure 4-6: Photomicrographs of scalp terminal hair samples in four categories based on their type and quantity of melanin. (a) light blond hair with a low quantity of predominant pheomelanin; (b) dark blond hair with a high quantity of predominant pheomelanin; (c) light brown hair with a low quantity of predominant eumelanin; (d) dark brown hair with a high quantity of predominant eumelanin. The black square spot illustrates where the light is focused.

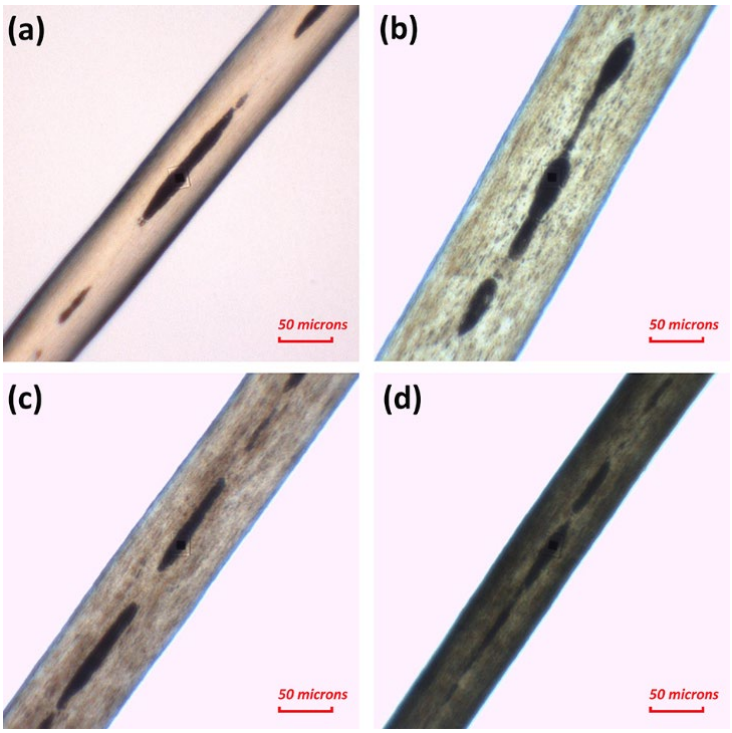

Figure 4-7: Photomicrographs of scalp terminal hair samples with the presence of medulla in the centre of the cortex (a) light blond hair, (b) dark blond hair, (c) light brown hair, (d) dark brown hair. The typical Caucasian scalp hair exhibits discontinuous medulla distribution along the length of the hair shaft. Regardless of hair colour, medulla appears black under the microspectrophotometer.

4.3.2 Transmission and attenuation coefficient spectra of the cortex and medulla

It is generally accepted that lighter colour hair would have higher light transmission. As demonstrated in Fig. 4-8, the average light transmission (within the wavelength range of 200 – 900 nm) in light blond hair was found to be the highest among the four colours of hair, which is followed by dark blond, light brown and dark brown hair in a descending order. The transmittance spectra of the four colours of hair exhibit V shapes with troughs of about 10% at 300 nm. As compared to the other three colours of hair, the transmittance spectrum of light blond hair experiences a more rapid increase in the wavelength range of 300 to 400 nm. The transmittance spectra of hair depend on its diameter. Although the transmittance spectra of the four hair categories share similar troughs, each of them is averaged from hair samples with different diameters. After taking into consideration of hair diameter, their optical properties (attenuation coefficients) can be compared. The signature characteristics of these transmittance spectra agree well with those determined from the absorbance spectra of hair reported by Barrett et al. [74].

As can be seen from Fig. 4-9, the attenuation coefficients of the cortex of these four colours of hair share similar profiles, peaking at a wavelength of around 300 nm and decreasing towards shorter and longer wavelengths. Dark brown hair has the highest attenuation coefficient in the entire wavelength range, which is considerably higher than the other three colours of hair. In the wavelength range of about 220 to 315 nm, light brown, dark blond and light blond hairs have similar attenuation coefficients. Nevertheless, light blond hair still exhibits the lowest value. From 315 to 900 nm, the difference in the attenuation coefficient of the cortex of these three colours of hair becomes more pronounced. The greatest difference is observed in the wavelength range of around 390 to 420 nm and decreases gradually with an increase in wavelength. The wavelength dependency of attenuation coefficient of hairs agrees well with the findings from Kharin et al. [79], who studied the attenuation coefficients of human hairs in the wavelength range of 400 to 1100 nm.

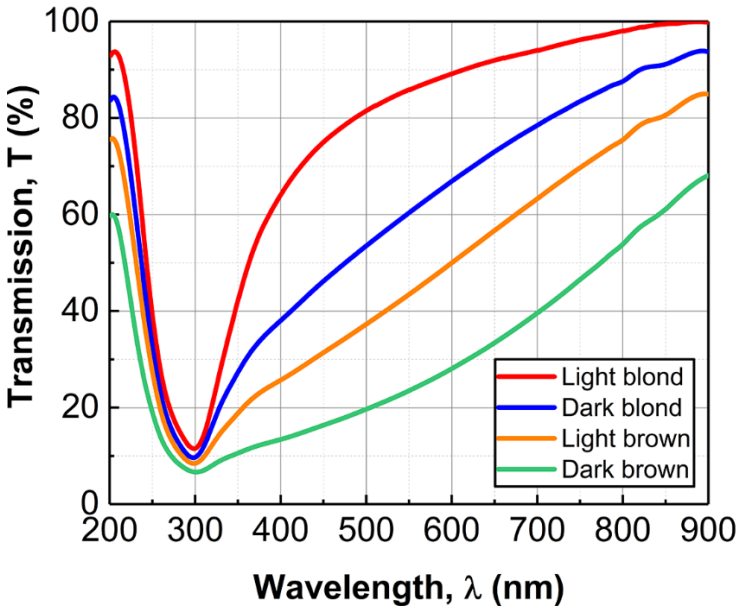

Figure 4-8: Average transmittance spectra of the cortex of light blond, dark blond, light brown and dark brown hair in the wavelength range of 200 to 900 nm.

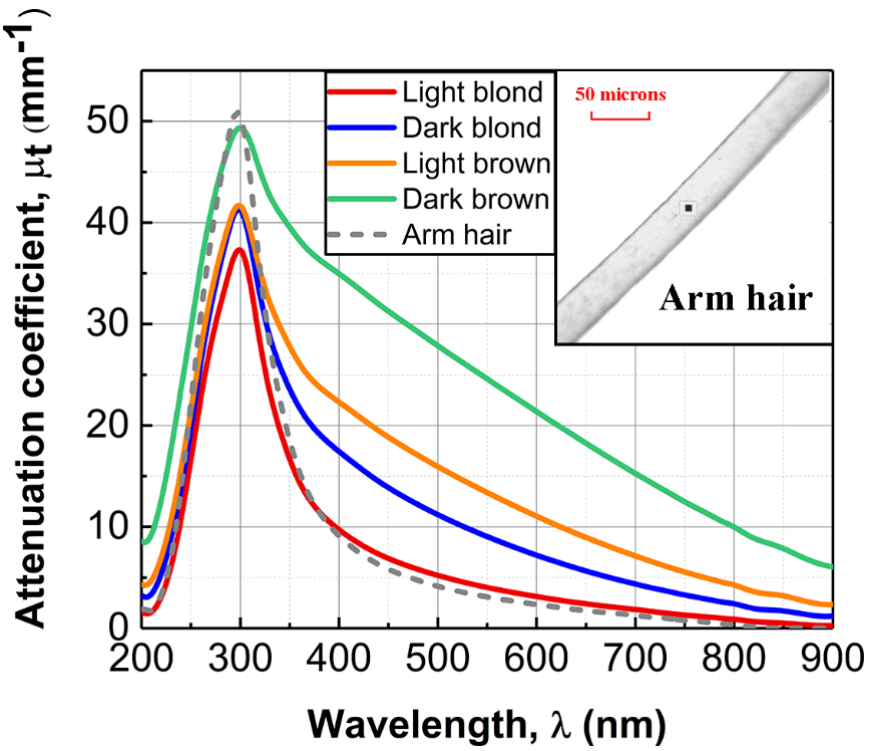

Figure 4-9: Average attenuation coefficient of light blond hair, dark blond hair, light brown hair, dark brown hair and arm hair in the wavelength range of 200 to 900 nm. The attenuation coefficient profiles exhibit an inverse pattern to the transmittance spectra, as expected. There are minor differences between the profiles of light brown, dark blond and light blond in the wavelength range of 200 and 315 nm. From 315 to 900 nm, light blond hair demonstrates the lowest attenuation profile. The attenuation coefficient of the arm hair closely follows that of light blond scalp hair, except in the UVB wavelength range. A photomicrograph of the arm hair is included in the figure.

The attenuation coefficients of the cortex of hair calculated in this study are slightly higher than the results reported by Kharin et al. [79]. This could be attributed to the facts that ethyl cinnamate (which has a refractive index closer to hair than glycerine) was used as the mounting medium in Kharin et al.'s measurement, as well as their different confocal setup.

The non-medullated arm hair samples are used as a representative of vellus hair (although vellus hair contains even less melanin), as shown in the photomicrograph in Fig. 4-9. Figure 4-9 also demonstrates that the attenuation coefficient profile of the body hair closely follows that of the light blond scalp hair, with an exception in the UVB wavelength range, where the attenuation coefficient of the body hair is noticeably higher than that of the scalp hair. Nevertheless, the light blond scalp hair is still considered to have an attenuation coefficient closest to that of vellus hair among all the four colour categories.

The standard deviations of the different hair categories are presented in Appendix B. The relatively large standard deviation of the cortex of hair is consistent with the findings in the literature [76, 77]. The possible reasons for this variation could be due to the variations of hair colour from individuals in each hair category and the assumption of the circular shape for the hair shaft. The low dispersion of the attenuation coefficient of hair reported in Kharin et al's study [79] is most likely due to the fact that only five samples (from the same participant) were measured in that case.

From the data analysis of the attenuation coefficient of the medulla, no clear hair colour-dependency has been found. The reason is that most of the hair melanin is distributed in the cortex; the medulla contains little or no melanin, implying that the optical properties of hair medulla is not colour-dependent. Therefore, average transmittance and attenuation coefficient were obtained from all the four colour categories. Fig. 4-10 shows the average transmittance of medullated hair samples and the attenuation coefficient of the medulla. It can be seen that the transmittance is at its lowest in the wavelength range of 300 to 600 nm, where it fluctuates around a value of 10%. Approaching shorter and longer wavelengths, the transmittance increases rapidly. The attenuation coefficient of medulla reaches its maximum at a wavelength about 590 nm and decreases rapidly towards shorter and longer wavelengths. The attenuation coefficient of medulla at 633 nm [79], measured by Kharin et al. falls within one standard deviations of our calculated sample mean.

To the best of our knowledge, this research is the first study to investigate the attenuation coefficient and wavelength dependency of medulla. The hair medulla has demonstrated strong attenuation effect on photons in the wavelength range of 300 to 800 nm. This is consistent with a study which shows high scattering characteristics from porous hair medulla in wavelength 400 nm and 700 nm [48]. The spectral behaviour of the attenuation coefficient of the medulla differs noticeably to that of the cortex (Fig. 4-9). This may be due to the fact that the medulla cells in hair have distinct keratins, and differ from all other cells of the hair follicle and epithelium [41]. In addition, the medulla is not only made up of keratinized cells but large air spaces [126], which may result in no clear wavelength dependency on its attenuation coefficient. Nevertheless, the medulla of hair still shows significantly higher attenuation coefficient than that of the cortex, implying that photons would transmit along the cortex of the hair shaft considerably more easily than the medulla. The uncertainty in medulla diameter measurement, and, more importantly, the variance of the medulla cells and their packing density, are considered to be responsible for the large standard deviation in the attenuation coefficient measurements.

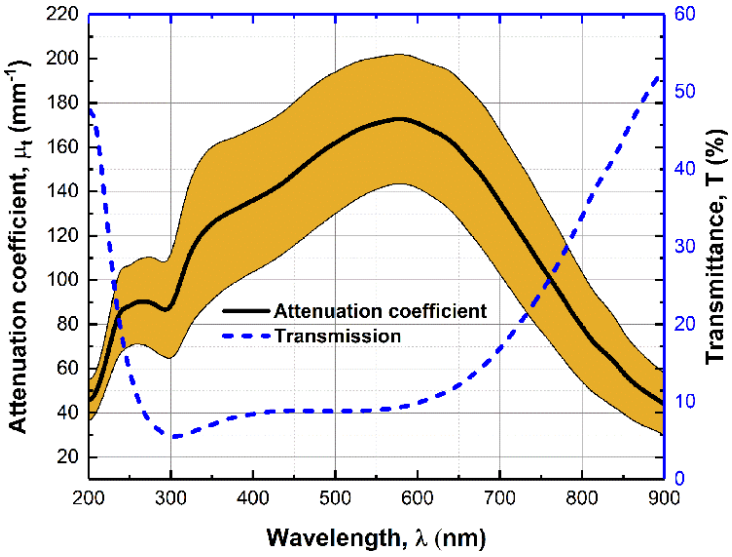

Figure 4-10: Average transmittance spectra of medullated scalp hair samples (dashed line), average attenuation coefficient (solid line) and one standard deviation (shaded region) graph of medulla as a function of wavelength from 200 to 900 nm. The transmittance spectra are obtained from the medullated hair (a combination of the cuticle, cortex and medulla). The attenuation coefficient spectra are estimated for the medulla only.

4.3.3 Comparison of the average attenuation coefficient of the cortex of hair

To examine whether vellus hair transmits UV photons more readily than terminal hair, it is considered reasonable to compare the average attenuation coefficient in the UVA and UVB wavelength ranges of light blond scalp hair, a representative of vellus hair, with the other three colour categories of terminal scalp hair. Therefore, an analysis of variance (ANOVA) test is performed in IBM SPSS Statistics to evaluate the differences between them.

The average attenuation coefficients of the sample hairs in the UVA and UVB regions are considered normally distributed after performing the Shapiro-Wilk test. Using the Levene's test, it was found that the assumption of homogeneity of variances is applicable only to the results in the UVA wavelength range. Therefore, the ANOVA & Tukey's HSD tests are performed to calculate the statistical significance p-value in the UVA wavelength range, whereas the Welch's test and Games-Howell's test are used in the UVB wavelength range. The results are summarized in Fig. 4-11.

In the UVA range, the average attenuation coefficient of the cortex of the light blond hair is found to be significantly lower than that of the dark blond, light brown and dark brown ($p < 0.0001$). The main reason is that the relatively low quantity of pheomelanin present in the light blond hair results in relatively low UV absorption and scattering, as compared to the other three colour categories of hair with their higher contents of pheomelanin and eumelanin. In contrast, no significant difference is found between the average attenuation coefficients in the UVB wavelength range of the cortex of light blond hair and dark blond or light brown hair.

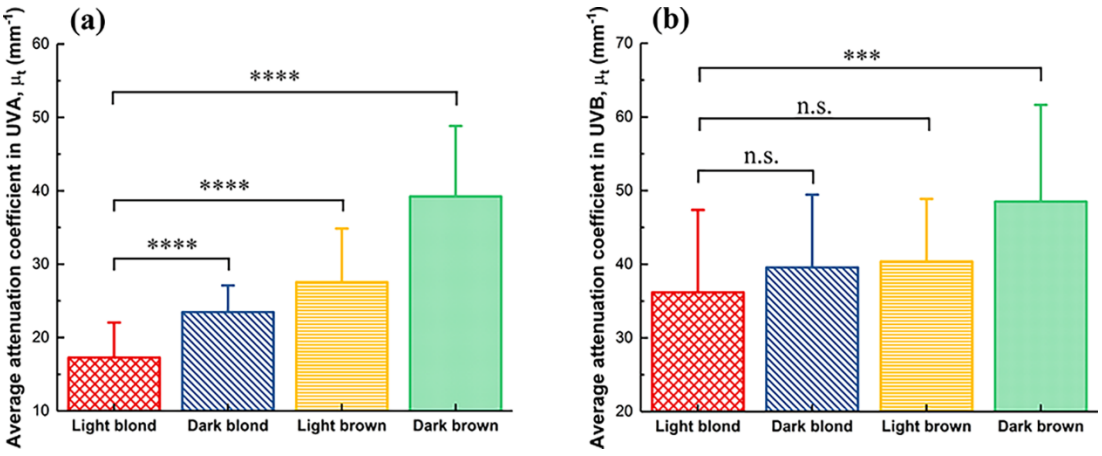

Figure 4-11: Comparison of the average attenuation coefficients of the cortex of the light blond, dark blond, light brown and dark brown scalp hair in the (a) UVA and (b) UVB wavelength ranges. *** = $p < 0.001$, **** = $p < 0.0001$, n.s. = no statistically significant difference.

The possible explanations for this phenomenon are 1) the difference between the light attenuation effect of pheomelanin and eumelanin decreases with a decrease in wavelength, with almost no difference at 280 nm [96]; 2) as the wavelength decreases from 310 to 280 nm, the attenuation effect of keratin (the protein composing the cortex) increases rapidly [127], implying that the keratin in the cortex of hair may be responsible for more photon attenuation than melanin in the UVB wavelength range. Nevertheless, light blond hair still shows significantly lower attenuation coefficient than dark brown hair in the UVB wavelength range ($p < 0.001$).

4.3.4 Comparison of the attenuation coefficient of hair and skin

The attenuation coefficient of tissues indicates how easily the photons at a specific wavelength can penetrate. As it can be seen from Fig. 4-12, the attenuation coefficient of non-medullated light blond hair ('vellus-like hair) is significantly lower than that of skin layers. This implies that vellus hair in the skin may contribute to the solar UV transmission deeper into the skin, reaching the follicular stem cells.

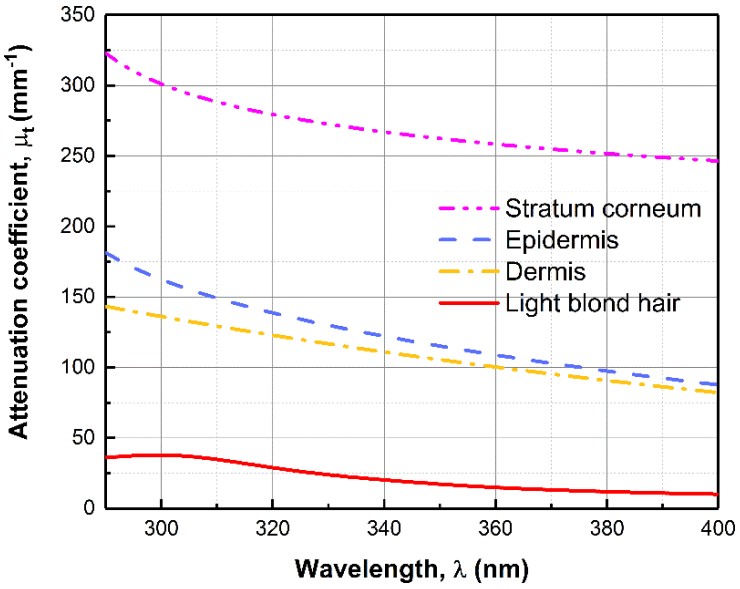

Figure 4-12: Comparison of the attenuation coefficients of the cortex of light blond hair and the skin layers (stratum corneum, epidermis and dermis) in the wavelength range of 290 to 400 nm. Attenuation coefficients of the stratum corneum, epidermis and dermis are acquired from the data reported by Van Gemert et al. [111]. The average attenuation of light blond hair is about 13.7, 6.3 and 5.6 times lower that of stratum corneum, epidermis and dermis respectively in the wavelength range of 290 to 400 nm.

4.4 Chapter summary

The average attenuation coefficient of the cortex of 'vellus-like' hair is found to be significantly lower than that of terminal hairs in the UVA and UVB wavelength ranges. In addition, the medulla, present in terminal hair, has a significantly higher attenuation coefficient than that of the cortex of hair. These results indicate that UV photons from the sun would transmit through vellus hair into skin more easily than through terminal hair. Furthermore, the attenuation coefficients of the 'vellus-like' hairs in the UV wavelength range are dramatically lower than those of the skin layers. Therefore, it is hypothesized that vellus hair could play a role in melanoma development by contributing to the passage of solar UV photons to the bulge region of the hair follicle, where the melanocyte stem cells reside. This hypothesis will require further investigation of the optical properties of hair in the UV wavelength range. In chapter 5, a planned Monte Carlo simulation of photon transport in the skin with and without vellus hair will reveal its contribution to UV photon delivery to the bulge region of hair follicle and potential melanoma development.

Chapter 5 Simulation of UV transmission in realistic skin models

5.1 Introduction

Skin alone is traditionally considered as the main pathway for transporting harmful UVR to skin cells that causes skin cancer development. However, this chapter considers the contribution of hair in transmitting UVR into the skin.

In Chapter 4, the attenuation coefficient of light blond, non-medullated hair has shown to be significantly lower than that of more pigmented non-medullated and medullated hair. In this chapter, we apply the measured hair properties to realistic skin-hair models to investigate the roles different types of hair play in solar UV transmission into the skin. The hair shafts in our models were constructed to be bent towards the skin surface, which is considered to be more realistic than hair models built with straight shapes [98-100, 130]. The simulations are performed in TracePro software, with the implementation of the MC method for photon transport.

The morphology and optical properties of non-medullated light blond hair are considered to be mimics of vellus hair; so the absorption and scattering coefficients of light blond hair are applied to the vellus hair in the simulation. The non-medullated brown hair is selected as an example of terminal hair. Due to the lack of the optical properties of the hair medulla, hair shafts have always been modelled as homogeneous structure in the MC simulation. An attempt has been made to investigate the presence of hair medulla on the UV transmission in the skin (Section 5.3.3).

The legs of women consist of noticeable amount of vellus hair. And, the incidence of melanoma in legs of women is relatively high. It is speculated that this is associated with the tendency for women to shave their legs [27]. Thus, a skin model with shaved vellus hairs has also been setup for comparison with the model comprised of unaltered vellus hairs.

Similar to Chapter 3, the UV absorption in the stem cell layer of skin models will be compared. As noted in Chapter 3, the terminal hair follicle stem cell layer is situated about three times deeper than that of vellus hair and it has been realized that the stem cells at such deep location in the skin are less likely to be involved in melanomagenesis [123].

5.2 Materials and methods

TracePro (Lambda Software) with the implementation of the Monte Carlo method was used for constructing and simulating the skin-hair models in this chapter. Fig. 5-1 shows the three-dimensional models of (a) skin with the absence of hair, (b) presence of vellus hair, (c) terminal hair and (d) shaved vellus hair respectively. Since the focus of this chapter is to differentiate the influence of the vellus hair and terminal hair in UV transmission in the skin, we have used the typical geometry of Caucasian child skin for all the models. The thicknesses of the stratum corneum and epidermis are constructed to be 30 μm and 60 μm respectively [31]. Sufficient depth of dermis (1.5 mm) is constructed to examine the UV absorption in the stem cell layer.

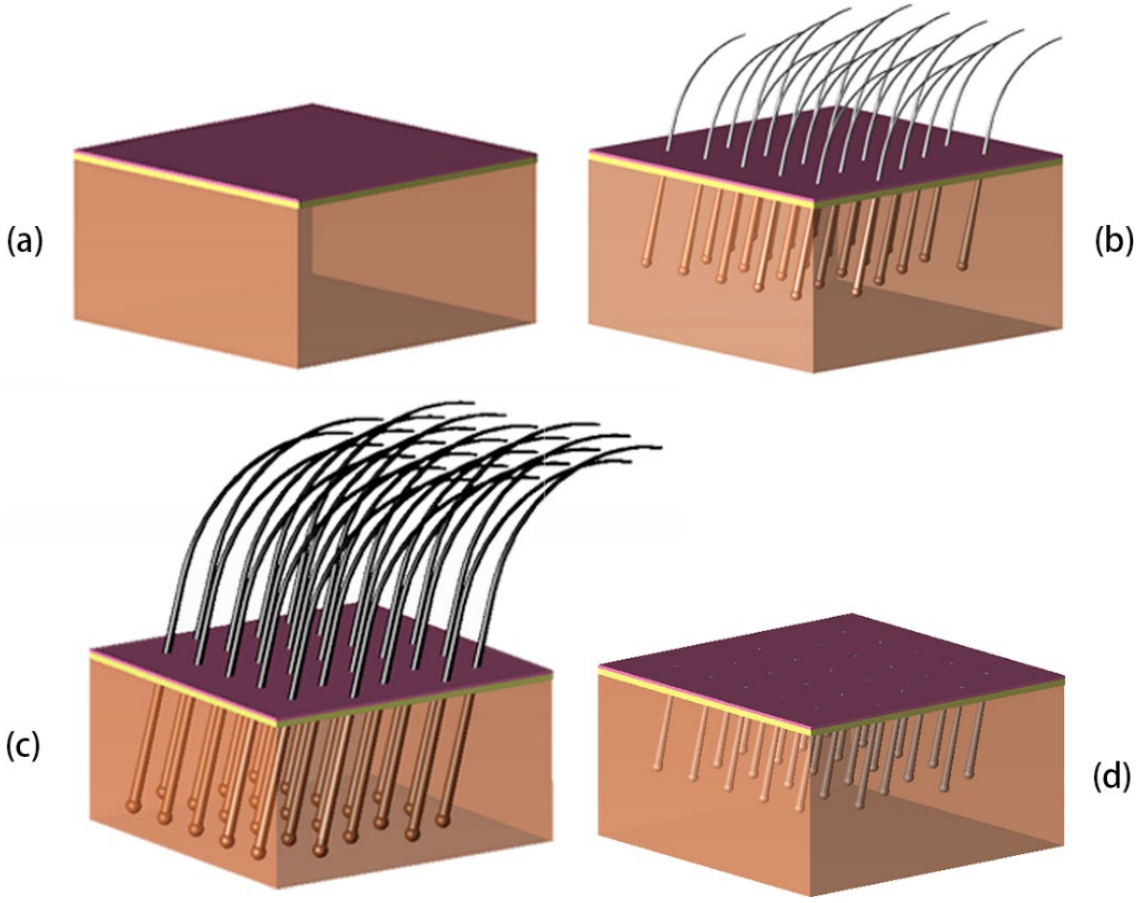

Figure 5-1: Three-dimensional skin-hair models constructed in TracePro software. (a) Three-layered hairless skin; (b) three-layered skin with vellus hair; (c) three-layered skin with terminal hair; (d) three-layered skin with shaved vellus hair.

The density of vellus hair varies with body site. The typical vellus hair density on the forehead is 280/cm^2 [131]. To correspond to this, the top view dimension of the three skin models are created to be 3 mm x 3 mm and the count of hair is 25. A typical diameter of vellus hair (30 μm) and terminal hair (60 μm) at the skin surface are assigned to the hair models. The lengths of the unaltered vellus and terminal hair shafts are 2 and 4 mm respectively. Hair shafts below the skin surface are tilted at an angle of 15 degrees to the vertical plane. The hair above the skin was modelled to be bent towards the surface of the skin for the purpose of achieving more realistic simulations. The shielding effect of hairs (absorption and scattering of photons) above the skin surface is considered in the simulations.

The skin is modelled as three flat layers (stratum corneum, epidermis and dermis in order of downward direction) with uniform optical properties. The optical properties of the Caucasian skin layers can be found in Chapter 3. The vellus hair is unpigmented whereas the terminal hair is highly pigmented. Therefore, it is considered reasonable to apply the optical properties of the non-medullated light blond and dark brown hair to the vellus and non-medullated terminal hair models respectively in TracePro. The absorption coefficient of blond and brown hair increases exponentially with a decrease in wavelength. Their absorption coefficients at UV wavelengths are extrapolated from Bashkatov et al.'s study [76]. The attenuation coefficient is the sum of the absorption and scattering coefficient. Therefore, the scattering coefficients of blond and brown hair are derived from deducting the absorption coefficients from the attenuation coefficients. They are summarized in Fig. 5-2. The refractive index (1.54) and the anisotropy factor (0.79) of hair are treated as constant in UV wavelength range [80, 98-100]. However, similar to the skin [44, 114], the minor variation of these properties in the UV wavelength range is considered to have insignificant influence on the results. The optical properties of the Caucasian skin layers can be found in Chapter 3.

We apply the same UV irradiance from Chapter 3 in this chapter [15]. The wavelength is varied from 310 to 370 nm in an interval of 20 nm to examine both UVA and UVB wavelength ranges. In each simulation, over 2 million photons are launched from a light source perpendicularly onto the top surface of the skin-hair model, constructed to share the same dimensions as the flux area of the light source (Fig. 5-3). After the completion of the simulation, the absorption fraction in each voxel of the model is multiplied by the irradiance to calculate the absorbed radiant flux inside the skin. The result will be

presented as the radiant flux absorbed in the stem cell layer along the depth in an interval of 2 μm (Fig.5-5).

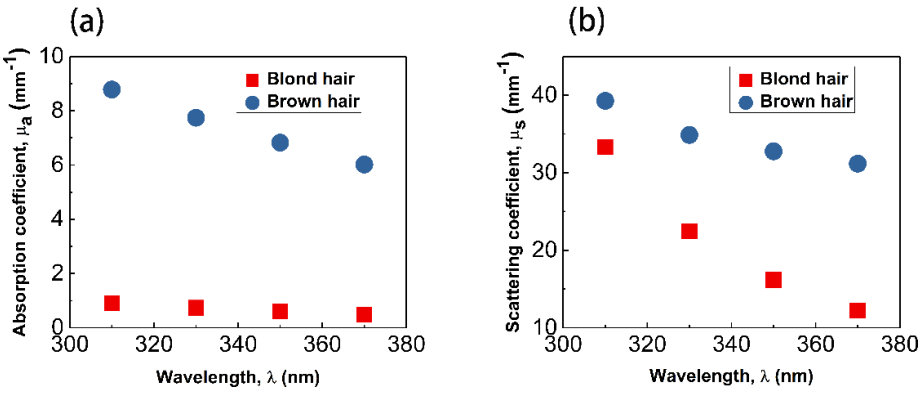

Figure 5-2: Absorption and scattering coefficient of blond (vellus) and brown hair (terminal). The scattering coefficients are derived from deducting the absorption coefficients from the attenuation coefficients determined in this study.

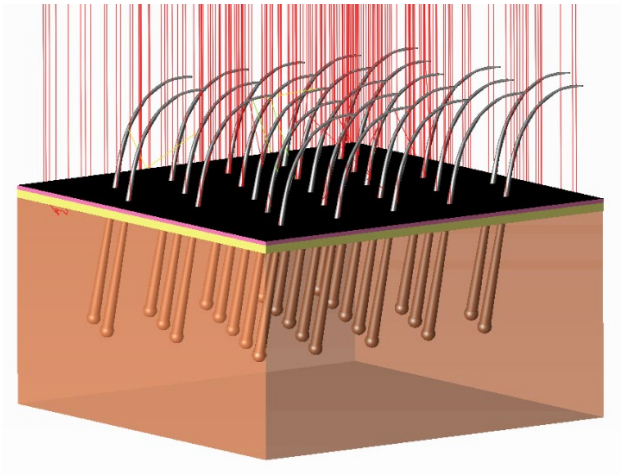

Figure 5-3: Diagram of launching photons onto a skin-vellus hair model in TracePro. For clarity, only a small number of photons are shown and the photons exiting from the model domain are not shown.

5.3 Results and discussion

5.3.1 The influence of hair in UV transmission into skin

As illustrated in Fig. 5 – 4 (a – d), a portion of the incident photons are scattered by the hair shafts above the skin or reflected by the skin surface. A much larger portion of rays are observed to be shielded by the terminal hairs above the skin surface than vellus hairs. Without the attenuation of photons by the hair above the skin surface, more photons can effectively enter into the skin, as shown in model (a) and (d).

The McSCs in the VHF reside in the skin layer with depths from 315 to 405 µm. Figure 5-5 illustrates that the radiant UV flux absorbed in the skin declines over the depth of the stem cell layer. Over the entire stem cell layer, the skin model with vellus hair shows noticeably higher absorption than the hairless skin and the skin with terminal hair.

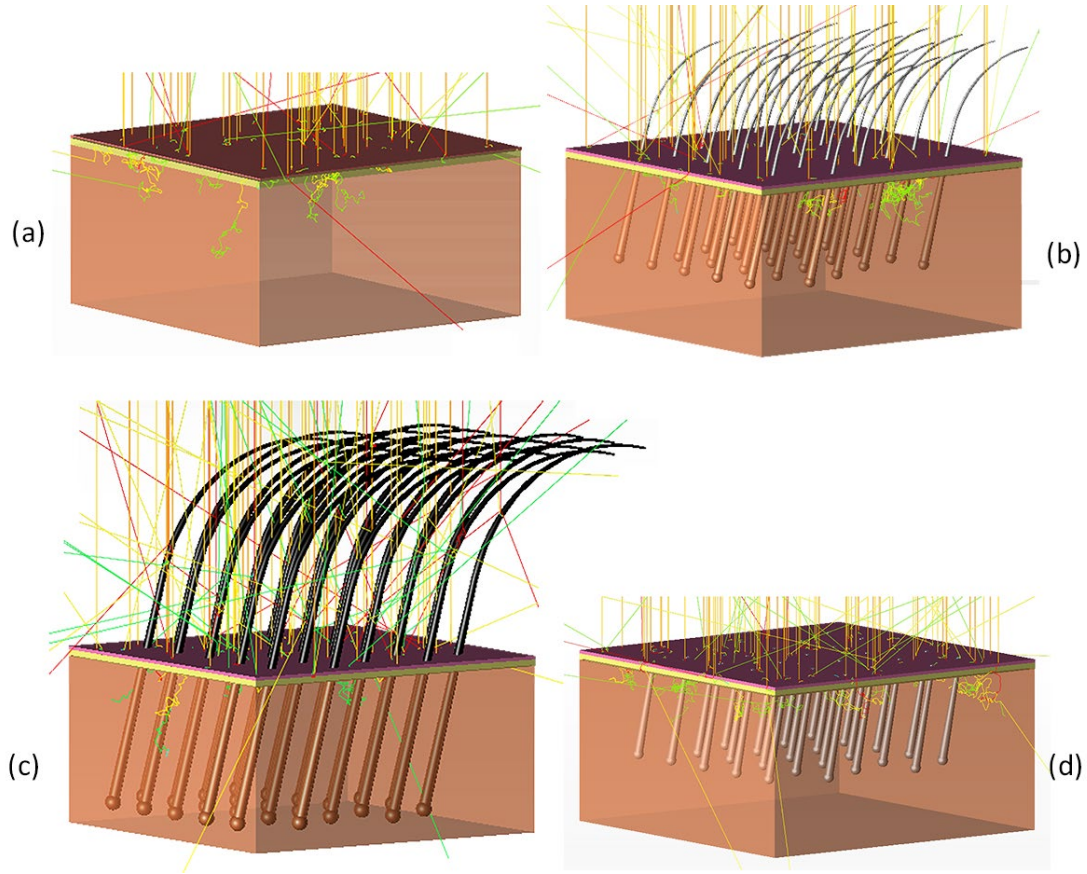

Figure 5-4: Diagrams showing interactions between photons and (a) skin with no hair, (b) skin with unaltered vellus hair, (c) skin with terminal hair and (d) skin with shaved vellus hair. The weight of each photon packet attenuates as it is experiencing absorption, which is represented by different colours (red, yellow, green and blue, in an order of decreasing photon packet weight). A small and equal number of photons are launched in these three models respectively for demonstration. Only the scattered but not the incident rays are shown in these diagrams.

More specifically, compared to hairless skin, the presence of vellus hair in the skin has increased the total absorption in the stem cell layer by 4.6%, 7.7%, 16.9% and 52.0% at wavelengths of 370 nm, 350 nm, 330 nm and 310 nm respectively. In contrast, compared with skin with terminal hair, the skin with vellus hair absorbs 16.7%, 20.0%, 28.7% and 55.6% higher UV at wavelengths of 370 nm, 350 nm, 330 nm and 310 nm respectively. A higher level of UV photons is delivered to the stem cell layer in the skin with vellus hair as compared to hairless skin and skin with terminal hair. This is because vellus hair exhibits significantly lower attenuation coefficients and, more importantly, lower absorption coefficients compared to the skin layers in the UV wavelength range (see Appendix C). As a result, harmful UV photons are able to transmit deeper into the skin and into the stem cell layer.

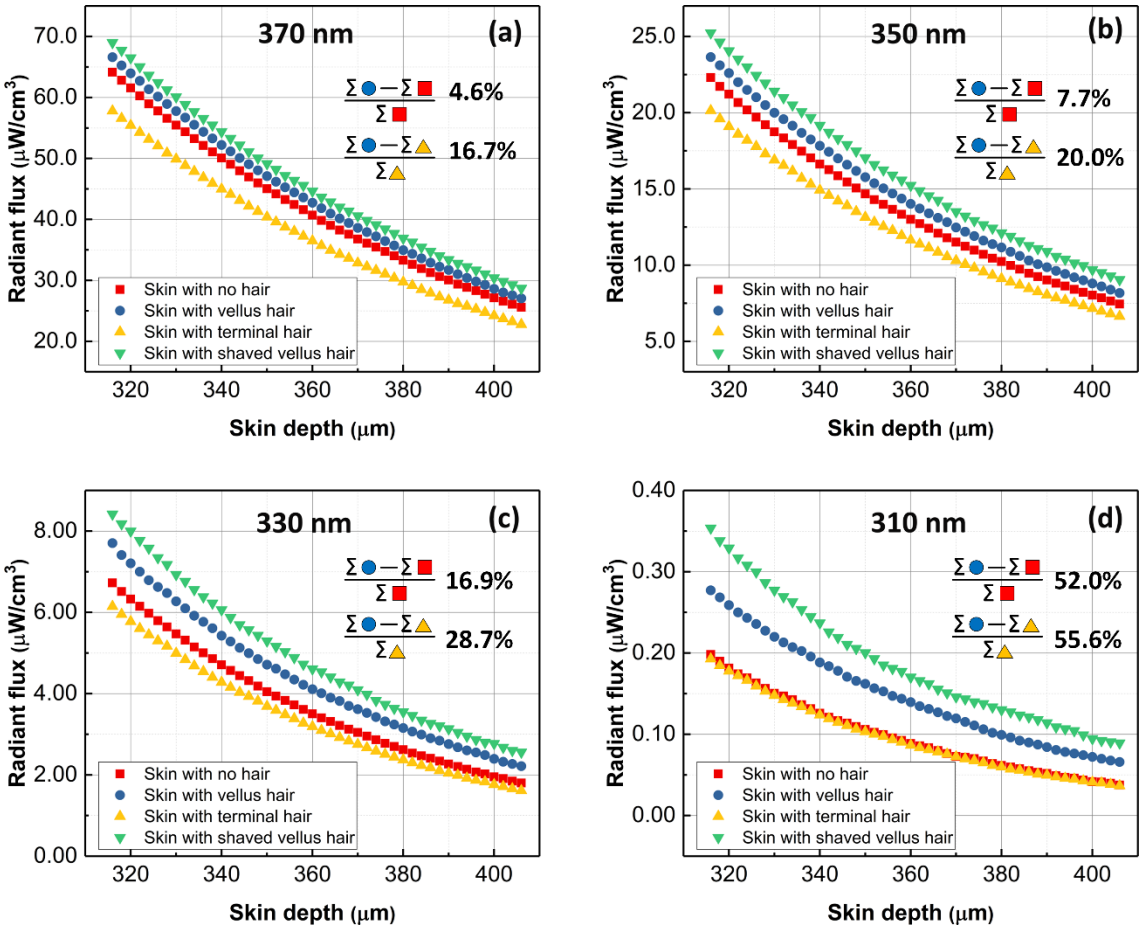

Figure 5-5: Radiant flux absorbed over the depth of the stem cell layer where the follicular melanocyte stem cells are situated, in different skin-hair models, at wavelength (a) 370 nm, (b) 350 nm, (c) 330 nm and (d) 310 nm. Noticeably higher absorption occurs in the skin model with vellus hair than the hairless skin and the skin with terminal hair models. The increase in UV absorption in the entire stem cell layer due to the presence of vellus hair, compared to hairless skin and skin with terminal hair are given in percentages.

Although vellus hairs above the skin surface also shield a portion of the incident photons from effectively entering the skin, this effect is considered as insignificant. Since the hair shafts are tapered, the average diameter of the portion of vellus hairs above the skin is smaller than that below the skin. The relatively larger portion of the vellus hairs underneath the skin contributes to the UV transmission deeper into the skin and this contribution effect is significantly greater than the attenuation effect created by the portion of vellus hairs above the skin surface.

It is important to note that the contribution of vellus hair in transmitting UV energy increases with a decrease in wavelength (see Fig. 5-5 (a) to (d)). More specifically, skin with vellus hair has increased the energy absorption in the stem cell layer from about 5% at 370 nm to around 50% at 310 nm, as compared to hairless skin. This is due to the fact that the differences between the attenuation coefficient of vellus hair and skin layers [123] also increases with a decrease in wavelength. Therefore, photons would transmit more easily in shorter wavelengths in the volume occupied by the vellus hair shafts underneath the skin. Both UVA and UVB can initiate melanoma. Our simulated results show that the presence of vellus hair on the body can contribute to the transmission of UVA, and more significantly UVB, to melanocyte stem cells.

For terminal hair, its attenuation coefficient is also less than the skin layers however, due to the presence of melanin, its absorption coefficients are higher than the dermis (see Appendix C), which results in lower photon transmission. Consequently, skin with terminal hair actually acts as a shield to the penetration of UV radiation into the stem cell layer. However, this shielding effect is observed to decrease with wavelength towards the UVB region. This is because although the attenuation coefficients of the skin layers increase rapidly as the wavelength decreases in the UVB region, the rise in attenuation coefficient of terminal hair is not as significant.

Due to the lack of knowledge about the absorption coefficient of medulla in the literature, it is not included in the skin-hair model. However, its significantly higher attenuation coefficient (Fig. 4-10) is considered to block photons as strongly as pigmented cortex. This will be demonstrated in Section 5.3.3.

The solar radiant UV flux reaching the stem cell layer is transmitted by way of paths through the hair and the skin layers. The radiant flux absorbed in the stem cell layer can be an indication of the relative risks for melanoma development. We hypothesize that the presence of vellus hair would increase the risk of melanoma by contributing higher dose

of UV transmission to the follicular stem cells, which can cause damage or mutations. If the hypothesis holds true, it may not only explain the vulnerability of children to sun exposure but also the positive correlation found between the incidence of melanoma in adults' bodies and the number of vellus hair follicles in these areas [27].

5.3.2 Influence of shaved vellus hair on UV transmission

As can be seen from Fig. 5-5, even more UV is absorbed in the stem cell layer in the skin model with shaved vellus hair. This is because that after shaving the portion of vellus hair above the skin surface, which can shield UV photons by absorption and scattering, more photons will effectively transmit into the skin. In addition, shaved vellus hairs are exposed to UV photons more directly, meaning a portion of UV photons can penetrate into the skin by entering the flat hair cross-sectional surfaces. This geometry of hair has enhanced UV transmission along the skin, resulting in more radiant flux absorbed in the stem cell layer, as compared to unaltered vellus hair.

The high density of vellus hair in women's legs would contribute to the solar UV transmission in the skin to McSCs, as shown in Section 5.3.1. Furthermore, after shaving vellus hair, the increase in UV transmission will be even greater. We hypothesize that the particularly high melanoma incidence seen in women's legs are not only associated with the high density of vellus hair but also the tendency of shaving.

5.3.3 Influence of terminal hair medulla on UV transmission

Although the attenuation coefficient of the hair medulla has been determined in Chapter 4, modelling medulla inside hair cortex requires the input of its absorption and scattering coefficient. Differentiating between the absorption and scattering coefficient requires additional measurement involving the use of an integrating sphere. However, as noted previously, since the hair medulla has an average thickness about 10 μm, determining its absorption and scattering coefficient is technically challenging in this apparatus. Here, we vary K from 0.1 to 0.5 and 0.9 to investigate a range of medulla's possible optical properties, where K is the ratio of absorption coefficient/attenuation coefficient of medulla.

$$K = \frac{\mu_a}{\mu_t} \qquad 5\text{-}1$$

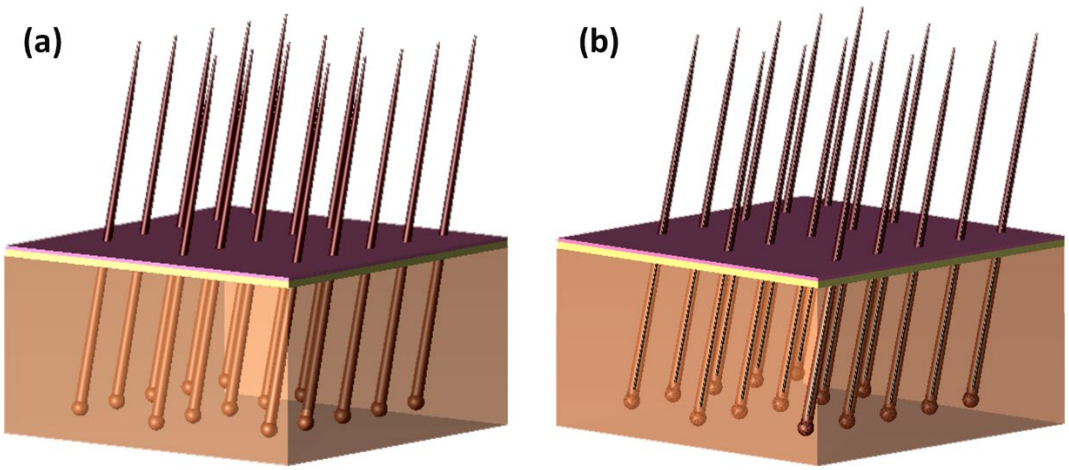

Figure 5-6: Skin and terminal hair models in TracePro software. (a) non-medullated terminal hair, (b) medullated terminal hair

Due to the complexity of constructing medullated hair with the same geometry as Fig. 5-1, simplified skin-hair models, as shown in Fig. 5-6, were used for the purpose of investigating the presence of medulla on UV transmission in the skin. Figure 5-6 (a) and (b) are the skin with non-medullated terminal hair and medullated terminal hair respectively. They share the same geometry, except for the presence of medulla in (b), which is set up to be about 25% of the hair shaft diameter.

The hair density is set to be 167/cm^2 [130]. The hair shafts are constructed to be straight with lengths of 3 mm, which are different to bent hair models in Fig. 5-1. The rest of the geometries are the same as Fig. 5-1.

Figure 5-7 represents the radiant flux absorbed over the depth of the stem cell layer for Caucasian skin with medullated hair and non-medullated hair when exposed to solar UVR at wavelengths of (a) 370 nm, (b) 350 nm, (c) 330 nm and (d) 310 nm respectively. As can be seen in all four wavelengths of Fig.5-7, varying K from 0.1 to 0.5 and 0.9 has a negligible effect on the radiant flux transmitted through the skin. In addition, as compared to non-medullated hair, no obvious difference in radiant flux has been observed. There are two main reasons for these phenomena. 1) the heavily pigmented terminal hair tends to absorb photons once they have entered the hair shaft, resulting fewer photons reaching the inner medulla; 2) although the medulla exhibits higher attenuation coefficient than the cortex of hair, its small size has a negligible effect on the overall photon transmission along the hair shaft.

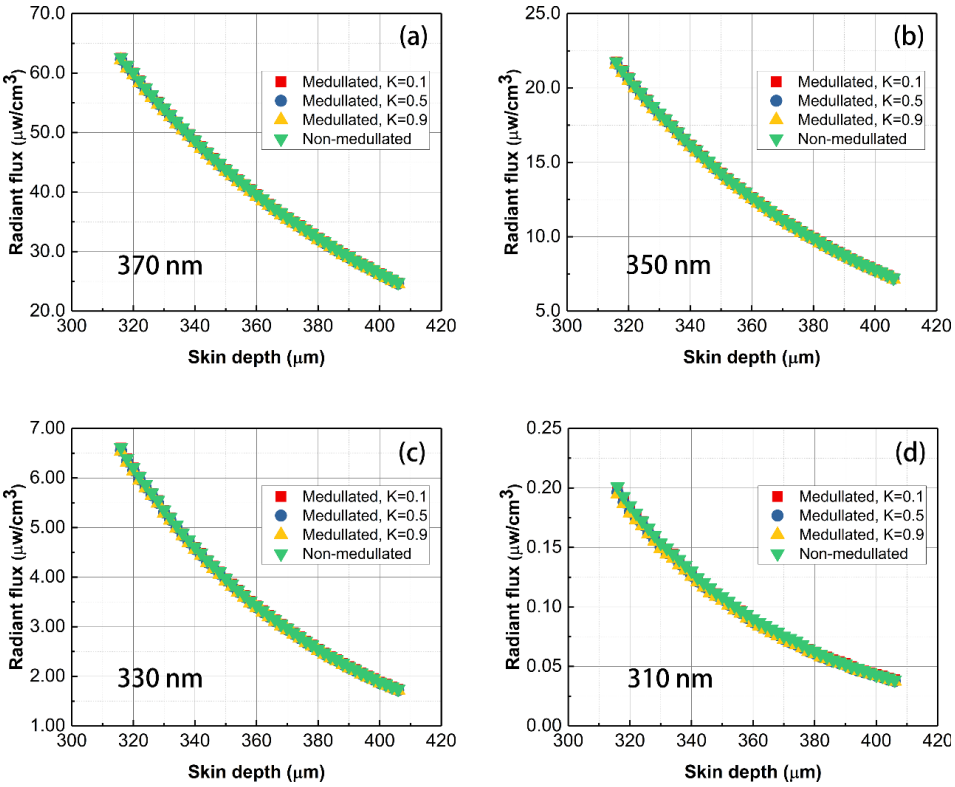

Figure 5-7: Comparison of the radiant flux absorbed along the depth of the skin with medullated and non-medullated terminal hairs, from solar exposure at (a) 370 nm, (b) 350 nm, (c) 330 nm and (d) 310 nm.

5.4 Chapter summary

The hypothesis of vellus hairs contributing to the solar UV transmission in the skin has been validated by the MC simulation. Skin with vellus hair results in significantly higher energy absorption in the stem cell layer as compared to hairless skin. The relative increase in energy absorbed in the stem cell layer when vellus hair is present to hairless skin varies from 4.6% to 52.0% over the UVA – UVB wavelength ranges. For skin with terminal hair (medullated or non-medullated), this relative increase in energy absorbed varies from 16.7% to 55.6% over the same wavelength range. Skin with shaved vellus hair will enhance the UV transmission in the skin even greater. In reality, the relative increase in the UV delivery will vary, depending on the hair density.

In conclusion, this chapter shows that the presence of vellus hair in skin could play a major role in melanoma development by contributing to the passage of solar UV photons to the bulge region of the hair follicle, where the melanocyte stem cells reside. Our research helps to explain the vulnerability of children to sun exposure, and the positive correlation between the incidence of melanoma in adults' bodies and the number of vellus hair follicles in these areas.

Chapter 6 Discussion

The literature review, experimental and theoretical work have been comprehensively discussed in their respective chapters. In this chapter, we will discuss the aspects that have not been extensively discussed previously.

6.1 Assumptions

There are several assumptions made in the course of the data analysis and simulations (Chapter 3 – 5). Some of them have been discussed previously, the others are discussed below.

6.1.1 Actual UV absorption by stem cells and melanoma development

Human hair follicles are often distributed irregularly in the body. To reveal the relative UV absorbed by the McSCs, the UV absorption in the entire stem cell layer is determined and compared. The UV absorption in the stem cell layer can be an indication of the relative risk of melanoma development. However, it should be noted that the McSCs are not distributed evenly in the entire stem cell layer. They are situated in the bulge region of hair follicles (Fig.1-1). Therefore, to estimate the UV absorbed by the bulge region, one can multiply the radiant power absorbed in the skin ($\mu W/cm^3$), determined in Chapter 3 or 5, by the volume of the bulge. The actual energy absorbed can be derived from the radiant flux absorbed by multiplying it with the duration of sun exposure.

6.1.2 Neglecting hair in the skin simulations

Since skin is the main optical path for solar UV delivery, any differences present in the anatomy or optical properties of skin will play a more significant role in influencing the UV transmission in the skin than any differences from hairs.

In Chapter 3, the influence of hair in affecting UV transmission is removed. Chapter 3 focuses on investigating how the skin thickness and the depth of McSCs affect the UV dose received by McSCs. It is shown that the stem cells in the VHF have been found to receive and absorb significantly more (over 250 times) UVR than those in the THF due to their shallower locations. As demonstrated in Chapter 5, the presence of vellus hair can contribute to the UV transmission in the skin, whereas terminal hair provides a degree of shielding to the penetration of UV. Therefore, when vellus and terminal hairs are included

in the skin models in Chapter 3, the difference between in UV abosrption by the stem cells in VHF and THF will be even greater than the original estimate.

6.1.3 Applying optical properties of scalp hair to body hair

Note that it was technically difficult to source vellus hair samples for measurement and analysis. The optical properties of non-medullated light blond scalp hair were applied to the vellus hair on the skin. The reasons are that 1) non-medullated light blond scalp hair has the least melanin content, which is the closest hair type to vellus hair among all the measured hair categories; 2) it exhibits the closest spectral attenuation coefficient to non-medullated and lightly pigmented arm hair, which is a representative of vellus hair.

Vellus hair is non-medullated with little or no melanin. Its attenuation coefficient is expected to be lower than pigmented terminal hairs, which has been shown in Chapter 4. The absorption and scattering coefficients of vellus hair are primarily determined by the keratins of the cortex. The wavelength dependency of the absorption and scattering coefficients of light blond hair determined in this thesis follow closely to the spectral behavior of the keratin. Therefore, it is considered reasonable to apply the optical properties of non-medullated light blond scalp hair to vellus hair in the skin model, to examine the effect of low hair melanin content in UV transmission in the skin.

6.2 Comparing results from MCX and TracePro™

Two different software packages (MCX and TracePro) have been used in this project to simulate the photon transport in the skin. They both use the MC method but have their own advantages and disadvantages. MCX allows calculations of multiple photons at the same time on a modern graphics processing unit (GPU), which speeds up the simulation process dramatically. Since enormous numbers of calculations were needed to obtain the power absorption in the stem cell layer over the UV wavelength range, MCX was chosen. However, constructing realistic skin-hair models in Matlab using MCX was found to be difficult. TracePro has an easier user interface. Therefore, it was chosen to construct the more realistic skin-hair models. The drawback of TracePro is that the photon transport calculations were performed in a single standard central processing unit (CPU), which was time-consuming. To not exceed the calculation capacity of the CPU in TracePro, a smaller number of photons (about 2 million) were simulated, as compared to 10^8 in MCX.

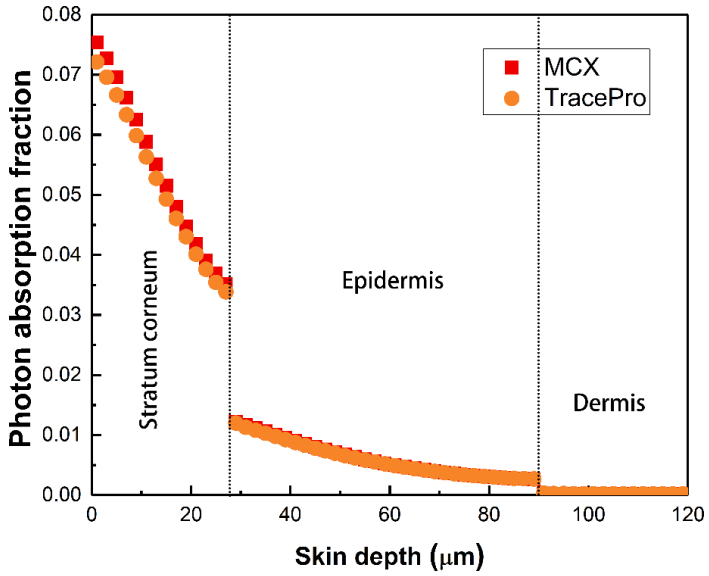

Figure 6-1: Comparison of results from MCX and TracePro software for λ = 350 nm.

MC simulations were performed on the skin with no hair using both software types (Chapters 3 and 5) and results for comparison were generated. The radiant flux absorbed depends on the area of exposure on the skin, and the two skin models have different dimensions. Therefore, the photon absorption fraction is compared along the depth of the skin, which is independent of exposure area. Fig. 6-1 shows the comparisons for the absorption fraction of photons at 350 nm along the depth of the skin.

The absorption fraction results from both software types show great agreement, especially in the epidermis and dermis layer. Therefore, it is expected that the simulation results from the skin-hair models in TracePro are considered reliable.

6.3 Comparing two different skin-terminal hair models in TracePro

Two different skin-terminal hair (non-medullated) models have been created in TracePro (Chapter 5) and presented here for comparison purposes. The two physical models are presented in Fig. 6-2 (a) and (b), and the results of the UV absorption along the depth of the two skin models are shown in (c).

The physical differences between the two models are the hair density, length and orientation.

The hairs above the skin surface in model (a) are longer and bent towards the skin surface, which results in larger effective shielding areas, than the straight and shorter hairs in model (b). In addition, the higher density of hair in model (a) provides stronger UV

protection for the skin by absorbing and scattering photons both above and underneath the skin surface. As a result, fewer photons are delivered into the skin in model (a) than (b), as shown in Fig. 6-2 (c).

All in all, higher density and more effective shielding area of terminal hair on the body site will provide better UV protection on the skin.

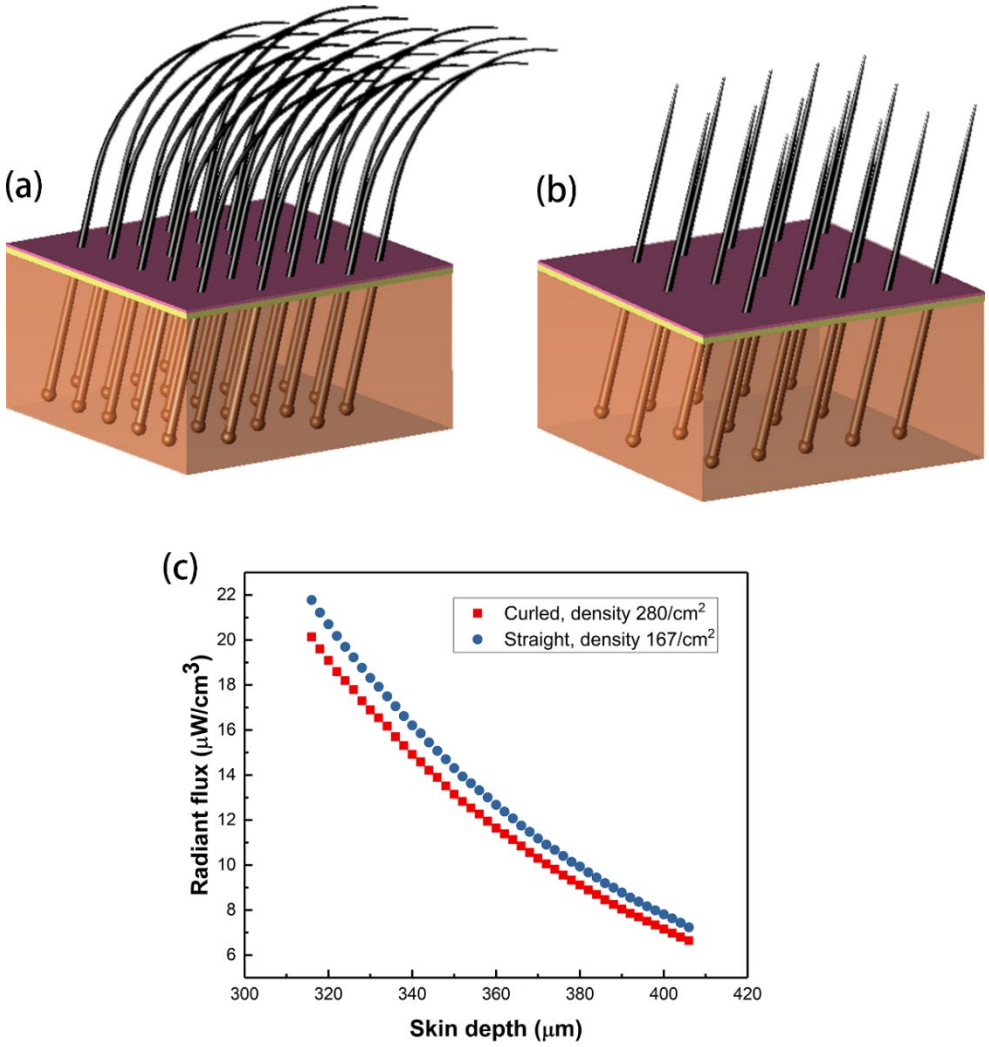

Figure 6-2: Two different skin-terminal hair models in TracePro. (a) Hair density and length are 280/cm^2 and 4 mm; (b) Hair density and length are167/cm^2 and 3 mm; (c) Radiant flux absorbed along the depth of the stem cell layer from two skin-terminal hair models at 350 nm.

6.4 Vulnerability of children to sun exposure

We hypothesize that children's McSCs before puberty receive relatively higher doses of UV, as compared to adults. In this thesis, we have investigated a few of the main characteristics of child skin, which can result in the higher dose of UV received by MsSCs.

1. The most important factor is that MsSCs in children before puberty are primarily situated three times shallower in the dermis than those in adults. Due to the shallower depth in the skin, the MsSCs can receive significant doses of UV as compared to adults.
2. Children having typically thinner epidermis allow more UV to transmit deeply into the skin, reaching the MsSCs.
3. The presence of vellus hair in child skin provides an additional optical pathway, allowing the easier passage of UV and overall contributing to the higher dose of UV absorbed by follicular MsSCs.

These three factors provide possible explanations for the vulnerability of children to sun exposure, and the positive correlation between the incidence of melanoma in adults' bodies and the number of vellus hair in these areas. Although the MsSCs in childhood receive higher doses of UV, they may remain quiescent (stable) while leaving the potential to materialize into melanoma in the future. This may explain why there is a fourfold increase of melanoma risk in adults who have experienced excessive sun exposure in their childhood.

6.5 Validation of the simulation results

Due to the difficulty of getting child and adult skin biopsies, the simulation results have not been validated. Using human skin samples for experimental purposes requires a strict process of ethical approval. This is also the reason that the optical properties of child skin are rarely studied in the literature.

Ideally, a skin phantom can be developed to validate the simulation results. Aqueous solution of gelatine and agar are commonly used to construct analogues of skin layers [132]. Black ink and intralipid are usually added to the solution to provide absorption and scattering coefficients mimicking the optical properties of skin [133, 134].

An optical phantom can be constructed similar to the schematic diagram in Fig. 6-3. Half of the phantom has hair samples embedded. The half of phantom without hair can be used to measure its optical properties, which will be applied to MC simulation for comparison.

Measuring the optical properties of a phantom (absorption coefficient, reduced scattering coefficient and refractive index) will require the use of optical instruments, such as integrating sphere, UV light source, spectrometer and refractometer.

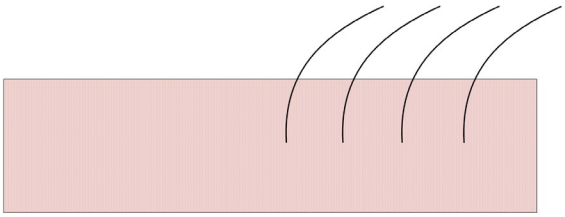

Figure 6-3: Schematic diagram of optical skin-hair phantom

However, there are a few challenges involved. First, ensuring the phantom has realistic skin optical properties can be time-consuming. Second, constructing two optically and physically identical skin phantoms (one with terminal hair attached and one with vellus hair attached) is technically difficult. Small differences in the physical models and their optical properties will mask the effect of different types of hair in UV transmission. Third, setting up a sophisticated optical bench for measurement is expensive. Lastly, embedding delicate hair shafts in an aqueous solution can be technically difficult. All in all, constructing a skin phantom for the purpose of validating the simulation results will require meticulous material preparation and sophisticated optical equipment. This could be investigated in the future.

6.6 Application for improvement of sunscreen

Nowadays, sunscreen is commonly used to provide skin protection against the harmful effects of solar UV. The active ingredients contained in the sunscreens are to provide broad-spectrum UV protection by absorbing, reflecting or scattering the incident radiation. Based on their mechanism of attenuating UV, sunscreen can be classified as either “chemical” or “physical” [135]. In chemical sunscreen, the active ingredient is an organic compound, which attenuates UV by absorption and dissipating the energy into heat. Whereas in physical sunscreen, the active ingredient is an inorganic compound that

physically reflects or scatters UV. Ideally, sunscreen should only remain on the skin surface.

Many commercially available organic sunscreens and some inorganic sunscreen (nanoparticles), can penetrate through the stratum corneum, or via hair follicles, into epidermis and dermis [136, 137], which can cause a variety of adverse effects, including cellular damage and carcinogenesis [138-140]. Micronized zinc oxide (ZnO) and titanium dioxide (TiO_2) are the two active ingredients that are generally recognized as safe and effective [141]. A combination of these particles assures a broad-band UV protection [142]. However, owing to their large particles size, they are opaque (i.e. appear white on the skin). To overcome this, nanoparticles of Zinc oxide and titanium dioxide offer more transparent suspensions on the skin. Paradoxically, these nanoparticles have not been demonstrated to be safe for tissue cells [143-145].

Our research has raised the importance of minimizing UV from entering hair follicles. It leads to a good opportunity for research on sunscreen development, possibly incorporating a combination of safe nano- or micronized particles as the active ingredients. Particles of approximately 600 nm in diameter has been demonstrated to penetrate efficiently along hair follicles (see Fig. 6-4) [146]. Applying such sunscreen on the skin surface will not only block UV from penetrating into the skin surface, but also prevent it from entering hair follicles, ultimately reducing the amount of UV reaching McSCs.

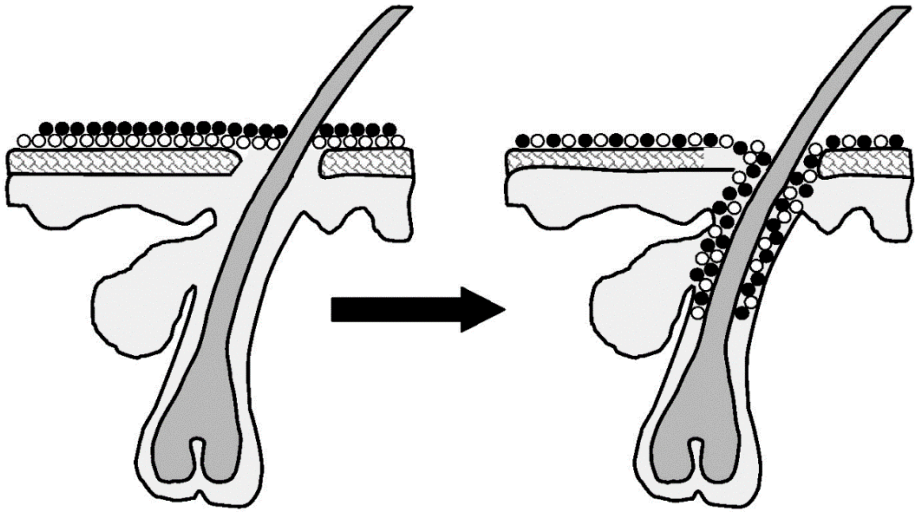

Figure 6-4: Schematic diagram of penetration of nanoparticles. Reproduced figure [147]

Chapter 7 Conclusion

7.1 Summary

Studies show that children are particularly vulnerable to sun exposure; excessive sun exposure during childhood will lead to increased risk of melanoma in later life. The explanation of this phenomenon is not yet known. Because the predominant type of body hair in children (fine and unpigmented vellus hair) and adult (long and dark terminal hair) are significantly different, and the melanocyte stem cells (McSCs) in hair follicles could be the origin of melanoma upon the exposure to UV, we hypothesize that it is because the McSCs in children before puberty can receive higher doses of UV than in adulthood; the quiescent McSCs will materialize into melanoma in later life after being affected by the cumulative UV damage. The shallower depth of McSCs, the thinner thickness of skin and the higher density of vellus hair in childhood all contribute to the solar UV transmission in the skin.

Using the MC simulations, it is shown that the McSCs in the VHF can absorb over 250 times higher UV energy than those in the THF due to their shallower location. As a consequence of the thinner epidermis, the McSCs in VHF of child skin will absorb about 1.9 and 3.2 times greater UVA and UVB respectively, than that in adult skin.

Due to the technical difficulty of acquiring and measuring bodily vellus hair, scalp hairs from three European families (children and adults) have been used. Their transmission properties are measured using a CRAIC microspectrophotometer in the wavelength range of 200 – 900 nm. By comparing the morphologies and the attenuation coefficient spectra of light blond scalp hair and body hair, it is considered reasonable use the attenuation coefficient of light blond scalp hair to represent the property of vellus hair.

The attenuation coefficient of the cortex of light blond hair is found to be significantly lower than that of more pigmented hair in the UVA and UVB wavelength ranges. Besides, the hair medulla shows significantly higher attenuation coefficient than the cortex. These two findings suggest that non-medullated and unpigmented vellus hair have significantly lower attenuation coefficients than medullated and pigmented terminal hair in the UV wavelength range.

To reveal how the presences of vellus and terminal hairs affect the solar UV transmission into the skin, the attenuation coefficients of light blond hair and dark brown hair, which

are the representatives of vellus and terminal hairs, are applied to skin-hair models to simulate the UV photon transport in the skin. The simulations are performed using the MC method in TracePro software.

The results show that skin with vellus hair results in significantly higher energy absorption in the stem cell layer as compared to hairless skin. The relative increase in energy absorbed in the stem cell layer when vellus hair is present to hairless skin varies from 4.6% to 52.0% over the UVA – UVB wavelength ranges. For skin with terminal hair (medullated or non-medullated), this relative increase in energy absorbed varies from 16.7% to 55.6% over the same wavelength range. Skin with shaved vellus hair will further enhance the UV transmission into the skin.

The objectives of this research have been met: The McSCs in the VHF receive and absorb significantly higher dose of UV primarily due to their shallower depth in the skin; The thinner skin layer and the presence of vellus hair also increase the solar UV transmission to the McSCs further. These three factors overall indicate that the McSCs in childhood will absorb significantly higher doses of UV, as compared to adulthood. This is believed to result in a higher risk of developing melanoma in later life, in which McSCs will undergoes several complex processes to form melanoma.

7.2 Future work

Measuring the transmittance spectra of human hair in its transverse direction is relatively more convenient than the longitudinal direction. The optical properties in the longitudinal direction of hair have not been measured in this work. Preliminary work has been done for preparing hair samples for the measurement, as briefly introduced below.

Figure 7-1 shows a schematic diagram of the procedures for hair sample preparation. Hair samples are firstly mounted perpendicularly into a paraffin wax. Then the wax block is sectioned into thin slices using a microtome. The wax slice containing the cross sections of hair can be mounted onto a quartz slide for transmittance spectra measurement using the CRAIC microspectrophotometer. Due to the difficulty of accessing the facilities for preparing the cross sections of hair at the measurement site, these transmittance spectra were not acquired. However, it was possible to obtain the micrographs of the cross sections of black scalp hair using a conventional microscope (Fig. 7-2).

Despite the difficulties and disadvantages of this method (Section 2.5.1), it is still considered to be the optimal approach to investigate whether the transmission property of human hair is different in its transverse and longitudinal directions.

Figure 7-1: Preparing the cross sections of hair using microtome.

Figure 7-2: Images of the cross sections of (a) medullated (b) non-medullated black scalp hair samples.

Although light blond hair has been considered to have close optical properties to vellus hair, real bodily vellus hair has not been measured. Measuring the optical properties of bodily vellus hair will more solidly confirm the hypothesis.

The optical properties of child skin are rarely known. Understanding the optical properties of child skin will improve the accuracy of the child's skin-hair model, which will make the comparison of the UV absorption in the stem cell layers of child and adult skin more realistic.

This research will also lead to testing the efficacy of sunscreens, in terms of UV filtering on the hair follicles.

Appendices

Appendix A – Publications during PhD

Journal articles

1. X. Huang, M. D. Protheroe, A. M. Al-Jumaily, S. P. Paul, and A. N. Chalmers, "Review of human hair optical properties in possible relation to melanoma development," *Journal of biomedical optics,* vol. 23, no. 5, pp. 050901, 2018 – **Chapter 2**
2. X. Huang, M. D. Protheroe, A. M. Al-Jumaily, A. N. Chalmers, S. P. Paul, and X. Fu, "Simulation of UV power absorbed by follicular stem cells during sun exposure and possible implications for melanoma development," *JOSA A,* vol. 36, no. 4, pp. 628-635, 2019 – **Chapter 3** (editor's pick)
3. X. Huang, M. D. Protheroe, A. M. Al-Jumaily, S. P. Paul, A. N. Chalmers, S. Wang, J. Diwu, and W. Liu, "Contribution of Human Hair in Solar UV Transmission in Skin: Implications for Melanoma Development," *Annals of Biomedical Engineering*, pp. 1-12, 2019 – **Chapter 4 & 5**
4. "Effect of hair removal on solar UV transmission into skin and implications for skin cancer development" (manuscript under review)

Conference proceedings

1. X. Huang, M. D. Protheroe, A. M. Al-Jumaily, S. P. Paul, A. N. Chalmers, and X. Fu, "Characterising UV transmission property of red hair using microspectrophotometer." in *Medical Laser Applications and Laser-Tissue Interactions IX* (2019) p. 1107914
2. X. Huang, M. D. Protheroe, A. M. Al-Jumaily, and S. P. Paul "Influence of human hair medulla in solar UV transmission through skin" in *ASME 2019 International Mechanical Engineering Congress and Exposition* (2019)
3. X. Huang, M. D. Protheroe, A. M. Al-Jumaily, and S. P. Paul, "The Significance of Hair Thermal Diffusivity on Melanoma Incidence." in *ASME 2017 International Mechanical Engineering Congress and Exposition* (2017), pp. V003T004A060-V003T004A060

Appendix B – Standard deviations of attenuation coefficient of hair

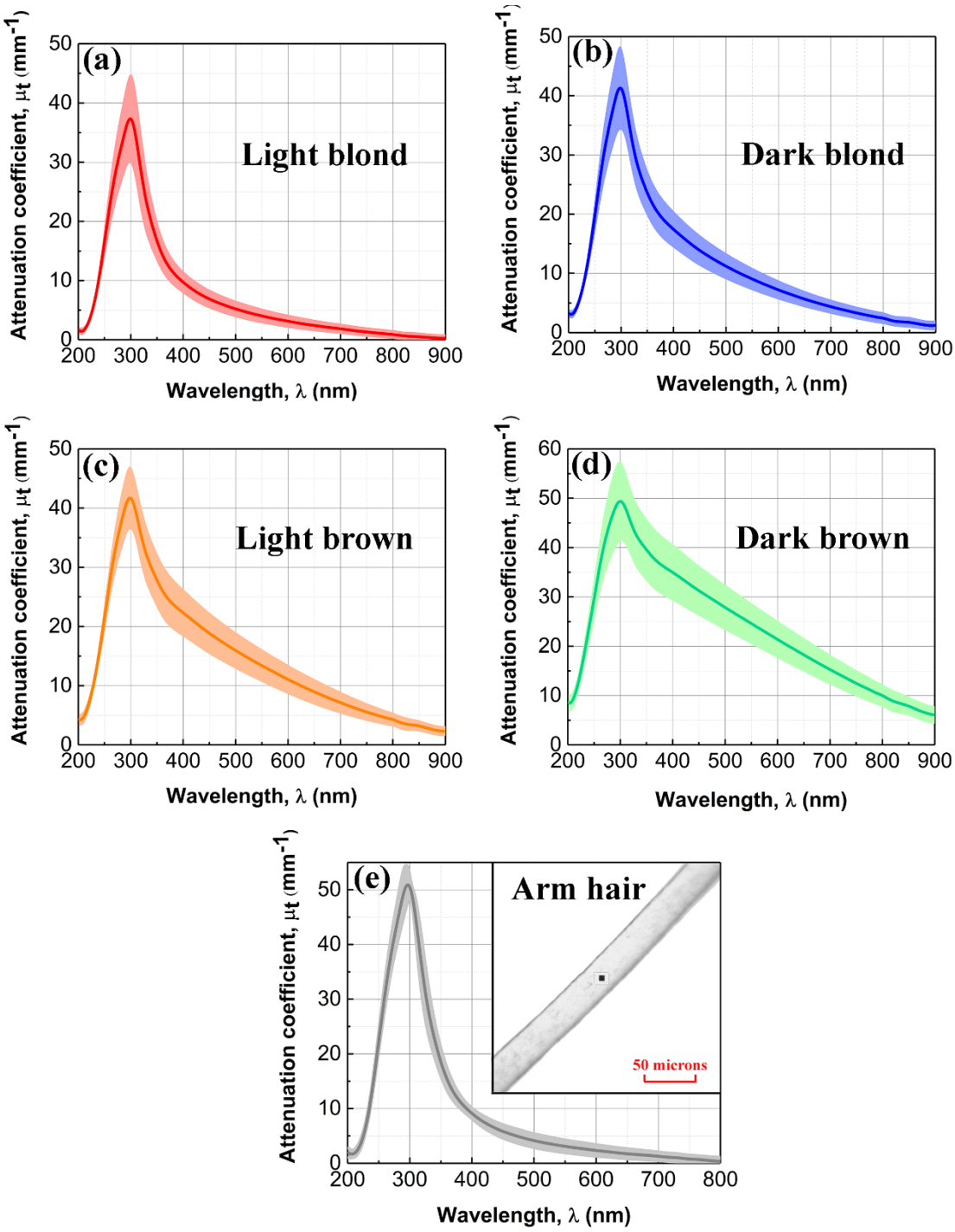

Figure B-1: Average attenuation coefficient (solid line) and one standard deviation (shaded regions) of (a) light blond hair (b) dark blond hair (c) light brown hair (d) dark brown hair (e) arm hair in the wavelength range of 200 to 900 nm

Appendix C – Absorption and scattering coefficients of skin and hair

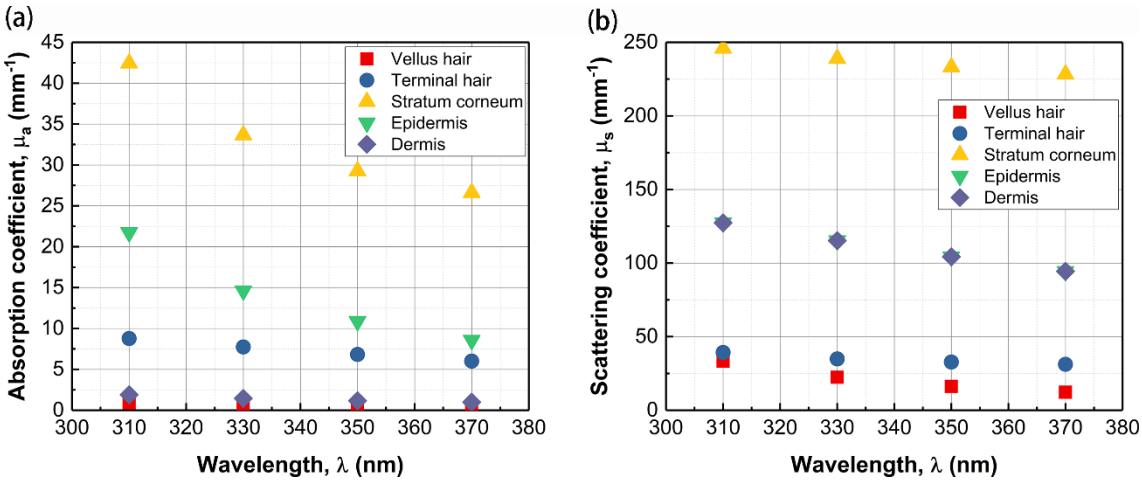

Figure C-1: (a) Absorption coefficient (b) scattering coefficient of stratum corneum, epidermis, dermis, vellus and terminal hair. The properties of the skin layers are from Fig. 3-1.

Appendix D – Ethics approval

AUTEC Secretariat

Auckland University of Technology
D-88, WU406 Level 4 WU Building City Campus
T: +64 9 921 9999 ext. 8316
E: ethics@aut.ac.nz
www.aut.ac.nz/researchethics

12 March 2018

Mike Protheroe
Faculty of Design and Creative Technologies

Dear Mike

Re Ethics Application: **18/11 An investigation of the UV properties of human hair and the implications for melanoma development**

Thank you for providing evidence as requested, which satisfies the points raised by the Auckland University of Technology Ethics Committee (AUTEC).

Your ethics application has been approved for three years until 9 March 2021.

Standard Conditions of Approval

1. A progress report is due annually on the anniversary of the approval date, using form EA2, which is available online through http://www.aut.ac.nz/researchethics.
2. A final report is due at the expiration of the approval period, or, upon completion of project, using form EA3, which is available online through http://www.aut.ac.nz/researchethics.
3. Any amendments to the project must be approved by AUTEC prior to being implemented. Amendments can be requested using the EA2 form: http://www.aut.ac.nz/researchethics.
4. Any serious or unexpected adverse events must be reported to AUTEC Secretariat as a matter of priority.
5. Any unforeseen events that might affect continued ethical acceptability of the project should also be reported to the AUTEC Secretariat as a matter of priority.

Please quote the application number and title on all future correspondence related to this project.

AUTEC grants ethical approval only. If you require management approval for access for your research from another institution or organisation then you are responsible for obtaining it. If the research is undertaken outside New Zealand, you need to meet all locality legal and ethical obligations and requirements. You are reminded that it is your responsibility to ensure that the spelling and grammar of documents being provided to participants or external organisations is of a high standard.

For any enquiries, please contact ethics@aut.ac.nz

Yours sincerely,

Kate O'Connor
Executive Manager
Auckland University of Technology Ethics Committee

Figure D-1: Ethics approval

References

[1] A. Jemal, R. Siegel, E. Ward, Y. Hao, J. Xu, T. Murray, and M. J. Thun, "Cancer statistics, 2008," *CA Cancer J Clin,* vol. 58, no. 2, pp. 71-96, 2008.

[2] G. P. Pfeifer, and A. Besaratinia, "UV wavelength-dependent DNA damage and human non-melanoma and melanoma skin cancer," *Photochemical & photobiological sciences,* vol. 11, no. 1, pp. 90-97, 2012.

[3] S. Bhatia, S. S. Tykodi, and J. A. Thompson, "Treatment of metastatic melanoma: an overview," *Oncology (Williston Park, NY),* vol. 23, no. 6, pp. 488, 2009.

[4] P. H. Dean, M. Bucevska, C. Strahlendorf, and C. Verchere, "Pediatric Melanoma: A 35-year Population-based Review," *Plast Reconstr Surg Glob Open,* vol. 5, no. 3, pp. e1252, 2017.

[5] C. D. Holman, and B. K. Armstrong, "Cutaneous malignant melanoma and indicators of total accumulated exposure to the sun: an analysis separating histogenetic types," *J Natl Cancer Inst,* vol. 73, no. 1, pp. 75-82, 1984.

[6] P. Autier, J. F. DorÃ©, O. Gefeller, J. P. Cesarini, F. Lejeune, K. F. Koelmel, D. Lienard, and U. R. Kleeberg, "Melanoma risk and residence in sunny areas. EORTC Melanoma Co-operative Group. European Organization for Research and Treatment of Cancer," *British Journal of Cancer,* vol. 76, no. 11, pp. 1521-1524, 1997.

[7] T. M. Mack, and B. Floderus, "Malignant melanoma risk by nativity, place of residence at diagnosis, and age at migration," *Cancer Causes and Control,* vol. 2, no. 6, pp. 401-411, 1991.

[8] K. Cooke, and J. Fraser, "Migration and death from malignant melanoma," *International journal of cancer,* vol. 36, no. 2, pp. 175-178, 1985.

[9] D. R. English, and B. K. Armstrong, "Identifying people at high risk of cutaneous malignant melanoma: results from a case-control study in Western Australia," *British medical journal (Clinical research ed.),* vol. 296, no. 6632, pp. 1285, 1988.

[10] S. A. Oliveria, M. Saraiya, A. C. Geller, M. K. Heneghan, and C. Jorgensen, "Sun exposure and risk of melanoma," *Archives of Disease in Childhood,* vol. 91, no. 2, pp. 131-138, 2006.

[11] M. Brenner, and V. J. Hearing, "The protective role of melanin against UV damage in human skin," *Photochemistry and photobiology,* vol. 84, no. 3, pp. 539-549, 2008.

[12] W. O. Jones, C. R. Harman, A. K. Ng, and J. H. Shaw, "Incidence of malignant melanoma in Auckland, New Zealand: highest rates in the world," *World journal of surgery,* vol. 23, no. 7, pp. 732-735, 1999.

[13] J. X. Wang, M. Fukunaga-Kalabis, and M. Herlyn, "Crosstalk in skin: melanocytes, keratinocytes, stem cells, and melanoma," *Journal of Cell Communication and Signaling,* vol. 10, no. 3, pp. 191-196, 2016.

[14] X. Huang, M. D. Protheroe, A. M. Al-Jumaily, and S. P. Paul, "The Significance of Hair Thermal Diffusivity on Melanoma Incidence." pp. V003T04A060-V003T04A060.

[15] B. L. Diffey, "Sources and measurement of ultraviolet radiation," *Methods,* vol. 28, no. 1, pp. 4-13, 2002.

[16] U. Leiter, and C. Garbe, "Epidemiology of melanoma and nonmelanoma skin cancer--the role of sunlight," *Adv Exp Med Biol,* vol. 624, pp. 89-103, 2008.

[17] E. C. De Fabo, F. P. Noonan, T. Fears, and G. Merlino, "Ultraviolet B but not ultraviolet A radiation initiates melanoma," *Cancer Res,* vol. 64, no. 18, pp. 6372-6, 2004.

[18] F. P. Noonan, M. R. Zaidi, A. Wolnicka-Glubisz, M. R. Anver, J. Bahn, A. Wielgus, J. Cadet, T. Douki, S. Mouret, and M. A. Tucker, "Melanoma induction by ultraviolet A but not ultraviolet B radiation requires melanin pigment," *Nature communications,* vol. 3, pp. 884, 2012.

[19] W. A. Bruls, H. Slaper, J. C. van Der Leun, and L. Berrens, "Transmission of human epidermis and stratum corneum as a function of thickness in the ultraviolet and visible wavelengths," *Photochemistry and photobiology,* vol. 40, no. 4, pp. 485-494, 1984.

[20] S. Q. Wang, R. Setlow, M. Berwick, D. Polsky, A. A. Marghoob, A. W. Kopf, and R. S. Bart, "Ultraviolet A and melanoma: a review," *J Am Acad Dermatol,* vol. 44, no. 5, pp. 837-46, 2001.

[21] H.-T. Wang, B. Choi, and M.-s. Tang, "Melanocytes are deficient in repair of oxidative DNA damage and UV-induced photoproducts," *Proceedings of the National Academy of Sciences,* vol. 107, no. 27, pp. 12180-12185, 2010.

[22] N. H. Cox, B. L. Diffey, and P. M. Farr, "The relationship between chronological age and the erythemal response to ultraviolet B radiation," *British Journal of Dermatology,* vol. 126, no. 4, pp. 315-319, 1992.

[23] B. Volkmer, and R. Greinert, "UV and Children's skin," *Progress in Biophysics and Molecular Biology,* vol. 107, no. 3, pp. 386-388, 2011.

[24] S. J. Balk, "Ultraviolet radiation: a hazard to children and adolescents," *Pediatrics,* vol. 127, no. 3, pp. e791-e817, 2011.

[25] H. Moon, L. R. Donahue, E. Choi, P. O. Scumpia, W. E. Lowry, J. K. Grenier, J. Zhu, and A. C. White, "Melanocyte stem cell activation and translocation initiate cutaneous melanoma in response to UV exposure," *Cell stem cell,* vol. 21, no. 5, pp. 665-678. e6, 2017.

[26] C. Köhler, D. Nittner, F. Rambow, E. Radaelli, F. Stanchi, N. Vandamme, A. Baggiolini, L. Sommer, G. Berx, and J. J. van den Oord, "Mouse cutaneous melanoma induced by mutant BRaf arises from expansion and dedifferentiation of mature pigmented melanocytes," *Cell stem cell,* vol. 21, no. 5, pp. 679-693. e6, 2017.

[27] A. M. G. Garcia, C. E. McLaren, and F. L. Meyskens, "Melanoma: is hair the root of the problem?," *Pigment cell & melanoma research,* vol. 24, no. 1, pp. 110-118, 2011.

[28] W. C. Chou, M. Takeo, P. Rabbani, H. Hu, W. Lee, Y. R. Chung, J. Carucci, P. Overbeek, and M. Ito, "Direct migration of follicular melanocyte stem cells to the epidermis after wounding or UVB irradiation is dependent on Mc1r signaling," *Nature medicine,* vol. 19, no. 7, pp. 924, 2013.

[29] A. N. Mull, A. Zolekar, and Y.-C. Wang, "Understanding melanocyte stem cells for disease modeling and regenerative medicine applications," *International journal of molecular sciences,* vol. 16, no. 12, pp. 30458-30469, 2015.

[30] D. Fang, T. K. Nguyen, K. Leishear, R. Finko, A. N. Kulp, S. Hotz, P. A. Van Belle, X. Xu, D. E. Elder, and M. Herlyn, "A tumorigenic subpopulation with stem cell properties in melanomas," *Cancer research,* vol. 65, no. 20, pp. 9328-9337, 2005.

[31] Y. Chiou, and U. Blume-Peytavi, "Stratum corneum maturation," *Skin pharmacology and physiology,* vol. 17, no. 2, pp. 57-66, 2004.

[32] J. M. Waller, and H. I. Maibach, "Age and skin structure and function, a quantitative approach (I): blood flow, pH, thickness, and ultrasound echogenicity," *Skin research and technology,* vol. 11, no. 4, pp. 221-235, 2005.

[33] A. Vogt, S. Hadam, M. Heiderhoff, H. Audring, J. Lademann, W. Sterry, and U. Blume-Peytavi, "Morphometry of human terminal and vellus hair follicles," *Exp Dermatol,* vol. 16, no. 11, pp. 946-50, 2007.

[34] J. Wells, “Hair light guide,” *Nature,* vol. 338, no. 6210, pp. 23-23, 1989.

[35] B. Iyengar, “The hair follicle: a specialised UV receptor in the human skin?,” *Biol Signals Recept,* vol. 7, no. 3, pp. 188-94, 1998.

[36] F. M.-L. Robertson, and L. Fitzgerald, “Skin cancer in the youth population of the United Kingdom,” *Journal of cancer policy,* vol. 12, pp. 67-71, 2017.

[37] A. J. Miller, and M. C. Mihm Jr, “Melanoma,” *New England Journal of Medicine,* vol. 355, no. 1, pp. 51-65, 2006.

[38] R. M. Siervogel, A. F. Roche, J. H. Himes, W. C. Chumlea, and R. McCammon, “Subcutaneous fat distribution in males and females from 1 to 39 years of age,” *Am J Clin Nutr,* vol. 36, no. 1, pp. 162-71, 1982.

[39] A. C. Green, S. C. Wallingford, and P. McBride, “Childhood exposure to ultraviolet radiation and harmful skin effects: Epidemiological evidence,” *Progress in biophysics and molecular biology,* vol. 107, no. 3, pp. 349-355, 2011.

[40] M. R. Schneider, R. Schmidt-Ullrich, and R. Paus, “The hair follicle as a dynamic miniorgan,” *Curr Biol,* vol. 19, no. 3, pp. R132-42, 2009.

[41] L. Langbein, H. Yoshida, S. Praetzel-Wunder, D. A. Parry, and J. Schweizer, “The Keratins of the Human Beard Hair Medulla: The Riddle in the Middle,” *Journal of Investigative Dermatology,* vol. 130, no. 1, pp. 55-73, 2010.

[42] P. Riley, “Melanin,” *The international journal of biochemistry & cell biology,* vol. 29, no. 11, pp. 1235-1239, 1997.

[43] S. Ito, and K. Fujita, “Microanalysis of eumelanin and pheomelanin in hair and melanomas by chemical degradation and liquid chromatography,” *Analytical Biochemistry,* vol. 144, no. 2, pp. 527-536, 1985.

[44] R. R. Anderson, and J. A. Parrish, “The Optics of Human Skin,” *Journal of Investigative Dermatology,* vol. 77, no. 1, pp. 13-19, 1981.

[45] V. A. Randall, “Androgens and hair growth,” *Dermatol Ther,* vol. 21, no. 5, pp. 314-28, 2008.

[46] U. Blume-Peytavi, D. A. Whiting, and R. M. Trüeb, *Hair growth and disorders*, Berlin: Springer Science & Business Media, 2008.

[47] J. G. Marks, and J. J. Miller, *Lookingbill and Marks' Principles of Dermatology E-Book*: Elsevier Health Sciences, 2017.

[48] S. Nagase, S. Shibuichi, K. Ando, E. Kariya, and N. Satoh, “Influence of internal structures of hair fiber on hair appearance. I. Light scattering from the porous structure of the medulla of human hair,” *J Cosmet Sci,* vol. 53, no. 2, pp. 89-100, 2002.

[49] E. M. Wynkoop, “A study of the age correlations of the cuticular scales, medullas, and shaft diameters of human head hair,” *American Journal of Physical Anthropology,* vol. 13, no. 2, pp. 177-188, 1929.

[50] R. Sinclair, D. Jolley, R. Mallari, J. Magee, A. Tosti, B. M. Piracinni, C. Vincenzi, R. Happle, J. Ferrando, and R. Grimalt, "Morphological approach to hair disorders." pp. 56-64.

[51] W. Montagna, and K. Carlisle, "Considerations on hair research and hair growth," *Hair Research*, pp. 3-11: Springer, 1981.

[52] T. B. Fitzpatrick, “The validity and practicality of sun-reactive skin types I through VI,” *Archives of dermatology,* vol. 124, no. 6, pp. 869-871, 1988.

[53] S. L. Jacques, “Optical properties of biological tissues: a review,” *Physics in medicine and biology,* vol. 58, no. 11, pp. R37, 2013.

[54] W.-F. Cheong, S. A. Prahl, and A. J. Welch, "A review of the optical properties of biological tissues," *IEEE journal of quantum electronics,* vol. 26, no. 12, pp. 2166-2185, 1990.

[55] O. Hamdy, J. El-Azab, T. A. Al-Saeed, M. F. Hassan, and N. H. Solouma, "A Method for Medical Diagnosis Based on Optical Fluence Rate Distribution at Tissue Surface," *Materials,* vol. 10, no. 9, pp. 1104, 2017.

[56] B. Wilson, M. Patterson, and S. Flock, "Indirect versus direct techniques for the measurement of the optical properties of tissues," *Photochemistry and photobiology,* vol. 46, no. 5, pp. 601-608, 1987.

[57] A. J. Welch, and M. J. Van Gemert, *Optical-thermal response of laser-irradiated tissue*, New York: Springer, 2011.

[58] A. N. Bashkatov, E. A. Genina, and V. V. Tuchin, "Optical properties of skin, subcutaneous, and muscle tissues: a review," *Journal of Innovative Optical Health Sciences,* vol. 4, no. 01, pp. 9-38, 2011.

[59] M. Friebel, A. Roggan, G. Müller, and M. Meinke, "Determination of optical properties of human blood in the spectral range 250to1100nm using Monte Carlo simulations with hematocrit-dependent effective scattering phase functions," *Journal of biomedical optics,* vol. 11, no. 3, pp. 034021-034021-10, 2006.

[60] V. Peters, D. Wyman, M. Patterson, and G. Frank, "Optical properties of normal and diseased human breast tissues in the visible and near infrared," *Physics in medicine and biology,* vol. 35, no. 9, pp. 1317, 1990.

[61] E. Salomatina, B. Jiang, J. Novak, and A. N. Yaroslavsky, "Optical properties of normal and cancerous human skin in the visible and near-infrared spectral range," *Journal of biomedical optics,* vol. 11, no. 6, pp. 064026-064026-9, 2006.

[62] L. V. Wang, and H.-i. Wu, *Biomedical optics: principles and imaging*: John Wiley & Sons, 2012.

[63] L. Wang, S. L. Jacques, and L. Zheng, "MCML--Monte Carlo modeling of light transport in multi-layered tissues," *Comput Methods Programs Biomed,* vol. 47, no. 2, pp. 131-46, 1995.

[64] G. W. Lucassen, W. Verkruysse, M. Keijzer, and M. J. van Gemert, "Light distributions in a port wine stain model containing multiple cylindrical and curved blood vessels," *Lasers in surgery and medicine,* vol. 18, no. 4, pp. 345-357, 1996.

[65] V. Periyasamy, and M. Pramanik, "Monte Carlo simulation of light transport in turbid medium with embedded object--spherical, cylindrical, ellipsoidal, or cuboidal objects embedded within multilayered tissues," *J Biomed Opt,* vol. 19, no. 4, pp. 045003, 2014.

[66] S. L. Jacques, "Coupling 3D Monte Carlo light transport in optically heterogeneous tissues to photoacoustic signal generation," *Photoacoustics,* vol. 2, no. 4, pp. 137-142, 2014.

[67] L. Zhang, X. Wang, M. Sun, Y. Chai, Z. Hao, and C. Zhang, "Monte Carlo simulation for the light propagation in two-layered cylindrical biological tissues," *Journal of Modern Optics,* vol. 54, no. 10, pp. 1395-1405, 2007.

[68] C. Zhu, and Q. Liu, "Review of Monte Carlo modeling of light transport in tissues," *Journal of biomedical optics,* vol. 18, no. 5, pp. 050902-050902, 2013.

[69] H. K. Bustard, and R. W. Smith, "Studies of factors affecting light scattering by individual human hair fibres," *Int J Cosmet Sci,* vol. 12, no. 3, pp. 121-33, 1990.

[70] A. Guiolet, J. Garson, and J. Levecque, "Study of the optical properties of human hair," *International journal of cosmetic science,* vol. 9, no. 3, pp. 111-124, 1987.

[71] H. K. Bustard, and R. W. Smith, “Investigation into the scattering of light by human hair,” *Applied Optics,* vol. 30, no. 24, pp. 3485-3491, 1991.

[72] R. F. Stamm, M. L. Garcia, and J. J. Fuchs, “The optical properties of human hair I. Fundamental considerations and goniophotometer curves,” *J. Soc. Cosmet. Chem,* vol. 28, no. 9, pp. 571, 1977.

[73] R. F. Stamm, M. L. Garcia, and J. J. Fuchs, “The optical properties of human hair II. The luster of hair fibers,” *J. Soc. Cosmet. Chem,* vol. 28, no. 9, pp. 601, 1977.

[74] J. A. Barrett, J. A. Siegel, and J. V. Goodpaster, “Forensic Discrimination of Dyed Hair Color: I. UV-Visible Microspectrophotometry*†,” *Journal of Forensic Sciences,* vol. 55, no. 2, pp. 323-333, 2010.

[75] X. Wang, R. Dhond, W. Sorin, J. Nelson, S. Newton, and T. Milner, “Characterization of human scalp hairs by optical low-coherence reflectometry,” *Optics letters,* vol. 20, no. 6, pp. 524-526, 1995.

[76] A. N. Bashkatov, E. A. Genina, A. V. Volokh, S. A. Murikhina, G. B. Altshuler, and V. V. Tuchin, "Optical properties of hair shafts estimated using the digital video microscopic system and inverse Monte Carlo method." pp. 1-9.

[77] T.-Y. Lin, C. C. Dierickx, V. B. Campos, W. A. Farinelli, J. Rosenthal, and R. R. Anderson, “Reduction of regrowing hair shaft size and pigmentation after ruby and diode laser treatment,” *Archives of dermatological research,* vol. 292, no. 2, pp. 60-67, 2000.

[78] E. Nicholls, “Microspectrophotometry in the study of red hair,” *Annals of Human Genetics,* vol. 32, no. 1, pp. 15-26, 1968.

[79] A. Kharin, B. Varghese, R. Verhagen, and N. Uzunbajakava, “Optical properties of the medulla and the cortex of human scalp hair,” *J Biomed Opt,* vol. 14, no. 2, pp. 024035, 2009.

[80] M. Greenwell, A. Willner, and P. L. Kirk, “Human hair studies. III. Refractive index of crown hair,” *Journal of Criminal Law and Criminology (1931-1951),* vol. 31, no. 6, pp. 746-752, 1941.

[81] A. Douglas, “A new method of cross-sectioning hair of larger mammals,” *South African Journal of Wildlife Research-24-month delayed open access,* vol. 19, no. 2, pp. 73-76, 1989.

[82] M. C. Pepper, and S. D. Lantis, “A new technique for cross sectioning free hairs,” *Journal of Investigative Dermatology,* vol. 68, no. 2, pp. 111-112, 1977.

[83] W. B. Shelley, and S. Öhman, “Technique for Cross Sectioning Hair Specimens** From the Department of Dermatology, University of Pennsylvania School of Medicine, University Hospital, 3400 Spruce Street, Philadelphia, Pennsylvania 19104,” *Journal of Investigative Dermatology,* vol. 52, no. 6, pp. 533-536, 1969.

[84] M. Kneberg, “Improved technique for hair examination,” *American Journal of Physical Anthropology,* vol. 20, no. 1, pp. 51-67, 1935.

[85] M. Steggerda, “Cross sections of human hair from four racial groups,” *Journal of Heredity,* vol. 31, no. 11, pp. 474-476, 1940.

[86] F. Formanek, Y. De Wilde, G. Luengo, and B. Querleux, “Investigation of dyed human hair fibres using apertureless near‐field scanning optical microscopy,” *Journal of microscopy,* vol. 224, no. 2, pp. 197-202, 2006.

[87] T. Lister, P. A. Wright, and P. H. Chappell, “Optical properties of human skin,” *Journal of biomedical optics,* vol. 17, no. 9, pp. 0909011-09090115, 2012.

[88] D. W. Koon, “Is polar bear hair fiber optic?,” *Applied optics,* vol. 37, no. 15, pp. 3198-3200, 1998.

[89] H. Tributsch, H. Goslowsky, U. Küppers, and H. Wetzel, “Light collection and solar sensing through the polar bear pelt,” *Solar energy materials,* vol. 21, no. 2-3, pp. 219-236, 1990.

[90] G. Kalyuzhny, A. Vaskevich, G. Ashkenasy, A. Shanzer, and I. Rubinstein, “UV/Vis spectroscopy of metalloporphyrin and metallophthalocyanine monolayers self-assembled on ultrathin gold films,” *The Journal of Physical Chemistry B,* vol. 104, no. 34, pp. 8238-8244, 2000.

[91] S. Walkbridge-Jones, “Microspectrophotometry for textile fiber color measurement,” in Identification of Textile Fibers, CRC Press, Boca Raton, FL, 2009, pp. 165-180.

[92] E. M. Chamot, and C. W. Mason, *Handbook of chemical microscopy*: John Wiley And Sons; Newn York, 1938.

[93] H. Van de Hulst, “Light Scattering by Small Particles 1Dover,” *New York,* vol. 19812, pp. 127, 1981.

[94] M. Wolbarsht, A. Walsh, and G. George, “Melanin, a unique biological absorber,” *Applied Optics,* vol. 20, no. 13, pp. 2184-2186, 1981.

[95] R. Anderson, and J. Parrish, "Optical properties of human skin," *The science of photomedicine*, pp. 147-194, New York: Springer, 1982.

[96] I. A. Menon, S. Persad, H. F. Haberman, and C. J. Kurian, “A Comparative Study of the Physical and Chemical Properties of Melanins Isolated from Human Black and Red Hair,” *Journal of Investigative Dermatology,* vol. 80, no. 3, pp. 202-206, 1983.

[97] G. Lask, M. Elman, M. Slatkine, A. Waldman, and Z. Rozenberg, "Laser-assisted hair removal by selective photothermolysis preliminary results," *Dermatologic surgery,* vol. 23, no. 9, pp. 737-739, 1997.

[98] F. Sun, A. Chaney, R. Anderson, and G. Aguilar, “Thermal modeling and experimental validation of human hair and skin heated by broadband light,” *Lasers in surgery and medicine,* vol. 41, no. 2, pp. 161, 2009.

[99] C. Ash, K. Donne, G. Daniel, G. Town, M. Clement, and R. Valentine, “Mathematical modeling of the optimum pulse structure for safe and effective photo epilation using broadband pulsed light,” *Journal of applied clinical medical physics,* vol. 13, no. 5, pp. 290-299, 2012.

[100] C. Ash, M. Dubec, K. Donne, and T. Bashford, “Effect of wavelength and beam width on penetration in light-tissue interaction using computational methods,” *Lasers in medical science,* vol. 32, no. 8, pp. 1909-1918, 2017.

[101] Z. D. Draelos, “Sunscreens and Hair Photoprotection,” *Dermatologic Clinics,* vol. 24, no. 1, pp. 81-84, 2006.

[102] C. R. Robbins, and C. R. Robbins, *Chemical and physical behavior of human hair*, New York: Springer, 2002.

[103] J. SaNogueira, and T. Russo, "Sunscreen for the scalp hair and hair," Google Patents, 2001.

[104] J. P. Ciaudelli, and E. Brand, "Sunscreen composition for hair protection," Google Patents, 1986.

[105] C. D. Vaughan, "Ultraviolet resistant sunscreen compositions," Google Patents, 1993.

[106] M. E. Nambudiry, and V. N. Collur, "Sunscreen compositions comprising pongomol," Google Patents, 1992.

[107] J. F. Grollier, G. Lang, S. Forestier, and G. Rosenbaum, "Cosmetic composition containing aloesin as an agent for protection against sunlight and its use for skin and hair protection," Google Patents, 1987.

[108] S. V. Patwardhan, A. P. Dhawan, and P. A. Relue, “Monte Carlo simulation of light-tissue interaction: three-dimensional simulation for trans-illumination-based imaging of skin lesions,” *IEEE transactions on biomedical engineering,* vol. 52, no. 7, pp. 1227-1236, 2005.

[109] J. D. Atencio, S. L. Jacques, and S. V. y Montiel, "Monte Carlo modeling of light propagation in neonatal skin," *Applications of Monte Carlo Methods in Biology, Medicine and Other Fields of Science*: InTech, 2011.

[110] I. R. M. Barnard, P. Tierney, C. L. Campbell, L. McMillan, H. Moseley, E. Eadie, C. T. A. Brown, and K. Wood, “Quantifying Direct DNA Damage in the Basal Layer of Skin Exposed to UV Radiation From Sunbeds,” *Photochemistry and photobiology*, 2018.

[111] M. Van Gemert, S. L. Jacques, H. Sterenborg, and W. Star, “Skin optics,” *IEEE Transactions on biomedical engineering,* vol. 36, no. 12, pp. 1146-1154, 1989.

[112] Q. Fang, and D. A. Boas, “Monte Carlo simulation of photon migration in 3D turbid media accelerated by graphics processing units,” *Optics express,* vol. 17, no. 22, pp. 20178-20190, 2009.

[113] D. A. Boas, J. Culver, J. Stott, and A. Dunn, “Three dimensional Monte Carlo code for photon migration through complex heterogeneous media including the adult human head,” *Optics express,* vol. 10, no. 3, pp. 159-170, 2002.

[114] W. A. Bruls, and J. C. Van Der Leun, “Forward scattering properties of human epidermal layers,” *Photochemistry and photobiology,* vol. 40, no. 2, pp. 231-242, 1984.

[115] S. Seidenari, G. Giusti, L. Bertoni, C. Magnoni, and G. Pellacani, “Thickness and echogenicity of the skin in children as assessed by 20-MHz ultrasound,” *Dermatology,* vol. 201, no. 3, pp. 218-22, 2000.

[116] J. G. Derraik, M. Rademaker, W. S. Cutfield, T. E. Pinto, S. Tregurtha, A. Faherty, J. M. Peart, P. L. Drury, and P. L. Hofman, “Effects of age, gender, BMI, and anatomical site on skin thickness in children and adults with diabetes,” *PLoS One,* vol. 9, no. 1, pp. e86637, 2014.

[117] J. Lock-Andersen, P. Therkildsen, F. F. de Olivarius, M. Gniadecka, K. Dahlstrem, T. Poulsen, and H. C. Wulf, “Epidermal thickness, skin pigmentation and constitutive photosensitivity,” *Photodermatology, Photoimmunology & Photomedicine,* vol. 13, no. 4, pp. 153-158, 1997.

[118] T. Tadokoro, N. Kobayashi, B. Z. Zmudzka, S. Ito, K. Wakamatsu, Y. Yamaguchi, K. S. Korossy, S. A. Miller, J. Z. Beer, and V. J. Hearing, “UV-induced DNA damage and melanin content in human skin differing in racial/ethnic origin,” *The FASEB Journal,* vol. 17, no. 9, pp. 1177-1179, 2003.

[119] S. L. Jacques, C. Alter, and S. A. Prahl, “Angular dependence of HeNe laser light scattering by human dermis,” *Lasers Life Sci,* vol. 1, no. 4, pp. 309-333, 1987.

[120] D. Huafeng, Q. L. Jun, A. W. William, J. K. Peter, and H. Xin-Hua, “Refractive indices of human skin tissues at eight wavelengths and estimated dispersion relations between 300 and 1600 nm,” *Physics in Medicine & Biology,* vol. 51, no. 6, pp. 1479, 2006.

[121] N. Maddodi, and V. Setaluri, “Role of UV in cutaneous melanoma,” *Photochemistry and photobiology,* vol. 84, no. 2, pp. 528-536, 2008.

[122] A. H. Shain, and B. C. Bastian, “From melanocytes to melanomas,” *nature reviews Cancer,* vol. 16, no. 6, pp. 345, 2016.

[123] X. Huang, M. D. Protheroe, A. M. Al-Jumaily, A. N. Chalmers, S. P. Paul, and X. Fu, “Simulation of UV power absorbed by follicular stem cells during sun exposure and possible implications for melanoma development,” *JOSA A,* vol. 36, no. 4, pp. 628-635, 2019.

[124] X. Huang, M. D. Protheroe, A. M. Al-Jumaily, S. P. Paul, A. N. Chalmers, S. Wang, J. Diwu, and W. Liu, "Contribution of Human Hair in Solar UV Transmission in Skin: Implications for Melanoma Development," *Annals of Biomedical Engineering*, pp. 1-12, 2019.

[125] X. Huang, M. D. Protheroe, A. M. Al-Jumaily, S. P. Paul, A. N. Chalmers, and X. Fu, "Characterising UV transmission property of red hair using microspectrophotometer." p. 1107914.

[126] X. Huang, M. D. Protheroe, A. M. Al-Jumaily, S. P. Paul, and A. N. Chalmers, "Review of human hair optical properties in possible relation to melanoma development," *Journal of biomedical optics,* vol. 23, no. 5, pp. 050901, 2018.

[127] E. Bendit, and D. Ross, "A technique for obtaining the ultraviolet absorption spectrum of solid keratin," *Applied Spectroscopy,* vol. 15, no. 4, pp. 103-105, 1961.

[128] M. G. Larson, "Analysis of variance," *Circulation,* vol. 117, no. 1, pp. 115-121, 2008.

[129] A. Hilton, and R. Armstrong, "Statnote 6: post-hoc ANOVA tests," 2006.

[130] F. H. Mustafa, M. S. Jaafar, and A. H. Ismail, "Control Light Delivery in PDT by Taking Account the Optical Properties of Hair Density on the Skin Surface," *Modern Applied Science,* vol. 5, no. 2, pp. 149, 2011.

[131] N. Otberg, H. Richter, H. Schaefer, U. Blume-Peytavi, W. Sterry, and J. Lademann, "Variations of hair follicle size and distribution in different body sites," *J Invest Dermatol,* vol. 122, no. 1, pp. 14-9, 2004.

[132] A. I. Chen, M. L. Balter, M. I. Chen, D. Gross, S. K. Alam, T. J. Maguire, and M. L. Yarmush, "Multilayered tissue mimicking skin and vessel phantoms with tunable mechanical, optical, and acoustic properties," *Medical Physics,* vol. 43, no. 6Part1, pp. 3117-3131, 2016.

[133] R. Cubeddu, A. Pifferi, P. Taroni, A. Torricelli, and G. Valentini, "A solid tissue phantom for photon migration studies," *Physics in medicine and biology,* vol. 42, no. 10, pp. 1971, 1997.

[134] B. W. Pogue, and M. S. Patterson, "Review of tissue simulating phantoms for optical spectroscopy, imaging and dosimetry," *Journal of biomedical optics,* vol. 11, no. 4, pp. 041102, 2006.

[135] S. Tampucci, S. Burgalassi, P. Chetoni, and D. Monti, "Cutaneous permeation and penetration of sunscreens: formulation strategies and in vitro methods," *Cosmetics,* vol. 5, no. 1, pp. 1, 2018.

[136] C. Hayden, S. Cross, C. Anderson, N. Saunders, and M. Roberts, "Sunscreen penetration of human skin and related keratinocyte toxicity after topical application," *Skin pharmacology and physiology,* vol. 18, no. 4, pp. 170-174, 2005.

[137] X. Liu, J. E. Grice, J. Lademann, N. Otberg, S. Trauer, A. Patzelt, and M. S. Roberts, "Hair follicles contribute significantly to penetration through human skin only at times soon after application as a solvent deposited solid in man," *British journal of clinical pharmacology,* vol. 72, no. 5, pp. 768-774, 2011.

[138] A. S. Barnard, "One-to-one comparison of sunscreen efficacy, aesthetics and potential nanotoxicity," *Nature nanotechnology,* vol. 5, no. 4, pp. 271, 2010.

[139] E. Kimura, Y. Kawano, H. Todo, Y. Ikarashi, and K. Sugibayashi, "Measurement of skin permeation/penetration of nanoparticles for their safety evaluation," *Biological and Pharmaceutical Bulletin,* vol. 35, no. 9, pp. 1476-1486, 2012.

[140] A. Vogt, B. Combadiere, S. Hadam, K. M. Stieler, J. Lademann, H. Schaefer, B. Autran, W. Sterry, and U. Blume-Peytavi, "40 nm, but not 750 or 1,500 nm, nanoparticles enter

epidermal CD1a+ cells after transcutaneous application on human skin," *Journal of investigative dermatology,* vol. 126, no. 6, pp. 1316-1322, 2006.

[141] M. K. Matta, R. Zusterzeel, N. R. Pilli, V. Patel, D. A. Volpe, J. Florian, L. Oh, E. Bashaw, I. Zineh, and C. Sanabria, "Effect of sunscreen application under maximal use conditions on plasma concentration of sunscreen active ingredients: a randomized clinical trial," *Jama,* vol. 321, no. 21, pp. 2082-2091, 2019.

[142] T. G. Smijs, and S. Pavel, "Titanium dioxide and zinc oxide nanoparticles in sunscreens: focus on their safety and effectiveness," *Nanotechnology, science and applications,* vol. 4, pp. 95, 2011.

[143] Z. Pan, W. Lee, L. Slutsky, R. A. Clark, N. Pernodet, and M. H. Rafailovich, "Adverse effects of titanium dioxide nanoparticles on human dermal fibroblasts and how to protect cells," *Small,* vol. 5, no. 4, pp. 511-520, 2009.

[144] B. Trouiller, R. Reliene, A. Westbrook, P. Solaimani, and R. H. Schiestl, "Titanium dioxide nanoparticles induce DNA damage and genetic instability in vivo in mice," *Cancer research,* vol. 69, no. 22, pp. 8784-8789, 2009.

[145] H. Zhang, Y. Shan, and L. Dong, "A comparison of TiO2 and ZnO nanoparticles as photosensitizers in photodynamic therapy for cancer," *Journal of biomedical nanotechnology,* vol. 10, no. 8, pp. 1450-1457, 2014.

[146] J. Lademann, F. Knorr, H. Richter, S. Jung, M. Meinke, E. Rühl, U. Alexiev, M. Calderón, and A. Patzelt, "Hair follicles as a target structure for nanoparticles," *Journal of Innovative Optical Health Sciences,* vol. 8, no. 04, pp. 1530004, 2015.

[147] W. C. Mak, A. Patzelt, H. Richter, R. Renneberg, K. K. Lai, E. Rühl, W. Sterry, and J. Lademann, "Triggering of drug release of particles in hair follicles," *Journal of controlled release,* vol. 160, no. 3, pp. 509-514, 2012.